THE SINTERABILITY OF ULTRA-FINE IRON POWDERS

by

DAVID MICHAEL COULSON, B.Met.Hons

Submitted for the degree of Master of Philosophy

University of Surrey

1973

ProQuest LLC.
789 East Eisenhower Parkway
P.O. Box 1346
Ann Arbor, MI 48106 – 1346

The Sinterability of Ultra-Fine Iron Powders

D. M. COULSON

Submitted for M.Phil Degree of University of Surrey. April 1973.

SUMMARY

Iron powders, having a high specific surface area compared to current industrial powders, have been prepared by two different routes. These were (a) the decomposition of ferrous oxalate and subsequent reduction of the resulting oxide and (b) the direct reduction of a high purity oxide, in hydrogen atmospheres. The resulting powders were suvstantially in the submicron size range, and were pyrophoric, necessitating handling in glove boxes. The morphology of the powders was studied using electron microscopy and BET (krypton sorption) methods and this study showed many differences between the initial oxide powders and the iron powders obtained from them by reduction.

Sintering studies were carried out on these powders, together with a commercial iron powder of the carbonyl type which was used as a reference material. All sintering was carried out in the α-phase at temperatures up to 900°C for times up to 16½ hours. Two of the powders showed conventional behaviour on sintering up to 900°C and also showed a marked decrease in density at 900°C. The powder, ex ferrous oxalate showed rapid initial densification for periods of about 30 minutes, but sintering apparently ceased after that time. Sintering at 900°C produced only a slight decrease in density. Measurements of grain size on the sintered compacts showed marked rapid increases after sintering at 900°C for two of the powders, but the third powder, from ferrous oxalate, showed much more gradual grain growth at 900°C. These differences were accounted for in terms of powder purity and were related to the anomalies noted in the densification of the powders. Dilatometric studies were also carried out to determine whether the powders were in the α or γ ranges on sintering at 900°C. However, the results obtained were not consistent with observed variations in sintering behaviour.

ABSTRACT

Iron powders having a high specific surface area, compared to current industrial iron powders, have been prepared by the decomposition and subsequent reduction of ferrous oxalate, and by the reduction of a high purity grade of oxide, at 300°C, under a hydrogen atmosphere. The iron powders obtained were pyrophoric, so that all handling was carried out in glove boxes, under an argon atmosphere.

The morphology of the powders was studied using electron microscopic and krypton sorption (B.E.T.) techniques. Both preparation routes yielded powders of similar shape and size although considerable differences existed in the oxides from which they were prepared.

The sintering behaviour of the powders was studied at temperatures up to 900°C and for times up to 16½ hours. A typical industrial iron powder viz carbonyl iron, was sintered alongside the fine powders to provide a basis for comparison. Marked differences were observed in sintering behaviour, the iron powder ex oxalate showing a rapid initial densification followed by an apparent cessation of densification. The other two powders showed more conventional behaviour up to 900°C. However on sintering at 900°C rapid drops in density were observed in both these powders, accompanied by an abnormal rate of grain growth at this temperature. The other powder, ex ferrous oxalate, showed a smaller drop in density and a more gradual rate of grain growth. Activation energies for sintering fell below the established values for grain boundary diffusion in iron, and this is interpreted in terms of the operation of more than one sintering mechanism acting in parallel with each

other. Diffusion distances obtained from bulk diffusion data, are compared with actual grain sizes present in the materials, in order to discuss the relative contributions of both boundary and volume diffusion in terms of the proximity of grain boundary sinks. It was concluded that finer grain sizes resulted in a larger contribution of volume diffusion to sintering owing to a longer contact between pores and the grain boundary sink. Differences between the iron powder ex oxalate, and the other two materials are accounted for in terms of purity, since the much lower rate of grain growth in this former powder is primarily responsible for its densification characteristics, and such grain growth is markedly affected by purity.

A dilatometric investigation was carried out on the sintered compacts, in order to determine the temperature of the α/γ phase change in the materials. It was found that both carbonyl iron and iron powder ex oxalate would contain γ phase on sintering at 900°C, whereas transformation in the powder from high purity oxide occurred above this sintering temperature.

ACKNOWLEDGEMENTS

I wish to express my thanks and gratitude to Dr. D.H. Houseman, and to Mr. J. Towner for their help and guidance through various stages of this work.

My thanks are also due to Dr. J. Castle and his former colleagues of the Chemistry Department of the C.E.G.B. Research Laboratories, Leatherhead, Surrey, for permission to use, and guidance in the use of, equipment for gas sorption analysis.

I am also indebted to the Governors and Principal of Derby College of Art & Technology for permission to complete this work during my time at the College.

CONTENTS

		Page
1.	INTRODUCTION	8
2.	LITERATURE SURVEY	10
	2.1. Phenomenological Approach to Sintering	10
	2.2 Model Experiments and the Initial Stages of Sintering	14
	2.3 The Importance of Grain Boundaries and last Stage Models of Sintering	20
	2.4 The Sintering of Metal Powders	23
	2.5 Other Factors affecting the Sintering Process	27
	2.5.1 The Effect of Green Density on Sintering	27
	2.5.2 The Effect of Oxide Films on the Metal Surface	28
	2.5.3 The Effect of Sintering Atmosphere	29
	2.5.4 The Effect of Phase Change on Sintering	29
	2.6 The Production and Properties of Ultrafine Powders	30
3.	EXPERIMENTAL PROCEDURE	38
	3.1 Materials used and Methods of Preparation	38
	3.2 Apparatus	40
	3.2.1 Reduction Chambers	40
	3.2.2 Glove Boxes	41
	3.2.3 Pressing and Sintering of the Powders	42

3.3. Techniques for Studying Particle Morphology..... 43
3.3.1 Gas Sorption Analysis..... 43
3.3.2 Electron Microscopy of the Powders..... 43
4. RESULTS..... 47
4.1 Morphology of the Powders..... 47
4.2 Results of powder sintering experiments..... 48
4.2.1 Density/Time Plots..... 48
4.2.2 Semi logarithmic plots of sintering data..... 48
4.2.3 Activation energies for sintering..... 49
4.3 Determination of the α/γ phase change temperature in the powders..... 49
4.4 Results of Grain size measurements on the sintered powders..... 50
5. DISCUSSION..... 51
5.1 Morphology of the powders..... 51
5.1.1 Measurement of Surface Area..... 51
5.1.2 Electron Microscopy of the powders..... 52
5.2 Sintering Behaviour of the Powders..... 53
5.2.1 Effect of time and temperature on sintering behaviour..... 53
5.2.2 Effect of pressing pressure on the sintering process..... 59
5.2.3 The effect of phase transformations within the powders..... 61

5.2.4 Grain size variations during sintering..... 63

5.2.5 General discussion..... 66

6. CONCLUSIONS..... 71

7. Suggestions for future work..... 73

8. Tables..... 75

9. Figures..... 88

10. References..... 123

1. INTRODUCTION

Considerable interest has been shown in recent years, in the development of high strength alloys by dispersion hardening techniques. Such alloys rely for their strength on the interactions between dislocations and a finely dispersed refractory phase within the metal. The most successful methods of preparation of these alloys has been by the powder metallurgy route, where dispersoid particles are mixed with the metal powders, and the composite powder pressed and sintered in the normal way. However, the mechanical properties of the bulk alloy are strongly dependent on the interparticle spacing of the dispersed phase, which is determined principally by the size of the matrix metal powders. Most commercially available powders lie in the size range of 5 μm and above, as is the case for the carbonyl iron powder used in this work, which varies between 5 and 20 μm size. This places a limit on the interparticle spacings obtainable in alloys using this powder. Substantially closer spacings should be obtained if the refractory phase could be successfully dispersed throughout finer iron powders. Such powders, having a size range substantially less than one micron, have been exploited for many years in the field of iron powder magnets, but they suffer from the inherent disadvantage of being highly pyrophoric. This property dictates the use of glove box techniques for handling the powders, which would add substantially to the cost of production. However the high costs involved could no doubt be justified, if the technique enabled successful high strength, high temperature resistant alloys to be developed.

Two such routes for the preparation of fine iron powders, viz from the decomposition of ferrous oxalate and the reduction of fine

iron oxides have been utilised in this work, in order to study the sintering characteristics of fine iron powders prior to their use in dispersion hardening systems.

2. LITERATURE SURVEY

2.1 Phenomenological Approach to Sintering

The term "sintering" is usually applied to the ability of a powder mass to change into a bulk solid under the influence of heat, combined in most (but not all) instances with pressure. As such, it embraces many types of phenomena observed in materials in general viz. Diffusion, Grain Growth, Recovery and Recrystallisation, Interfacial Interactions to name but a few.

The term also covers multicomponent systems when more than one component is present in the powder e.g. Cu/Zn in the sintering of brass powders, and liquid phase sintering, when the process is carried out at a temperature above the melting point of one of the components. However, since the work described in this thesis deals with a single component system at temperatures of the order of 0.6 T_m (where T_m is the absolute melting point) these topics will not be dealt with, except to refer the reader to one of many pertinent reviews.[1]

As early as 1923, work was in progress to determine the "nature and causes of sintering"[2] with a view to establishing that completely solid state reactions i.e. in the absence of a liquid phase, were possible. Much of this early work, by such people as Tamman, Hedvall, Volmer, Huttig and Sauerwald, is reviewed by Eitel[3], Jones[4], and Goetzel.[5] The more theoretical approach to sintering, which characterises many of the current papers on the subject, started around 1945 with the investigation by Frenkel.[6] This work led to the development of a sintering theory based on the use of models in which the areas of contact between the models were well defined and easily observed. In this connection, the classic works of

Kuczynski[7] must be mentioned. However this aspect will be considered in more detail later in this survey.

Three distinct stages have been recognised during the sintering process. These have been defined as follows[1]:-

(a) Neck growth - in which the points of contacts between particles grow rapidly giving rise to a large decrease in electrical resistivity and a large increase in mechanical properties (e.g. UTS., of the sintering body). Very little densification occurs in this stage,[8] although surface activity as represented for example, by rate of chemical reaction, shows a marked decrease.

(b) The densification stage:- as the name suggests, most of the increase in density, up to about 95% of theoretical density, occurs during this stage. The pore structure changes from one of large interconnected pores, to one of isolated pores often joined by grain boundaries. Grain growth also proceeds and the original particles lose their identity as they are consumed by the moving grain boundaries. This grain growth is controlled by the spacing of the pores since these pores are known to act like inclusions in impeding grain boundary migration.[9]

(c) The final stage - in which the isolated voids shrink at a slower rate and slowly become spherodised. Exaggerated or discontinuous grain growth may occur, causing certain favourable grain boundaries to break away from their pore "captors" and grow, at the expense of neighbouring grains, to a large size.

This effect is discussed in detail by Coble and Burke[9]. The net result of this exaggerated growth is the isolation of pores within the grains themselves. Since grain boundaries are postulated as the most likely "sinks" for vacancies, this means that these pores within grains will shrink very slowly and contribute towards the residual porosity of the material. Another effect of the final stage is the growth of very large pores at the expense of smaller ones, the latter eventually disappearing[10].

Rhines[10] has interpreted these stages using the topological concept of "genus" where the genus is related to the number of particles and the total number of contacts, it being zero for a massive pore free body. Thus in stage (a) the genus remains constant as neck growth proceeds and contacts are neither created nor destroyed. Stage (b) the genus decreased towards zero as porosity decreases and grain growth occurs. Stage (c) a constant residual genus occurs corresponding to the presence of the residual porosity.

Thus the process of sintering occurs by the growth of inter-particle contacts followed by a decrease in porosity. The driving force for the process has its origin in the reduction of surface energy of the powder mass, and as a direct result of this energy it can be shown that the curved neck between the two particles is subjected to an outward facing, tensional stress given by[10]

$$\sigma = \frac{\gamma}{\rho} \quad \ldots\ldots\ldots (1)$$

σ = stress [2] in Nm^{-2}

γ = surface tension in Nm^{-1}

ρ = radius of curvature of the neck in metres.

For an iron powder of 40 microns diameter, taking the value of surface energy as 2 Nm^{-1} (2000 dynes/cm)[24], this stress is of the order of 39.4 MN/m^2, (N.B. Room Temperature Yield Point of Iron =

225 MN/m^2), which may be significant at high sintering temperatures. In addition to this, the pores formed in the powder mass are subjected to compressive stresses of the order of $\frac{2\gamma}{r}$, where γ is the surface tension of the material, as above, and r is the pore radius[9]. This stress operates in such a direction to make the pore shrink and is equivalent to an external hydrostatic pressure. For a one micron pore, taking $\gamma = 2Nm^{-1}$, this pressure is about 4 MN/m^2.

Two further effects associated with the thermodynamics of curved surfaces should be noted, since they both play important roles in the process of sintering. Firstly, there exists an excess concentration of vacancies beneath the concave surface of a pore, over and above that existing below a normal flat surface. This excess is given by the following equation[1, 9]

$$\frac{\Delta C}{C_o} = \frac{\gamma V_o}{RT\rho} \quad \ldots\ldots\ldots (2)$$

C_o = equilibrium concentration of vacancies beneath a flat surface

ΔC = excess concentration of vacancies above

γ = surface tension

ρ = radius of curvature of surface

V_o = molar volume of solid

T = temperature in degrees absolute

R = gas constant

Secondly the vapour pressure over a concave surface is lower than that above a flat surface by an amount given by

$$\frac{\Delta p}{p_o} = \frac{-\gamma V_o}{RT\rho} \quad \ldots\ldots (3)$$

where

Δp = decrease in vapour pressure over concave surface

p_o = vapour pressure above flat surface

and the other symbols have the same meanings as in the previous

equation. Thus the pressure in the neck area of a compact is smaller by Δp than that over a flat surface and providing that the vapour pressure is high enough, this suggests one possible mechanism of material transport during sintering, viz evaporation from regions having large convex radii of curvature and condensation in the concave neck region.

A consideration of the above effects suggests several possible transport mechanisms in addition to evaporation and condensation, that could occur during sintering. These are

(1) viscous flow

(2) plastic flow

(3) volume diffusion

(4) surface diffusion

(5) grain boundary diffusion.

All these transport mechanisms may operate under specific conditions during sintering and the relevant rate equations for the processes have been worked out, at least for the initial stages assuming one or other of these mechanisms to be operative. In order to test these equations, model experiments were devised in which the geometry of the sintering bodies could be carefully controlled.

2.2 Model experiments and the initial stages of sintering

The initial stage of sintering proceeds by the formation of necks between powder particles, and in order to study this behaviour models were devised which enabled direct measurements of neck growth to be made. The models used were sphere/plate, sphere/sphere, and bundles of wire wrapped round a former, thus enabling well defined geometrical interfaces to be observed and the rate of neck formation between these interfaces to be measured. The prime movers of this

approach were Frenkel [6] and Kuczynski[11]. The results of this work showed that the initial stages of sintering could be represented by an equation of the general form.

$$\frac{x^n}{a^m} = F(T)t \quad \ldots\ldots (4)$$

x = neck width
a = particle radius
) see Figure 1

F(T) = some function of temperature

t = time

n,m constants depending on neck growth mechanism.

Kuczynski[11] assumed different sintering mechanisms viz evaporation and condensation, surface, and volume diffusion, and calculated the theoretical neck growth rate between particles assuming these processes to be operating. He then devised model experiments to test the theoretical equations. This type of approach has been adopted by several investigators [9, 11, 14-16, 26] and typical results are given in Table 1. The Kuczynski exponent n = 5, denoting volume diffusion has been obtained in many model sintering experiments for both metal and oxide systems. Reference to the following reviews[1, 13], shows the vast amount of experimental evidence supporting this model, although as Bernard[13] points out the basic experiment is the same in each case.

Several investigators, principally Pines[14], Cabrera[15] and Schwed[16] have derived different exponents to those of Kuczynski and these are shown in Table 1. De Hoff, Baldwin and Rhines[17], on the basis of experiments conducted on bundles of copper wire found that the exponent 'n' in equation (1) varied markedly with the wire diameter. However Rieck and Rockland[18] claimed that by careful measurement on wire bundles the exponent 'n' proved to be equal to 5 (the Kuczynski exponent for volume diffusion) regardless of

the wire diameter.

Frenkel[6] considered neck formation to be a process dominated by a viscous flow mechanism, and derived the following equation for the rate of neck growth

$$\frac{x^2}{a} = \frac{3}{2}\left(\frac{\gamma}{\eta}\right) t \quad \ldots\ldots\ldots (5)$$

x and a are the radius of neck and particle respectively

η = coefficient of viscosity

γ = Surface Tension

t = time

Herring[12] formulated scaling laws from the model data, based on similarity considerations. According to these, at equal $\frac{x}{a}$ ratios, different particle diameters require sintering times, related to the diameter ratio by a power law. Thus:-

$$\frac{t_2}{t_1} = \left(\frac{a_2}{a_1}\right)^p \quad \ldots\ldots\ldots (6)$$

a = radius of particle

t_2, t_1 times to reach equal $\frac{x}{a}$ ratios, for particles of diameter a_2 and a_1 respectively.

p = exponent related to neck growth mechanism.

The exponent 'p' has a different value depending on the predominant neck growth mechanism (see Table 1). Its value can be related to the Kuczynski exponents 'n' and 'm' by the relationship $p = (n-m)^1$. In order to explain the shrinkage which occurs on sintering, one of the necessary postulates of the Kuczynski theory is that the centres of particles must approach each other during sintering. Thus, vacancies diffusing out of the pores between particles must be absorbed and destroyed, to allow the particles to shrink. Kuczynski[11] has suggested that the grain boundaries between the particle necks

act as "sinks" to absorb the vacancies. According to Clapson and Robins [19] and Barnes[20], these vacancies are absorbed at the grain boundaries, and destroyed by the removal of planes of atoms adjacent to the boundaries. Other possible sinks are the particle surface, and dislocations within the particles[9] but neither of these sinks produce an approach of particle centres, merely causing shape changes in the system. Van Bueren and Hornstra[126] postulate a mechanism of vacancy removal by the steady relative shear of a curved grain boundary, the shear stress necessary to accomplish this arising from vacancy gradients within the boundary. However Coble and Burke[9] point out the lack of metallographic evidence supporting this model. The possibility of dislocations absorbing vacancies by climb to form tilt boundaries has been considered[126]. Gifkins[127] reviews mechanisms by which grain boundaries can act as vacancy sinks after pores are closed off and concludes that they only act as sinks when they are linked to the free surface by a continuous path or when there is a small compressive applied stress which will help to remove vacancies by grain boundary sliding.

It has also been reported[21, 22] that the same time law of neck growth applies, with and without the presence of grain boundaries between the particles. Thus neck growth can occur with sinks other than grain boundaries in operation. It has been pointed out[1] that the total shrinkage accounted for by such models is extremely small, amounting to some 3% of the whole, and therefore has little value in describing the behaviour of real powder systems.

The formation of necks by pure surface or grain boundary diffusion mechanisms must not be overruled and has been supported by several authors[8, 23-25]. The latter authors[23-25] claim that

surface diffusion is important in the sintering of coarse powders, whilst volume diffusion is operating in finer powders. The basis for their argument is that coarse powders show very little shrinkage during sintering, whereas fine powders shrink to a much greater extent. Since a surface diffusion mechanism does not produce approach of centres i.e. shrinkage, it is assumed to be the operative mechanism with the coarse powders. Experimental evidence for this was provided by Fischmeister and Zahn[24] working on Iron, who compared Diffusion Coefficients and Activation Energies, obtained from scratch healing and thermal grooving experiments with those obtained from neck growth measurements on wire bundles and from the sintering of iron powders (see Tables 2 and 3). The results showed good agreement and therefore surface diffusion was considered to be the operative mechanism during the neck growth stage of sintering. They obtained an exponent n = 7 for the neck growth model which agrees with the value derived by Kuczynski for surface diffusion. The argument against surface diffusion mechanisms is based largely on the weight of experimental evidence from a wide variety of materials giving n = 5, the Kuczynski exponent for volume diffusion and also on the fact that no approach of centres is possible using this model. The Kuczynski exponent n = 7 for surface diffusion has been confirmed by Rockland[26], but criticised by other authors[13, 14, 15, 27]. Nichols[27] calculated theoretically that 'n' ranges from 5.2 to 6.5 for model sintering and concluded that surface diffusion was dominant in all wire sintering experiments to date, on the basis that values of n, close to 5.5 were obtained. Recent work by Matsumura[115] on iron wires has obtained the Kuczynski value of n = 7 at temperatures below 1050°C, whereas the value of n = 5 was obtained above 1250°C.

This fact was interpreted as a change in sintering mechanism from surface to volume diffusion at high temperatures as suggested by other authors[24].

Other possible mechanisms of sintering for which rate exponents have been calculated are Evaporation/Condensation[11], Viscous Flow and Plastic Flow[6]. However, support for these mechanisms is not widespread, owing to a lack of experimental evidence, except in certain specialised systems involving materials of high vapour pressure, or viscous solids. Thus, sintering by Evaporation/Condensation has been reported in Zinc Oxide at 1050°C[28] whilst flow has been identified by the movement of inert markers in glass and organic materials (e.g. Cellulose Acetate)[29]. Mackenzie and Shuttleworth[30] and Clark and White[31] have proposed theories of sintering based on plastic flow, motivated by surface tension, and obtained semi-empirical equations which agreed well with experimental shrinkage curves. However, considerable doubt exists as to whether the yield point for plastic flow is exceeded in most systems by the action of surface tension alone[1].

It is possible to reconcile the diffusion and plastic flow theories to some extent if one considers the transport mechanism to be a form of Herring-Nabarro Diffusion Creep, in which creep occurs by movement of vacancies from grain-boundaries under a tensile stress, to those under a compressive stress and is operative at high temperatures and under low stresses. Diffusion Creep has been suggested by Pines[32] and by Lenel and Ansell[33], the latter obtaining a shrinkage rate directly proportional to the stress. The stress concerned may be either an externally applied one or one generated in the neck due to surface forces. As this stress is increased during

sintering, so the shrinkage rate dependence on stress alters, becoming proportional to stress raised to some power which varies with mechanism. This change of stress exponent from unity to higher orders, is the demarcation point between pressureless sintering, where stresses occur in the necks of copper powders ($< 150\mu$m) of up to approximately 1 kg./cm.^{2}, (98.1 kN/m.^{2}) and hot pressing where higher externally applied loads are used. This value is considerably less than the stress in the necks of the particles calculated according to equation (1) given by other authors[11] and quoted as 4000 psi (27.6 mN/m^2) for 40μm copper powder. The differences are presumably due to particle size effects, and as pointed out by Johnson[125], the stress in the neck increases as particle size decreases, possibly exceeding the yield point in very small sizes. However, this contribution of plastic flow to sintering would decrease rapidly since the stress decreases as neck growth occurs.

2.3 The Importance of Grain Boundaries and Models of Last Stage Sintering

Mackenzie and Shuttleworth[30] argued that sintering could not occur by diffusion, because the observed rates were too great to be accounted for by the diffusion of vacancies to the free surface, which acted as the vacancy sink. However, Nabarro[34] and Herring[35] have shown that vacancies formed at pore surfaces can be discharged at grain boundaries adjacent to the pore, as well as at free surfaces. In this way, the need for large vacancy diffusion distances was obviated and experimental sintering rates were explained in terms of volume diffusion, with grain boundaries as the vacancy sinks.

Mackenzie and Shuttleworth[30] further proposed a shrinkage mechanism based on plastic flow, with surface tension as the motivating force. However this theory has been discounted[1] on the

grounds that the yield point of the material will not normally be exceeded, during sintering, by the action of surface tension alone.

The importance of grain boundaries as vacancy sinks during the densification stage of sintering was first emphasised by Alexander and Baluffi[36]. They studied the progress of shrinkage of tubular voids within a spool of copper wire, and noted that shrinkage occurred only so long as the voids were connected by grain boundaries. As soon as discontinuous grain growth occurred, many pores became isolated within grains, and virtually ceased to shrink. Kuczynski[37] examined the problem of shrinkage of cylindrical pores on a volume diffusion basis, postulating the grain boundary intersecting the pore, as the sink for vacancies. He arrived at the following equation for pore shrinkage.

$$r^3 = r_o^3 - \frac{3\gamma VD}{RT} t \quad \ldots\ldots(7)$$

r_o = original pore radius
r = radius at time 't'
D = coefficient of self diffusion of material
V = Atomic Volume
γ = Surface Tension
R = Gas Constant/mole
T = Absolute Temp
t = time from start of sintering

This relationship was verified experimentally by Kuczynski and Ichinose[38] working on tubular voids, obtained from twisting together three copper wires. In the same paper, an explanation was offered of the so called "Sauerwald temperature", which is the "temperature at which exaggerated grain growth occurs with sintering times of a

few hours". Kuczynski explained this in terms of the inhibiting action of pores on grain growth, using the well known Zener relationship[31]

$$\delta = {}^{4}/_{3}\,\frac{r}{f} \quad \ldots\ldots\ldots (8)$$

δ = Maximum limiting grain radius of curvature when restraining effect of pores exactly balances driving force for grain growth.

r = radius of inclusion or pore

f = volume fraction of inclusions

Thus, during sintering, 'r' and f alter continually, until the limiting grain size, given by δ , is larger than the actual grain size of the compact. When this occurs, rapid grain growth ensues, at this "Sauerwald" temperature.

The kinetics of grain growth in porous compacts have been studied by several authors[40, 41] and the relationship

$$d^3 - do^3 = K^1(T)t \quad \ldots\ldots\ldots (9)$$

do = initial grain size

d = grain size at time t

$K^1(T)$ = Constant which varies with Temperature

t = time of sintering

has been obtained both empirically and theoretically.

Further studies on the closure of isolated pores during sintering were carried out by J. Brett and L. Seigle[29]. They worked with copper and nickel wires containing dispersions of fine alumina powder and concluded that sintering in the nickel wire occurred by a diffusional process rather than a viscous flow mechanism, since in the latter case, movement of the alumina particles into the neck would have been observed, and this was not evident. However, in the

case of the copper/alumina wires, marked inhibition of sintering was noted and the central pore failed to disappear after very long sintering times, suggesting that the presence of the alumina markers interfered with the sintering process.

2.4 The Sintering of Metal Powders.

The use of model experiments provide valuable information on the initial and final stages of sintering, but the densification stage is largely absent from these models, and it is this stage which characterises the sintering of real powders.

Studies of the densification stage in real powders utilise the method of measuring the dimensions, or density of powder compacts as a function of sintering time. Often, the density or dimensions are better represented by standardised values, having maximum values of unity or infinity[1].

e.g. $\frac{Vo - Vs}{Vo - Vth}$ or $\frac{Ds - Do}{Dth - Do}$ where Do/Vo = pressed or "green" (density / volume) of compact

Ds/Vs = sintered (density / volume)

Dth/Vth = theoretical (density / volume) of bulk metal

The curves obtained from such experiments have been fitted to an equation of the form

$$D = kt^n \quad \ldots\ldots (10)$$

D = Density or standardised parameter

t = time

k and n are constants, n being called the rate exponent.

Physical significance has been attached to the values of 'n' determined from log/log plots of sintering data, in that values of 'n' (the slope of the log/log plot) between 0.4 and 0.5 were considered indicative of a lattice diffusion mechanism, whereas lesser slopes ($\simeq$0.3) were taken to indicate grain boundary or surface diffusion. The justification for these assumptions came from work by Kuczynski and Ichinose[42], who derived equations for the rate of shrinkage i.e. approach of centres, of the spheres used in their model experiments. However, as pointed out by Thummler and Thomma[1], these models account for only a few percent of the actual shrinkage that takes place in the sintering of a powder, and no account is taken in the model experiment, of the very important influence of grain boundaries on the process[36]. Thus the value of n = 0.4 can only be taken to represent lattice diffusion if it is obtained in experiments involving the very early stages of sintering. Larger amounts of shrinkage leading to values of 'n' of this order must be regarded as accidental[1].

Many workers in this field have attempted to compute activation energies for the sintering process from a study of the kinetics involved. The rate of sintering is assumed to follow the Arrhenius law

$$\text{Rate} = Ae^{-Q/RT} \quad \ldots\ldots (11)$$

T = Temp in ^{o}Abs

A = constant

R = Gas constant in cals/mole ^{o}K

Q = Activation energy Cals/mole

According to Jordan and Duwez[43], the rate may be computed from the time to achieve a constant densification, and the logarithm of this quantity, plotted against the reciprocal of Absolute temperature,

enables the activation energy to be determined from the slope of the graph. The values obtained from such a calculation can then be compared to the energies determined for pure volume, grain boundary or surface diffusion mechanisms, obtained from radio-active tracer measurements and other techniques. Tables 2 and 3 respectively, show activation energies and Diffusion coefficients for volume, grain boundary and surface diffusion in Iron, and also activation energies determined from sintering data for a range of Iron powders.

Many attempts have been made to summarise shrinkage data in the form of a general equation, and the form

$$\frac{\Delta l}{l_o} = (At \exp(-\frac{Q}{RT}))^n \quad \ldots\ldots (12)$$

$\frac{\Delta l}{l_o}$ = Fractional decrease in length

t = time

T = Temperature K

R = Gas Constant

A, Q, n - constants

has been widely used, since activation energies and values of the exponent 'n' can be determined, as mentioned previously. The fact that these calculated values, often are time and temperature dependent, throws the form of the equation open to doubt[1].

Sintering data can also be treated as a third order chemical reaction as in the case of Vanadium Carbide[70] which yielded an equation of the form

$$kt = \tfrac{1}{2}(1/p^2 - 1/p_o^2) \quad \ldots\ldots\ldots (13)$$

p_o = Initial Porosity in compact

p = Porosity after sintering for time t

k = constant

However, this approach does not appear to have been tested on the

sintering of metals.

One of the most successful equations is that due to Coble[71] who predicts a linear change in densification rate when plotted against log time. In its modified form[1] this equation is represented as

$$dp/dt = \frac{-KD_v \gamma V_o}{d^3 RT} \quad \ldots\ldots(14)$$

dp/dt = Rate of change of porosity with time

K = constant taking into account geometrical factors

D_v = Bulk Diffusion Coefficient

γ = Surface Energy

V_o = Volume of unit cell

d = grain size at sintering time t

R = gas constant

If the grain growth law, mentioned previously[40, 41] (Eqt^n 9 p.22) is combined with this equation, then the logarithmic form results e.g.

$$p = p_o - \frac{K''D_v \gamma V_o}{RT} \ln t/t_o \quad \ldots\ldots (15)$$

K'' = constant

p_o = Initial porosity at time t_o

p = porosity after sintering for time t

t_o = starting time for sintering.

This law has been confirmed experimentally by Coble himself, on alumina, with and without magnesia additions to control grain growth. The equations have been shown to represent the sintering data for iron of eight micron particle size[72] and for very fine

(2 - 5μm) cobalt and nickel powders[73].

Logarithmic shrinkage laws have also been obtained on a number of metal oxides[74 - 79], as well as on molybdenum[80] (particle size 2 - 6μm), and tungsten[81] (particle size 0.45 → 0.88μm). The mechanism of sintering proposed in the Coble model is one of pore elimination by the lattice diffusion of vacancies from the pore to the grain boundaries, where annihilation occurs. Thus the logarithmic law would seem to predict volume diffusion mechanisms for a wide range of fine powders.

The influence of grain growth on porosity in sintered carbonyl iron has been studied by Frydrych[123], who strain annealed this powder to induce grain growth and porosities in the range 9.7 → 10.3%. Subsequent sintering in hydrogen at temperatures in the range 700 - 890°C, gave rise to two activation energies viz 194 kJ/mole for fine grained iron and 335 kJ/mol. for coarse grained iron. He concluded that the shrinkage process can be arrested by controlling the grain growth.

2.5 Other Factors affecting the Sintering Process

Many other factors can be shown to influence the sintering process, and the principal ones are

(a) Effect of Green Density

(b) Effect of Oxide films on metal surface

(c) Effect of sintering atmosphere

(d) Effect of Phase Change.

2.5.1. (a) Effect of Green Density on Sintering -

The effects to be considered[1] are

(i) increasing contact area between particles with increasing green density

(ii) introduction of elastic or plastic deformation between particles

(iii) damage to surface layers such as oxides, and

(iv) entrapment of air and gas at high green densities.

The first two points (viz (i) and (ii) above) have received little attention in the literature, the main source of effort being directed to changes in pore structure during compaction[82] and the effect of green density on sintering rate[83]. The former work on changes in pore structure during compaction is outside the scope of this review, whilst in the latter case it was reported that sintering rate was greatest at low green densities when measured at the same time interval from the start, although the sintered densities attained were always less in the case of compacts pressed initially to low values of green density.

Cold welding at the interface between particles has been investigated by Nicholas[84], who showed that the oxide films are cracked by relative motion against each other rather than by the compacting pressure. Gas pressure effects are noted at high green densities, when gas inclusion in the pores can result in expansion rather than shrinkage. In this context, Pines, Sirenko and Sukhinin[85] observed growth in Copper compacts when the initial porosity was less than 14%. The effect increases with finer powders.

2.5.2. (b) Effect of oxide films on the metal surface

Oxide films on the surface of the metal drastically modify sintering behaviour. For rapid sintering to high temperatures, reduction of the oxide should be as complete as possible before shrinkage commences, in order to avoid isolation of the oxide film from the reducing atmosphere. Ramakrishnan etal have shown that the

sintered density of a number of metals, processed according to a standard cycle increased with thickness of initial oxide film, up to a maximum thickness (625A° for iron) and then decreased. The effect was attributed to the extra surface activity of the clean metal, when the oxide film is reduced. Other effects of such films are reviewed by Russell[88].

2.5.3. (c) Effect of sintering atmosphere.

The effect of atmosphere on sintering has been studied by several authors. Rhines[89] reports that a rapidly diffusing gas such as hydrogen has little effect on rate of change of pore size during sintering of copper powders, but a less mobile gas e.g. argon, can markedly affect the process. Also on copper, Calow and Tottle[90] report that the temperature of maximum shrinkage rate is approximately 300°C higher in argon than in hydrogen atmospheres. Fischmeister and Zahn[24] have shown a marked dependence of sintering kinetics on dewpoint for electrolytic iron bars sintered in hydrogen. The activation energies also changed from

$$191\,KJ/mole \rightarrow 224\,KJ/mole \rightarrow 306\,KJ/mole$$

$$45.5 \rightarrow 53.5 \rightarrow 73.0\ kcal/mole$$

for dewpoint changes from $-60^{\circ}C \rightarrow 0 \rightarrow +70^{\circ}C$, and they cite this as evidence for a surface diffusion mechanism of sintering.

2.5.4. (d) Effect of Phase Change.

The principal effects of phase change on sintering are associated with the volume changes which occur, and the change in diffusion rates, accompanying the change in crystal structure[1]. Detailed investigation of these points have been undertaken with particular reference to iron. Thus Gjostein[128] compared both surface and volume diffusion coefficients for α and γ iron, at a temperature of

910°C and found that

$$\frac{Ds^{\alpha}}{Ds^{\gamma}} = 8 \qquad \frac{Dlattice^{\alpha}}{Dlattice^{\gamma}} = 200.$$

Cizeron etal[45-47], working on iron powders have shown a greater rate of shrinkage on sintering in the α phase than in the γ phase. The α/γ transformation resulted in a large increase in grain size, thus entrapping pores within the grains and leading to a lowering of density. They obtained an activation energy for sintering in the α phase of 167.4 KJ/mole (40 k cal/gm atom) which they attributed to grain boundary diffusion, and 293 KJ/mole (70 k cal/gm atom) for γ phase sintering, which is close to the value for volume self diffusion obtained by tracer techniques (see table 2).

Poster and Hausner[86] report that lower densities are attained by sintering in the γ range than in the α range which they associate with the larger grains formed just after transformation, resulting in a decreased contribution of the grain boundaries to sintering. This is in general agreement with the increase in grain size observed by Cizeron[45-47] above. However, considerable grain size variations occur on heating to higher temperatures since Poster and Hausner[86] report a decreasing grain size on sintering at temperatures up to 2000°F (1093°C). Singh and Houseman[129] extend this temperature to 1400°C, noting that grain size decreases markedly between 1350 and 1400°C, but above 1400°C, abnormal grain growth seems to occur resulting in a lowering of densification and isolation of pores within grains.

2.6 Production and Properties of Ultra-fine Powders.

Interest in ultra-fine powders stems from their applications in fine particle magnets[91], aerospace applications[92, 93] and for

high temperature dispersion hardened alloys[94].

Fine powders have been of considerable interest in the magnetic field for many years, since they are capable of being compacted to form magnets of high remanence and coercivity, resulting in a high BH max value compared to other magnet materials. The main drawback to their use is associated with their inherent pyrophoricity arising from the fine particle size. The interest of the aerospace industries stems from the possible use of these materials as magnetic materials and as high strength, temperature resistant alloys. Attempts to overcome the pyrophoricity problem in this field, involve a combined reduction and sintering operation performed on iron oxides mixed with suitable disperse oxide phases[93]. A more recent attempt[117], giving powders stable up to 140 - 180°C, has been to coat the particles with a thin plastic film by a method of surface polymerisation. Such powder shows promise of application in the fields of permanent magnets and magnetic recording apparatus. Many other methods of manufacture of such powders have been reported in the literature. Vacuum evaporation[95] of powders has been tried successfully in the United States of America and a wide range of powders produced for use in dispersion hardened materials. Production of fine powders from plasma jets have been reported by several authors[96, 118, 119], producing both metal and ceramic powders in this way. The conventional method of ball milling has been tried by other workers. Quatinatz Schaeffer and Smeal[97] report that powders of five different metals (Cu, Cr, Te, Ag and Ni) were obtained in sizes less than 1.0μm, by grinding in alchohol using certain inorganic salts as grinding aids. A new type of micro-rolling mill has also been reported[98] as being capable of producing flake powders substantially in the sub-micron

range.

The preparation of fine iron powders for use in magnetic materials has been based mainly on the decomposition and low temperature reduction of ferrous oxalate, formate[99], or one of the oxides of iron[48, 91]. The subsequent pyrophoric powders made in this way were handled under benzene, and were pressed and sintered whilst still wet with benzene. Very little published information is available on the properties of these materials other than magnetic ones. However Cizeron, Hui and Breugnot[48], have prepared submicron iron powders by reduction of precipitated iron oxide, and have studied their sintering behaviour using a dilatometric method. They showed considerable shrinkage on sintering at temperatures of the order of 300°C for powders of specific surface area $8m^2/gm$ (prepared by reduction of oxide of specific surface $175m^2/gm$, at temperatures in the range 300 - 700°C). They noted that shrinkage stopped as soon as the specimen attained the furnace temperature under isothermal sintering conditions. Activation energies for sintering were in the range 58.5 → 83.5 kJ/mol. (14 → 20 k cals/mole) which is too low to correspond to any of the known diffusion processes. The authors consider that plastic flow is a possible mechanism. The conditions of preparation of the powders were also shown to be important in this paper. Thus both the temperature of reduction of the oxide, and the pressure of hydrogen used in the reduction, influence the subsequent sintering characteristics of the iron powder. In the first case, as the temperature of reduction is raised, the specific surface area of the powders decreases and the amount of shrinkage on subsequent sintering of the iron powder decreases. In the second case, powders prepared under reduced

pressures of hydrogen, or given a heating treatment in vacuo, prior to sintering showed greater shrinkage than those prepared under pressures of hydrogen close to atmospheric pressure. However the start of shrinkage was delayed compared to the powders prepared under high pressures of hydrogen. The effect was more pronounced during continuous sintering to 900°C, than during isothermal sintering, and this effect was interpreted by the authors in terms of a more rapid and greater desorption of hydrogen on continuous heating compared to that occurring under isothermal conditions.

Carmen[91] has also studied the preparation of iron powder, starting with fine iron oxides, and his results show similar trends to those of Cizeron etal[48], in that particle size increased with increasing reduction temperature from approximately 250 Å at 250°C to 500 Å at 350°C. Particle size was measured by electron microscopy and by examining back reflection X ray photographs using a micro-photometer. This latter method is usually accepted as being a measure of crystallite, rather than particle size. If this is the case, then the authors results of 110 Å for precipitated iron oxide, 180 Å for iron produced from this powder by reduction at 280°C, (both results obtained by measurement of electron micrographs) and the X ray value of 250 Å for the same powder, throw some doubt on the conclusion that the iron particles are separate crystallites. Presumably the high value obtained in the X ray work could be due to lattice strain, which does not seem to have been accounted for in the method used to determine particle size.

Franklin, Campbell and Weinman[130] have considered the problems of measuring particle size, by employing electron microscopy, X ray

line broadening and surface area measurements to measure the size of a number of fine iron powders. Their results showed good agreement between X ray and electron microscopy measurements, but surface area measurements were usually greater than either of the previous methods. The suggested reason for this was that the particles were coated with oxide, which is taken into account in surface area measurements, but not in the other techniques, being presumed transparent to the electron beam and not counted in the X ray method since line broadening was measured on the (110) line of iron only. The authors point out that this latter technique necessarily omits any consideration of line broadening due to strain, so the good agreement with electron microscopy results may be fortuitous. One of the powders studied in this work was of the carbonyl type, which gave very broad X ray lines, indicating a crystallite diameter of 80 Å, compared to the particle size measured by electron microscopy of 2 μm. Heating for two hours at 450°C considerably sharpened the lines, suggesting the relief of stresses and/or the growth of crystallites. These effects are well known with carbonyl iron and are referred to in the manufacturers information on the MCHP grade carbonyl iron used in the current work. Thus the spherical carbonyl particle consists of an onion skin type of structure composed of layers of fine crystallites which can be made to grow considerably by annealing.

The activity of iron oxides prepared by precipitation from solution and calcined at various temperatures, has been studied by both Gregg and Hill[131], and Pryor and Evans[132]. The former authors[131] showed a continuous decrease in specific surface area as calcination temperature is increased. This is in marked contrast

to the behaviour shown by other oxides, such as alumina and magnesia which show a peak in the surface area/calcination temperature curve. X ray evidence suggests that the reason for this is connected with a lattice change in both magnesia and alumina, whereas for the iron oxide, very broad, diffuse lines occur prior to heating which sharpen and increase in number on heating. All the lines however, correspond to α -Fe_2O_3. These results are largely supported by the work of Pryor and Evans[132] who showed a continuous decrease in the rate of dissolution of the iron oxide powder in acid, as the calcination temperature increases. However in this work, the X ray evidence suggests that the "amorphous" structure of the oxide, occurring at room temperature only in the previous work, persists up to 300°C, at which temperature the loss of combined or hydrated water commences.

The thermal decomposition of oxalates has been studied by Dollimore and his associates[120, 121] who showed that decomposition occurred initially by dehydration, followed by conversion to oxide, with a maximum in a plot of surface area against temperature occurring after the latter process. Iron oxalates also show a second maximum which is attributed to a change from an amorphous to a crystalline form of ferric oxide. Atmosphere effects were also noted, oxalates of Cr, Mn, Fe and Zn producing oxides after decomposition in both air and nitrogen, whereas Co, Ni, and Cu oxalates decomposed to oxides in air but to the metal under nitrogen. These results have been related by the authors to the stability of the oxides using free energy diagrams of the Ellingham type.

Several authors[99, 122] have studied the iron powders produced from ferrous formate by decomposition and reduction routes. Thus Franklin and Campbell[99], prepared hydrated ferrous formate below 150°C,

and then thermally decomposed it at temperatures from 220°C to 255°C in vacuo. X ray diffraction patterns of the resulting oxide, seemed to give a spinel structure and was thought to consist of an intimate mixture of Fe_3O_4 and metallic iron. The distribution and particle size of the iron was such that the iron lines were barely observable in the pattern. The resulting oxides were subsequently reduced at temperatures from 125°C to 450°C using Calcium Hydride (CaH_2) under a low pressure of hydrogen. Particle and crystallite sizes were measured by electron microscopy and X ray line broadening respectively, both methods showing reasonable agreement, particularly for the iron powders, although some of the oxides were poly-crystalline. The principal conclusion of the work was that each oxide crystallite produced one single crystal iron particle, a fact which was supported by the correspondence between observed crystallite and particle sizes, and values calculated on the assumption that one crystallite of oxide produced one particle of iron. It should be noted however that the X ray method employed is subject to the same limitations as those discussed previously for the work of Franklin, Campbell and Weinman[130]. (See page 33).

A final mention should be made of the work of Amiel and Malard[122] who studied the reduction of ferrous formate to iron, utilising thermogravimetry, differential thermal analysis and X-rays, to follow the process. The former two techniques revealed three stages in the decomposition, under different hydrogen flow rates, viz the formation of an anhydrous formate between 120° and 150°C, the formation of an oxide near 310°C, and finally iron forms near 580°C. The hydrogen flow rate plays an important part in the reduction, particularly on the form of the oxide occurring near

310°C. Thus at low flow rates, X ray examination of the products, revealed the presence of FeO, a divalent oxide having a spinel structure and traces of iron. At high flow rates only FeO and Iron are found. The spinel type oxide has been observed by other authors[133] and termed ɣ FeO. Iron powders were also prepared by isothermal heating at temperatures of 280° and 350°C, under different hydrogen flow rates, and measurements of line broadening, crystallite size and lattice parameter made on the powders after storing under benzene at room temperature. All these properties show marked changes at flow rates in the vicinity of 19 - 26 l/h/g, which the authors explain the terms of a change in oxygen content of the powders from 3.5 → 5.5%, to less than 0.05%. It should also be noted that the powders generally contained carbon contents from 0.15 up to 0.3%.

3. EXPERIMENTAL PROCEDURE

3.1. Materials Used and Methods of Preparation

Three main types of iron powder were used in this work:- (i) Carbonyl Iron. (ii) Powder obtained by the reduction of high purity iron oxide. (iii) Powder obtained from decomposition and reduction of Oxalates. Analyses of these powders and the raw materials for their preparation are given in table 5.

(i) The Carnonyl iron used as a basis for comparison in this work was obtained from International Nickel (MOND) Ltd., Grade MCHP, having an average particle size (as determined by air permeability methods) of 7μm (where 1μm = 10^{-6}m). This material was chosen as a standard because of the large amount of published information on its sintering behaviour.

(ii) Powder obtained from fine oxide reduction:- high purity ferric oxide (99.999%) was obtained from Johnson Mathey Ltd. Thirty gram lots of this were reduced at a temperature of 300°C in dry Hydrogen for 16½ hours. The hydrogen was purified by passing through a DEOXO unit (a catalytic purifier obtained from the Baker Platinum Division of Engelhard Industries Ltd). to remove Oxygen and then dried by passing over activated Molecular Sieves (obtained from Union Carbide Ltd). The Molecular Sieves were activated by heating at 250 - 300°C for 2 hours, under a rough vacuum (approximately 10^{-3} torr).

On completion of reduction the iron powder was transferred in the reduction chamber to a glove box containing an Argon atmosphere. Here, the reduction cell was opened and the caked powder broken up to a free flowing powder using a mortar and pestle. This powder was stored in a glass jar fitted with a tight lid, inside the glove box, since it tended to ignite spontaneously if warmed slightly in

air. All the powders stored in this way showed no weight increases over long periods of time.

(iii) Powder obtained from decomposition and reduction of Ferrous Oxalate:- The Ferrous Oxalate used was obtained from British Drug Houses Ltd. and was standard Laboratory Reagent Grade since no chemical firm, to our knowledge, manufactured an "Analar" grade of this material. Decomposition of the oxalate to a very fine iron oxide was carried out by heating on an ordinary hot plate at 100° - 150°C as measured with a Mercury/Glass thermometer. During the decomposition the temperature rose rapidly to about 180 - 200°C (indicating a strongly exothermic reaction) as the powder changed in colour from bright yellow to a brownish-red colour. Completion of the decomposition was indicated by the thermometer registering a fall in temperature again and a uniform red/brown colouration of the powder. This oxide, which was extremely fine, was then reduced under the same conditions as the powder produced from the very high purity oxide above. Even greater care was necessary in the handling of this powder since it was quite strongly pyrophoric even in the presence of very small amounts of oxygen. Previous attempts at combining the decomposition and reduction stages either by heating at 300°C in dry hydrogen or by vacuum decomposition and subsequent reduction were unsuccessful due to the presence in the final product of up to 0.3% Carbon (confirmed by analysis). This carbon probably came from the original oxalate during decomposition since fine iron oxides are known to catalyse the cracking of carbon dioxide giving deposits of fine carbon (cf Blast Furnace practice where carbon is deposited in the stack at around 300 - 500°C).

3.2. Apparatus

3.2.1. Reduction Chambers

The reduction chamber itself consisted of a 3 inch wide neck, round bottom, Pyrex glass jar which was sealed at the top by a silicone rubber '0' ring clamped between a brass ring and plate. Through the brass plate, on the top of the jar, passed two $\frac{1}{4}$ inch i.d. copper tubes, silver soldered into position, one for gas inlet and the other for gas outlet purposes. Both tubes were closed off on the top of the apparatus by small vacuum and gas tight brass taps, which in turn were fitted with compression type joints using brass or copper olives, so that the whole reduction chamber could be connected and disconnected from the gas pipe line and reheating furnace, without allowing air to enter the chamber itself. The inlet pipe to the chamber was long enough to extend right down to the base of the glass jar and had a closed end with very fine ($\simeq \frac{1}{16}$") diameter holes drilled in it, in order to ensure good dispersion of the gas through the powder bed. Provision was also made for a stirrer to pass through the centre of the brass plate, by means of an '0' ring seal, but this was found to be unnecessary since the stirrer tended to push the powder away from the central gas inlet, decreasing the gas/powder contact area. The chamber was heated by means of an Electrothermal type mantle which surrounded the chamber and was controlled by a Sunvic energy regulator. Heat losses were further minimised by lagging the apparatus with a fibre glass cover and covering the top brass plate by a layer of hard asbestos sheet (Pierrite). In this way a uniform temperature was achieved in the apparatus to about one inch above the base of the vessel, which depth more than exceeded the depth of the powder bed. The gas

preheating furnace consisted of two copper tubes, one inch diameter and half inch diameter brazed one inside the other so that the centre and ends of the larger tube were blocked off. Gas inlet and outlet tubes, $\frac{1}{2}$ inch i.d. were braised into the one inch diameter tube and the outlet tube connected up to the tap on the top of the reduction chamber by means of the compression joint. Heating of this furnace was achieved by means of an Electrothermal tape wound round the outside of the one inch diameter tube and well lagged with asbestos string. The furnace control was again, by means of a Sunvic energy regulator, set to ensure a uniform temperature distribution in the atmosphere of the reduction chamber, as described above. Figure 2 shows a general view of the whole apparatus. On completion of a reduction run, the hydrogen was turned off and the taps on the top of the chamber closed. After cooling, the compression joints were unscrewed and the whole chamber transferred to the glove box for unloading.

3.2.2. Glove Boxes

Two glove boxes were used in the current work, one containing a ten ton press (Fig. 3) for compacting the powders and the other containing an electric balance (Fig. 4) for weighing out samples of powder. Both glove boxes were filled with high purity argon, (Dew Point - 120^{o}F) supplied from large gas cylinders, and were flushed through with this gas at weekly intervals, in order to maintain the atmosphere. Access to the boxes was by means of transfer ports which were fitted with inlet and outlet taps so that the port could be sucked out by a rotary vacuum pump and then filled with Argon through the inlet tap. In this way the pyrophoric powders could be handled without contact with the atmosphere.

3.2.3. Pressing and Sintering of the Powders

Pressing and sintering of the powders was carried out in the following manner. Two gram samples of the powders were weighed out in the glove box and placed in small containers with tight fitting lids. These containers were then transferred to the second glove box for pressing. A $\frac{3}{8}$" diameter "floating" die was used and the die walls were lubricated with stearic acid, applied from a solution of the stearic acid in alcohol. No lubricant was used in the actual powder. After pressing, the "green" compacts could be safely handled in air, no weight increase being observed during the period of transference to the furnace.

The sintering furnace used was of the tube type, heated by six "Crusilite" (silicon carbide) elements, and controlled by an on/off, anticipatory controller giving temperature control over the periods of time involved in this work, to within $\pm 3^{o}C$.

In order that the samples might be sintered in Hydrogen atmospheres and that they might be transferred directly to the hot zone of the furnace (in order to minimise heating up times), the arrangement shown in Figure 5 was utilised. Thus the end of the furnace tube was sealed using the large neoprene stopper shown in Figure 5 and the compacts for sintering kept in the cool end of the furnace, whilst an argon flow was used to flush out the tube for a period of five minutes. The argon flow was replaced by hydrogen and the compacts transferred to the hot zone utilising the molybdenum rod passing through the 'O' ring seal. At the end of the sintering period, the reverse procedure was adopted to remove the compact to the cold end of the tube, so that cooling occurred rapidly under a stream of argon. No visible signs of oxidation were noted on the

compacts treated in this way. The dimensions and weight of the compacts were recorded both before and after sintering, so that "green" and sintered densities could be calculated.

3.3. Techniques for Studying Particle Morphology and Size

3.3.1. Gas Sorption Analysis

Measurement of particle size was carried out using a technique proposed by Aylmore and Jepson[100]. This is basically a modification of the well known B.E.T. (Brunauer, Emmett and Teller) method of surface area measurement[101], which utilises krypton as the adsorping gas, at liquid nitrogen temperatures. The amount of krypton adsorped on the solid surface is estimated from the change in volumes of gas, before and after sorption. The krypton used was doped with a small amount of the isotope ^{85}Kr so that the change in count rate, before and after sorption, is proportional to the volume change. From a series of readings of amount of krypton sorbed, as a function of relative pressure

$$\left(\text{Relative pressure} = \frac{\text{pressure in system}}{\text{saturated vapour pressure at } -196^{\circ}C}\right),$$ the

monolayer capacity i.e. volume of gas sorbed to form a monolayer on the surface of the solid, can be determined. Knowing the area of one gas molecule, the total surface area of the solid can be estimated.

The use of this technique for the measurement of low surface areas has been reviewed by Sing and Swallow[102].

3.3.2. Electron Microscopy of the Powders

The morphology of the powders was studied using an electron microscope technique. The main problem with such a technique is to obtain a very small sample for examination in the microscope which is still representative of the powder mass. Owing to the

pyrophoric nature of some of the powders used in this work, sampling had to take place inside the glove box. The procedure adopted for sampling was to utilise a hollow tube as a probe into the powder mass. Several such probes were taken from various parts of the powder and placed into a smaller container. The process was then repeated on this container and subsequently on others of decreasing size until a sufficiently small quantity of powder was obtained for use in preparation of the electron microscope samples. This sample of powder was transferred to a solution of 1% Formvar in an air tight container, for removal from the glove box. In order to prepare an electron microscope film, small droplets of this solution were placed on a clean slide and drawn out into films using a glass rod. The film was then cut into sections small enough for mounting on an electron microscope grid, and these sections stripped from the slide and collected in the conventional manner. In order to make the examination more representative, several films were studied from varying positions on the slide (to obviate the possibility of segregation occurring during drawing out of the film) for each of the powders studied in this work. No rigorous particle size classification was attempted, the object of the examination being to give a qualitative appreciation of size and shape, and to augment information obtained from B.E.T. work.

3.4. Dilatometric Study of Phase Changes occurring in Sintered Powders.

In view of the unusual behaviour of some of the powders during sintering in the neighbourhood of 900°C, it was decided to try to determine the exact temperatures of the α/γ phase change on actual powder compacts, to see if such behaviour could be explained

rationally in terms of this phase change. One compact was selected from each powder, which had been sintered for periods of time at 900°C, longer than those likely to be encountered in the dilatometer run, so that the tendency for further densification during the run, would be minimized.

The dilatometer used was a conventional one, employing a silica tube and a silica pushrod, fitting neatly onto the top of the compact. Movement in the pushrod was monitored by a linear displacement transducer and displayed on a digital readout monitor capable of recording 0.001mm. Oxidation of the sample was minimised by restricting the throat of the furnace tube and flushing through with Argon gas so that a back pressure of Argon was maintained in the tube during the run. Temperature was measured on a Chromel/Alumel couple, in contact with the sample, using a Cambridge potentiometer, reading to 0.01mVs. The couple was calibrated, prior to use, against a standard Platinum-Platinum/13% Rhodium couple. The heating rate employed was approximately 300°C/hour, and arrests were recorded both on heating and cooling.

3.5. Measurement of Grain Size in the Sintered Compacts.

Prior to the measurement of grain size, initial metallographic difficulties were encountered in showing up all the grain boundaries satisfactorily. The procedure adopted to overcome this, was to etch the sample for increasing lengths of time, observing the sample after each etch, until definite signs of over etching were obtained. The sample was then re-polished and etched for a time just short of that corresponding to over etching. The method of measurement of grain size used is a variant of the standard lineal analysis technique, and is due to Hilliard[116]. This method uses a circle of known

diameter as the test figure, in place of the more usual line, since a circle automatically randomises the direction of measurement to allow for variations away from the equi-axed shape in grains. In this work, two circles of 6cm and 8cm diameter were accurately drawn on a piece of transparent acetate film, which would be positioned accurately on the screen of a Vickers projection microscope. The magnification of the microscope on the screen was calibrated initially using a stage micrometer and accurately measuring the resultant image on the screen. To measure grain size, the circles were placed on the screen, and the number of boundaries intersecting the circumference were counted. In this method of counting, grain boundaries intersecting parallel to the circumference were counted in the same way as boundaries actually cutting it, and grain boundary triple junctions were counted as one and a half counts. In general, the pore phase interfered in only the finer grain sizes measured in this work, and for these fine grains, the boundary was considered to run down the middle of the pore (since most of the pores were situated at the boundaries). This would give rise to a small error in the size of the smaller grains, erring on too large a value for grain size, but it does not interfere with the general trends noted in the work, the more so since errors also arose from the fact that in some cases grain boundaries, obviously pinned by pores curved back on themselves, two or three times. In general, over one hundred grains were measured on each sample, spread over six or seven independent fields of view, to ensure accuracy of measurement.

4. RESULTS

4.1. Morphology of the Powders.

The results of B.E.T. analysis on the powders are summarised in Table 6, whilst Figures 6 - 10, show the respective adsorption isotherms, and the B.E.T. plots derived from them. These B.E.T. plots are obtained from the equation

$$\frac{x_J}{\Delta V_J\,(1-x_J)} = \frac{1}{VmC} + \frac{(C-1)}{VmC}\,x_J$$

due originally to Brunauer, Emmett and Teller[101], by plotting $\frac{x_J}{\Delta V_J(1-x_J)}$ against x_J, where the terms in this equation have the following meanings

x_J = equilibrium relative pressure

ΔV_J = Volume of gas sorbed at relative pressure x_J.

Vm = Monolayer capacity of gas, i.e. volume of gas required to form a monolayer on the powder surface.

C = Constant, related to the net heat of absorption on the surface.

From the resulting plot, the monolayer capacity Vm is calculated since Vm = (Slope + Intercept)$^{-1}$. This value can then be used to calculate the surface area of the powder, according to

$S = \frac{Vm}{V}$ N. Am. where V = volume of 1 mole of krypton at NTP

N = Avogadro's number

Am = Area of adsorbed krypton molecule $(19.5\ \text{Å})^2$ in this work[100].

The "point B" method for determining surface area, relies on the estimation of the start of the linear region of the $\frac{\Delta V_J}{x_J}$ isotherm,

the corresponding volume being a measure of the monolayer capacity[102]. The values used to plot the curves are given in Tables 7 - 11.

Electron micrographs of the oxide powders used in this work are shown in Figures 11 - 14, whereas the corresponding iron powders obtained by reduction are shown in Figures 15 - 18. A typical electron micrograph of carbonyl iron powder is shown in Figure 19. Figure 20 shows a selected area diffraction pattern obtained from the particle of iron oxide, ex ferrous oxalate shown in Figure 14. Good agreement with the (110), (202) (204) (214) and(220) rings for α-Iron oxide was obtained on indexing and comparing with the ASTM powder data file (Card reference number 60502). The spots appear to show evidence of a preferred orientation.

4.2. Results of Powder Sintering Experiments.

4.2.1. Density/Time Plots.

Densification curves for the powders after pressing at 15 t.s.i, (231 MN/m^2), and sintering for periods of time at 600, 700, 800, and 900°C, are presented in Figures 21 - 23, whereas the corresponding values of density after pressing at 50 t.s.i. (770 MN/m^2) and sintering, are shown in Figures 24 - 26. The data plotted in these figures is shown in Tables 12 - 14.

4.2.2. Semi Logarithmic Plots of Sintering Data

Figures 27 - 32 show sintering data plotted in the form of Porosity/log time plots, in order to test the results obtained in this work against the sintering model due to Coble[71]. (See Equation 15). The relevant data for these plots is given in Tables 12 - 14. For the purpose of these plots, densification is expressed in terms of fractional porosity, where

Fractional Porosity $P = \frac{Pt - Ps}{Ps}$ where Pt = Theoretical Density (7.87 gm/cc for Iron)

Ps = Sintered Density.

4.2.3. Activation Energies for Sintering

Table 2 shows values of activation energies calculated by other workers for diffusion in bulk samples, whereas Table 3 gives typical values obtained from sintering experiments on metal powders. For the purposes of comparison activation energies calculated in this work are shown in Table 4. These latter activation energies were calculated from the following equation

$\frac{1}{t} = Ae^{\frac{-Q}{RT}}$ where t = time to achieve a standard density

(6.0 → 6.2 gm/cc at 15 t.s.i.)
(7.15 → 7.2 gm/cc at 50 t.s.i.)

Q = Activation energy

R = Gas Constant = 8.31J/K mol.

T = Absolute Temperature ^{o}K.

A = Constant.

4.3 Determination of the α / γ Phase Change Temperature in the Powders.

A dilatometric method was used to determine the start and finish of the α/γ phase transformation in iron powders, and the results obtained on heating and cooling are shown in Table 15. From these results it will be noted that two of the powders, viz the carbonyl iron and the iron powder, ex ferrous oxalate had started to undergo the α/γ transformation on sintering at 900^{o}C. In the latter case, the start of transformation on heating and the finish on cooling, were uncertain due to a very gradual tailing off of the transformation volume change, rather than an abrupt one, as in the case of the

other powders.

4.4 Results of Grain Size Measurements on the Sintered Powders.

Grain size measurements were made on the powders using the method due to Hilliard[116], which is a modification of the basic lineal analysis method, utilising a circle as the reference figure. This figure has the advantage that it automatically randomises the direction of measurement. The average lineal intercept $\bar{L}$ is calculated from

$$\bar{L} = \frac{nP}{MN}$$ where nP = Total Perimeter of circle after 'n' measurements.

M = Magnification

N = Total number of intersections after 'n' application of the circle.

In some cases, as for iron powder ex ferrous oxalate, after sintering at 600 and 700°C, it proved impossible to etch up a suitable grain boundary structure due principally to the fineness of the grain and metallographic difficulties associated with the fine pore structure. In these cases no values can be quoted for grain size. Typical results of average lineal intercept plotted against sintering time are shown in Figures 33 - 35, and actual measurements are listed in Tables 16 - 18. Typical micrographs of some of the sintered compacts are shown in Figures 36 - 42.

5. DISCUSSION

5.1. Morphology of the powders

5.1.1. Measurement of Surface Area.

The results of B.E.T. measurements (see Table 6) show considerable differences in the surface areas of the oxides, prior to reduction to the metal. The major difference occurs in the comparatively large surface area of the oxide produced from ferrous oxalate, and this difference is supported by measurements of the apparent densities of the two powders, viz J.M. oxide 0.74g/cc, oxide ex oxalate, 0.48g/cc.

Figures 6 - 10 show the corresponding Isotherms and B.E.T. plots for the oxides, and values of the B.E.T. constant 'C' for these isotherms are respectively, 125 for the Johnson Mathey oxide, and 143 for the oxide ex oxalate. These values are important, since the higher the value of 'C', the sharper will be the knee of the isotherm and the closer the agreement between the B.E.T. and point 'B' surface areas (this latter, corresponding to the point at which the isotherm deviates from a straight line, the associated volume providing a direct measure of Vm, the monolayer capacity) as discussed by Sing and Swallow[102]. The values of 'C' above are high enough to give good agreement between the two surface areas, since C = 50 has been quoted[102] as being the value below which the knee becomes particularly indistinct. However in the case of the oxide produced from ferrous oxalate, the point 'B' method could not be applied since insufficient points were obtained on the isotherm to show clearly the departure from linearity.

In the examination of the B.E.T. isotherms of the metal powders, two features are outstanding, viz

(i) the large decrease in the surface area of the oxide

ex ferrous oxalate when reduced to the metal and

(ii) the negative intercept obtained on the B.E.T. plot of the data from the iron powder ex Johnson Mathey oxide.

The former i.e. (i) above, is undoubtedly associated with sintering of the powders during reduction, and further evidence supporting this will be discussed in the section on electron microscopy of the powders. The negative intercept obtained in the case of the iron powder from Johnson Mathey oxide is seemingly inexplicable, but similar effects have been reported by other workers[102]. The low surface area obtained on the carbonyl iron powder is in good accord with the size ranges published in the manufacturers advertising literature. Values of 'C' obtained on the metal isotherms are generally low, and this fact in the case of carbonyl iron, no doubt occounts for the large difference in the two calculated surface areas.

5.1.2. Electron Microscopy of the Powders

Electron micrographs of the individual powders support the information obtained from the B.E.T. work. In particular, photographs of the oxides (Figures 11 - 14) show marked differences. The Johnson Mathey oxide appears to consist of small isolated particles, whose density in the electron beam is roughly equal over each particle, which suggests a uniform plate-like shape. In comparison the oxide, ex oxalate, has a much less uniform shape, and the electron density is variable over the surface of each particle. This suggests that each "particle" of the oxide ex oxalate, is in fact an agglomerate of smaller particles. This fact alone is supported by the high surface areas found in the B.E.T. work, but a diffraction pattern is

shown in Figure 20, which was obtained from the particles shown in Figure 14, and this provides further evidence. The indexed rings obtained on this pattern agree well with those for α Iron oxide published in the A.S.T.M. index. The ring pattern shows a preferred orientation, and a number of fine isolated spots are evident in the pattern. Thus, the most likely interpretation of this pattern was that the preferred orientation arose from sub grains present within the larger particle, and the individual spots were due to a number of finer particles sticking to the larger one.

The metal powders corresponding to the above two oxides show very little difference to each other either in size or density to the electron beam (Figures 15 - 18). This again agrees well with the B.E.T. results. The major fact to be noted is the large amount of sintering which has occurred during the reduction of the oxide ex oxalate at 300°C to give such a large shape change and drop in surface area. The apparent minor increase in surface area of the Johnson Mathey iron oxide on reduction is not evident from the electron micrographs, and may possibly be due to slight shattering of the particles during reduction from oxide to metal. The carbonyl iron powder (Figure 19) shows the spherical shape normally associated with this powder.

5.2. Sintering Behaviour of the Powders

5.2.1. Effect of Time and Temperature on sintering behaviour

Examination of figures 21 - 26 allows the following general conclusions to be drawn from the curves. For powders pressed at 15 t.s.i. (231 MN/m^2), the general density level attained on sintering at 600, 700, and 800°C is less, in the case of carbonyl iron powder and powder produced from high purity oxide, than in the case of

powder ex ferrous oxalate. Also in these two former powders, a much greater decrease in density occurs on sintering at 900°C, than in the case of the powder ex ferrous oxalate, and the scatter of experimental points around the plots increases markedly at this temperature. Such density decreases on sintering close to the $\alpha - \gamma$ phase change have been observed by other workers[47, 86].

Another feature of the curves presented here is the apparent cessation of densification in the powder ex ferrous oxalate at 700, 800, and 900°C after rapid initial sintering for times of approximately two hours.

At the higher pressing pressure used (i.e. 50 t.s.i. or 770 MN/m^2), the general effects found at 15 t.s.i. (231 MN/m^2) with respect to decrease in density on sintering at 900°C, and greater experimental scatter of points at this temperature, still apply. However, the general level of density attained in the powder ex ferrous oxalate, is now slightly less than that achieved in the other two powders, particular in the 700 - 800°C temperature range.

Striking differences are apparent in the green densities attained in the compacts after pressing. At both the pressures used, the iron powder ex ferrous oxalate, exhibited a much lower green density than either of the other two powders. This is an apparent contradiction of information gathered on the morphology of the powders, since one would expect similar packing characteristics from powders of similar size and shape. From the data of the previous sections (5.1.1 and 5.1.2) this similarity of both size and shape would appear to exist for both the powders, ex ferrous oxalate and high purity oxide. No obvious explanation of this effect presents itself, but extremely low values of the constant 'C' in the B.E.T.

equation, such as are found for iron powder ex ferrous oxalate, in this work, can lead to errors in surface area calculated in this way[102]. The higher green density of the carbonyl powder is accounted for by its shape and size differences compared to the other powders.

Activation energies for the sintering process in the temperature range 600 - 800°C, have been calculated and are shown in Table 4. In general the values obtained lie close to that for grain boundary self diffusion in α - iron, if non-equilibrium effects are taken into account. (See page 56).

The exception to this is the carbonyl iron powder which gave a much lower activation energy of 92.1 kJ/mole. Forss[52] using electrolytic iron of mean particle size 75μm obtained a similar value for sintering in the α phase. However, this value is in marked contrast to the value of 232 $\pm$ 19.7 kJ/mole obtained by Fischmeister and Zahn[24] on electrolytic iron of a similar size.

No effect of pressing pressure on the activation energy of carbonyl iron was obtained in this work, which is in good agreement with Fischmeister and Zahn[24]. In the case of the other two powders, an increase in activation energy was found with increasing initial compacting pressure from 15 t.s.i. (231 MN/m^2) to 50 t.s.i. (770 MN/m^2).

Typical values of activation energies determined by other workers, utilising different experimental methods, are shown in Tables 2 and 3. The data in Table 2 relates to diffusion data determined by tracer techniques and, in the case of surface diffusion, by scratch healing techniques. These values may be compared with the values of activation energy obtained from the sintering of iron powders, given in Table 3, and also with the values obtained in this work. In Table 2, the diffusion constants show considerable scatter

in value, particularly in the α phase. Such wide variations have been attributed by other authors[105] to the effect of errors on the very small self diffusion coefficients obtained ($\simeq 10^{-11}$ cm^2 sec^{-1} at the transformation temperature), to the presence of parasitic grain boundary diffusion even at 800°C, and to the effect of sample purity. Some variation in both the diffusion coefficient[106] and activation energy[107] have been reported in the vicinity of the Curie point (768°C). The few values quoted for both grain boundary and surface diffusion show much better agreement, although it should be noted that the activation energy for surface diffusion in α - Fe lies well within the range of values obtained for volume diffusion. Thus it would appear that attempts to determine sintering mechanisms by a comparison of activation energies obtained from densification curves, with those of known diffusional processes, are likely to be unsuccessful. However surface diffusion is known to promote shape change but not shrinkage of powders[23 - 25], so that activation energies within the correct range, but accompanied by marked shrinkage would presumably be representative of volume diffusion only. The situation is further complicated by the results of Aucouturier[108] etal and Guiraldenq[109] who determined activation energies for grain boundary diffusion in α - iron, using both porous (96 - 99% TD) and bulk samples. Their values for diffusion in the porous samples were generally lower than in the bulk material (Typical values were 39 k Cals/mole (163 kJ mole^{-1}) for massive iron, and 30 k cals/mole (126 kJ mole^{-1}) for the porous iron). Such marked differences are attributed to the non-equilibrium vacancy concentrations expected in porous compacts.

Values of activation energies obtained from sintering data, and

shown in Table 3, are again extremely varied. However, such a wide degree of scatter might be expected from the wide variation in purity of powders, temperature ranges of sintering, particle size and sintering atmospheres used. The latter two effects have been shown by other authors[24] to have a marked effect on sintering. The results of this work lie generally on the low side of the values for grain boundary diffusion given in Table 2 and hence if these effects are attributed to non-equilibrium vacancy concentrations, then the results are in reasonable agreement with the accepted activation energies for grain boundary diffusion. An alternative explanation for the apparent low values is that the rate of sintering is dependent on more than one mechanism, over the temperature range considered, and that the measured activation energy is an apparent value as a result of more than one process operating, in parallel. Thus vacancies can arrive at grain boundary sinks as a result of diffusion through the lattice and also by grain boundary diffusion. This is in good agreement with the work of Forss[124], who concludes that for many iron powders, two sintering mechanisms are operative at moderate temperatures. A consequence of such mechanisms would appear to be that a variation in activation energy with temperature might result due to varying amounts of grain boundary and volume diffusion as temperature is increased. Such a variation was not observed in this work, but this can be attributed to an overall lack of experimental data, and a similar study conducted over more closely spaced temperature intervals, might reveal such changes in activation energy.

An alternative way of presenting sintering data, due to Coble[71], expresses porosity as a function of the logarithm of time (see equation 15, page 26). A good linear plot of experimental data

presented in this way is taken to represent volume diffusion of vacancies to grain boundary sinks, according to Coble's original model. Other workers[72] have tested this model on carbonyl iron powder at 800°C, and have fitted the data to the following expression

$$P = 0.1366 \ln \frac{t}{tf}$$ where P = Porosity at time t

tf = 235 hours = time for final densification i.e. when P = 0.

In the current work, reasonable straight lines were obtained for the three powders, pressed at both 231 and 770 MN/m^2, within the temperature range 600 - 800°C. (Figures 27 - 32). These plots greatly emphasise the effects noted previously on the sintering curves. Thus the slope of the lines for iron powder ex ferrous oxalate (Figures 28 and 31) show a marked decrease as temperature rises, becoming nearly horizontal at 800°C, a fact which agrees well with the virtual time independence of sintering noted earlier for these powders. In comparison, the change in slope with time for the other powders is very small. Extrapolation of the data to P = 0, in order to obtain a value for tf, does not seem justified to this author, since such a procedure implies the possibility of sintering to theoretical density at a fixed temperature, whereas in practice a residual porosity is a much more common occurrence. Indeed, in Coble's original work on alumina, the linearity of the semi log plots ceased at a porosity of about 95%, which he attributed to the isolation of pores within the centres of grains rather than at boundaries. The criterion used to judge the validity of the Coble model is solely the linearity of the semi log plot. Such a criterion is, in the opinion of this author,

open to criticism on the grounds that a semi log plot by its very nature, optimises the chances of obtaining straight lines, and that any such fit should be regarded as largely empirical, until more direct evidence of sintering mechanisms is available. (Such evidence might be found in the direct measurement of activation energies from pore shape and size changes during different stages of sintering). Furthermore, available evidence from both radioactive tracer diffusion work, and shrinkage kinetics, point to the presence of both grain boundary and volume diffusion over the temperature ranges in question in this work.

5.2.2. Effect of pressing pressure on the sintering process.

The noticeable feature of the effect of pressure on sintering, in this work is the marked increase in density which occurs at the higher pressing pressures used, in the case of the carbonyl iron and the powder from high purity oxide. This effect is well known and has been reported many times in the literature[24], but is in striking contrast with the results on the iron powder ex ferrous oxalate. In this latter case, the sintered densities obtained after pressing at 15 t.s.i. (231 MN/m^2) are much closer to the results obtained after pressing at 50 t.s.i. (770 MN/m^2). In particular the curve for (800°C and 15 t.s.i.), almost superimposes on the curve for (700°C and 50 t.s.i.), an effect which did not happen with the other iron powders used. Since the initial green densities of the metal from oxalate powder, pressed at 15 t.s.i. (231 MN/m^2) and 50 t.s.i. (770 MN/m^2) were respectively 3.70 gm/cc and 5.00 gm/cc, the much greater overall densification of the powder pressed at 15 t.s.i. (231 MN/m^2) is evident. Several workers have investigated the effects of pressing on the degree of plastic deformation and work hardening in powders,

with variable results. Thus work[110] on green compacts of brass, pressed at 50 t.s.i. (770 MN/m^2), yielded little metallographic evidence of plastic deformation. However Singh[111] has obtained electron microscopic evidence of gross plastic deformation within carbonyl iron powders pressed at 110 kgf/mm^2 (1100 MN/m^2), and results by Hirschhorn and Garey[112] confirm this on atomised iron powder pressed at 60 t.s.i. (924 MN/m^2) using micro-hardness measurements. These latter authors compared micro-hardness measurements on pressed compacts and sintered test bars subjected to known amounts of deformation by either tensile testing or rolling, and arrived at the conclusion that a pressure of 60 t.s.i. (924 MN/m^2) was equivalent to a tensile deformation of 12.5%, or a deformation on rolling of 2.5% respectively.

These results suggest an overall lack of work hardening in the materials, particularly at the stress levels employed in this work. This can probably be associated with a relatively small dislocation density within the powders, so that when plastic deformation takes place, these dislocations run completely through the powder particle leaving behind little residual strain. Such effects should be more evident, the smaller the particle size, and the higher the temperature at which the powder was produced (i.e. atomised and reduced powders would presumably have lower initial dislocation densities). Deformation would presumably be a maximum close to the necks between particles and increasing pressure would serve to weld together larger necks. A corollary to these effects and to the small apparent deformation noted in the particles[112], is a possible high temperature of re-crystallisation and grain growth across the interface, with its attendant effects on sweeping up of porosity. This however does not

seem to be borne out completely in this work, since well defined grain structures were evident in both the carbonyl iron and the powder from high purity iron oxide, after sintering at 600°C (see Figure 40). This value is, of course, comparable with the "re-crystallisation temperature" range for iron quoted in many standard text books. However, in the case of the powder obtained from ferrous oxalate, no grain structure was apparent until the much higher temperature of 800°C was reached. Such an effect could possibly be attributed to a low degree of strain in the powder, or alternatively, to a difference in purity of the powders.

The overall effect of pressure in this work would seem to be one of increasing green density as a direct result of increased interparticle contacts and necks between particles. The influence of the pressing operation on sintering appears to be more indirect in that compacts of higher green density will contain a lower volume fraction of pores, but have a wider spacing between pores. Thus, such an array of pores should lose contact with grain boundaries at an earlier stage than a more closely spaced array, resulting in a lower fractional densification (defined as $\frac{\text{Increase in Density}}{\text{Green Density}}$), due to the decreased contribution of grain boundary diffusion to densification.

The greatly enhanced densification of the powders ex oxalate is probably due to the very fine initial grain size and the attendant slow rate of grain growth, which would result in a prolonged grain boundary contribution to sintering.

5.2.3. The Effect of Phase Transformations within the Powders.

In view of the impure nature of the powders from ferrous oxalate (see Table 5), and of the irrational nature of sintering in the region

of 900°C, dilatometric studies of sintered compacts from each of the powders were carried out, in order to ascertain the actual transformation temperatures of the powders in question. From the results obtained (see Table 15), it would appear that both the carbonyl iron powder and the powder ex iron oxalate were, at least partially transformed to the γ (fcc) phase on sintering at 900°C. As can be seen from the results in table 15, the start and finish of transformation were clear cut and sharp for all the powders except the iron powder ex ferrous oxalate. This powder showed an uncertain start to transformation, below 900°C, but a well defined end to transformation on heating. All these arrests were reproduced in the cooling curves, so that the structure of the compacts on sintering at 900°C seems clearly defined, and variations in sintering behaviour might be expected on the basis of these results.

However, although variations in the densification of the powders did occur on sintering at 900°C, they do not follow the logical pattern suggested by the above results e.g. the powders showing the sharpest drops in densification at 900°C, are the carbonyl iron powder and the powder from high purity oxide, which, according to the dilatometric results are respectively in the γ (fcc), and the α (bcc) forms at this temperature. In contrast to this the powder ex ferrous oxalate, which was in the $(\alpha + \gamma)$ region showed relatively little drop in densification. Such effects may be explained more logically in terms of grain growth/phase change interactions which are discussed further in the following sections (5.2.4 and 5.2.5).

The effects of sintering wholly in the γ (fcc) phase have not been investigated in this work, but the results of other investigators have been reviewed in section 2.5.4, page 29.

5.2.4. Grain Size Variations during Sintering.

The results of grain size measurements, taken on the powders after isothermal sintering show considerable variations (see Figures 33 - 35). In spite of the rather wide scatter bands of the results at different temperatures (due principally to metallographic difficulties), certain well defined effects are noted. Firstly, grain growth is gradual in both the carbonyl Iron and the powder from high purity iron oxide, up to temperatures of 800°C. In fact it is difficult to distinguish clearly between the results at 700 and 800°C for both these powders, and this effect is attributed to experimental error. However, on sintering at 900°C, both powders undergo marked grain growth after very short sintering times. In the case of the iron powder ex ferrous oxalate, measurements were only possible at two temperatures, because of the exceedingly fine grain size. Even at 800°C, the grain size is much smaller than the values attained in the other two powders at 600°C, the actual value changing from 2 - 4 μ m, over the full time of sintering used in this experiment. Grain growth again occurs at 900°C, but is no longer rapid, and takes place gradually over the whole range of sintering time. In all these samples, no evidence was seen of second phase particles, at boundaries, or elsewhere, which might conceivably restrict grain growth. The extreme grain growth occurring on sintering at temperatures close to the α/γ transition has been noted by other authors[47, 87]. In particular, Cizeron etal[47] studied the effect using hot stage microscopy and dilatometry, and recorded the following effects:-

Marked γ grain growth was observed in iron powder compacts on heating through the α - γ change. However, much greater grain growth

of the α phase occurred during the reverse transformation on cooling. The ratios of the grain sizes in the initial α condition prior to transformation, in the intermediate γ phase, and in the final α condition following cooling back through the transformation range were as follows.

$$\frac{\text{Intermediate } \gamma \text{ grain size}}{\text{Initial } \alpha \text{ grain size}} \simeq 3 \text{ or } 4 \qquad \frac{\text{Final } \alpha \text{ grain size}}{\text{Initial } \alpha \text{ grain size}} = 25.$$

Subsequent cycling through the transformation temperature had a negligible effect on grain size. The experiments were also carried out on iron samples of differing purity machined from solid bar, with the result that no comparable grain growth was observed either on heating or cooling through the $\alpha - \gamma$ change. The kinetics of grain growth in the α region were more rapid for the solid machined samples than for the porous samples, and the rate of grain growth also increased as the purity of the solid, machined compacts increased.

Such effects are not in complete accord with the results of this work, since extreme grain growth was noted in both the carbonyl iron and iron powder ex high purity iron oxide, on cooling to room temperature. These two powders were respectively in the γ and α regions on sintering at 900°C, according to the dilatometric results given in Table 15, which suggests that heating <u>through</u> the transformation range is not essential to produce abnormal grain growth. Furthermore the grain sizes of these two powders after sintering at 900°C were very similar (see Figures 33 and 35) which suggests that the marked growth noted by Cizeron etal[47], which occurred on cooling through the $\gamma - \alpha$ change did not occur for the carbonyl powder used in this work. In Cizeron's work, the powders were transformed to γ, following long periods of heating in the α phase, (viz 24 hours and 96 hours at 870°C), and marked grain growth accompanied the trans-

formation. In the current work however, marked grain growth occurred rapidly, after heating for only $\frac{1}{2}$ hour at 900°C for the carbonyl iron powder and the powder from high purity oxide. It would be reasonable to suppose that the compacts used in this work were less dense than those used in the Cizeron work, due to the differences in sintering time, (direct comparison was not possible due to the lack of densification data in Cizeron's paper) and hence the conclusion may be drawn that quite large amounts of porosity have little influence on the abnormal grain growth. Taking the data from figures 21 and 23, and assuming the theoretical density of iron to be 7.87 gm/ml, the porosity after approximately $\frac{1}{2}$ hour at 900°C, would be 31%.

On sintering the high purity iron powder at 900°C, the structure would still be in the α range according to the dilatometric results, and a decrease in density was noted. This fact seems to be in accord with the statement by Poster and Hausner[86] that "the densification rate falls off sharply as sintering is raised to the low temperature side of the γ range".

Finally, the iron powder ex oxalate, shows a range of transformation which ends at 908°C, and hence was in the two phase ($\alpha + \gamma$) condition at 900°C, although owing to the closeness of the transformation temperature, the α phase would be small in amount. It is therefore surprising that no extreme grain growth occurred during the early stages of sintering in this powder, at 900°C. A possible explanation for this effect is found in the differences in purity of the powders, since the impure powder, ex oxalate, would be expected to show much slower grain growth kinetics as a result of grain boundary/impurity atom interactions. The much finer grain size of this powder initially and therefore its attendant finer pore structure

might also be expected to pin grain boundaries. Both these latter effects are well known and are amply discussed in text books dealing with recrystallisation and grain growth[113].

It has previously been noted in the literature survey (Section 2.5.4. page 29) that grain size decreases as the sintering temperature is raised in the γ fcc region, up to a maximum temperature of 1400°C[86, 129]. This effect could be interpreted in terms of nucleation difficulties and superheating of the transformation, since the higher the isothermal sintering temperature used in the γ range, the faster would be the rate of heating up of the specimen, through the α / γ transformation region, to the sintering temperature. Hence, superheating of the transformation should increase as the rate of heating up to the sintering temperature increases, and the higher the degree of superheat, the greater would be the numbers of effective γ nuclei, leading ultimately to a finer grain size once transformation is complete. In support of this theory, some evidence has been put forward for superheating of the α / γ transformation[134], albeit on very small iron whiskers (less than 50μm in width) which appeared to transform martensitically. The temperature of 1400°C would then represent the temperature at which growth of the nuclei became more important than the difficulties of nucleation. However, it is difficult to see why this temperature should be so high, in comparison say, to the grain coarsening temperatures of killed steels (950 - 1000°C), since nitride particles in the latter, should be as effective in restricting grain growth as the pore distribution in the sintered materials.

5.2.5. General Discussion.

On the basis of the results obtained in this work, it is

difficult to postulate a direct mechanism of sintering. The cases for both volume and grain boundary diffusion are shown diagrammatically in Figures 43 and 44, where the variation in diffusion distance, $x = \sqrt{Dt}$ (D = Diffusion coefficient, t = time), is plotted as a function of temperature. Also shown in Figure 43, is the maximum grain size attained, after $16\frac{1}{2}$ hours, in each of the powders used in this work. From these figures it can be seen that the diffusion distance is generally much less than the maximum grain size, for volume diffusion, but is considerably greater than the grain size, for grain boundary diffusion. These diffusion distances are calculated from "equilibrium" values of the diffusion variables Do and Q (References 59 and 66, Table 2), the values actually chosen being intermediate in the range of values shown in Table 2. This choice is further justified by the fact that as Do increases in Table 2, Q also increases, and since increases in either of these constants have opposite effects on the diffusion variable D, (increasing Do for a constant Q, increases D, whereas increasing Q for a constant Do reduces D), the argument adopted here is not radically altered. However, this same argument does not necessarily apply if the non-equilibrium effects discussed in section 5.2.1, are taken into account. Thus, according to the results of Aucouturier etal[108], and Guiraldencq[109], porous samples exhibit much lower activation energies for diffusion than massive samples. The value they obtained for grain boundary diffusion in porous compacts is 30 kcals/mole (126 kJ mol^{-1}), and if this result is used to calculate diffusion distances in iron at 800°C (assuming constant Do in the diffusion equation) values of 0.93mm and 5.4mm are obtained respectively for times of one half hour, and sixteen and one half hours. These values are considerably in excess of the grain sizes

shown in Figure 43. Similar effects might be expected for the case of non-equilibrium volume diffusion, however no information relating to porous compacts was found in the literature.

On the basis of the present results, it would appear that volume diffusion plays a relatively minor role in sintering, especially at the lower temperatures where the diffusion distance is small. The situation is best summed up in Figure 45 which shows the "range of effectiveness" of volume diffusion, for a pore situated in a grain boundary. Thus a flux of vacancies leaving the pore surface will only produce sintering, if a suitable vacancy sink is available. The most suitable sink appears to be the grain boundary, and the diagram shows, what proportion of the grain boundary lies within the (volume) diffusion distance of the pore. Areas of the pore surface lying outside the range of the grain boundary sink will have very low vacancy concentration gradients into the interior of the grain, and will therefore show a much smaller tendency to develop diffusion paths for the vacancies. Volume diffusion will obviously play a much larger role in sintering with smaller grain sizes, since a much greater surface area of the pore will lie within the diffusion distance of a grain boundary sink. This effect would appear to be operating in the current work, for the iron powder produced from ferrous oxalate, since the maximum grain size attained after $16\frac{1}{2}$ hours at 800°C, lies right on the limit of the diffusion distance at 800°C (see Figure 43). Hence the enhanced degree, and rate of densification in this powder is partially accountable to an increased contribution to sintering by a volume diffusion mechanism. This is in good agreement with the findings of Fischmeister and Zahn[24] who conclude that volume

diffusion is the most likely sintering mechanism in fine powders.

The contribution of grain boundary diffusion to the sintering process, appears to be very large, since the diffusion distances calculated on this model are generally well in excess of the measured grain size of the powder over the temperature range 600 - 800°C. In general, pores are situated at grain boundaries and the inter pore distance will bear some general relationship to the grain size, with smaller inter pore distances occurring in finer grain size materials. Thus in fine grain size materials, pore/vacancy sink distances will be short, and since diffusion distances even after half an hour at 600°C are in excess of the inter pore distances, sintering by such a mechanism should again be extremely rapid.

The extreme grain growth occurring at temperatures close to the $\alpha - \gamma$ transition in some of the powders was responsible for the marked drop in densification on sintering at 900°C, since during grain growth many pores become isolated within grains and no longer in contact with grain boundaries. The contribution of grain boundary diffusion to densification is therefore lost and subsequent shrinkage of the pores occurs only by volume diffusion across an enlarged pore/sink distance. Similar effects did not occur with the iron powder ex oxalate, since grain growth was more gradual, and comparable values with the other two powders were not obtained until approximately $16\frac{1}{2}$ hours of sintering time had elapsed. Thus the pores remained in contact with the boundaries for longer periods of time, and the pore/sink distances for volume diffusion would remain shorter, minimising the density decrease at 900°C in this powder. The slower rate of grain growth in this powder is attributable to its higher impurity content, and the boundary retarding effect such

impurities exert, as discussed previously. Similar effects have been noted on alumina[71], where the introduction of small amounts of impurity oxides, restricted grain growth and enabled sintered densities close to the theoretical density to be obtained.

One apparent anomaly arising from the current work is the contrasting behaviour of the powder ex iron exalate and that from the high purity oxide, since both these powders started from approximately the same initial particle size, as shown by electron micrographic and B.E.T. evidence. However, purity differences exist between the two powders, the purer powder showing the higher rate of grain growth, with its attendant effects on densification, as discussed previously. Differences may also exist between the two powders in other ways, e.g. the iron powder ex oxalate, was formed by reduction of a very fine iron oxide, whereas the iron powder from high purity oxide was obtained from oxide of a comparable size (Sections 5.1.1 and 5.1.2). Thus it is possible that crystallite size differences exist within individual particles from both types of powder, as a direct result of the method of preparation, the iron powder ex oxalate consisting of many fine crystallites, whereas the powder from high purity oxide having a crystallite size comparable with the particle size. However, it was not possible to obtain further evidence on this point. Further study by means of an X ray line broadening technique, of the powders in question would no doubt have helped to clarify this point.

6. CONCLUSIONS

The following conclusions can be drawn from this work.

1. Iron powders of substantially submicron size can be readily prepared by the methods utilised in this work, providing care is taken to obtain starting materials of a sufficiently high purity.

2. Very rapid sintering occurred in the case of the iron powder obtained from ferrous oxalate, although the general level of density obtained was much the same in all the powders used.

3. The extremely rapid sintering in the case of the iron powder ex ferrous oxalate, is associated with the extremely small grain size in this powder and the attendent low rate of grain growth, thus enabling both volume and grain boundary diffusion to play a larger part in the sintering process. The small grain size and low rate of grain growth are themselves associated with the lower purity of this powder and the inhibition of grain growth by such impurities.

4. Marked decreases in density occur on sintering in the region of the α / γ phase transition, and on the evidence of this work, would appear to occur on the low temperature side of the transformation temperature.

5. Such density decreases are associated with a marked increase in grain size, thereby divorcing pores from the grain boundaries and slowing down the sintering process. Similar effects were not noted with the iron powder ex ferrous oxalate, owing to the more gradual rate of grain growth occurring at 900°C and the increased time that the pores remained in contact with the boundaries.

6. Activation energies obtained for sintering in this work were generally low and this is attributed to the fact that no single process contributes towards densification, the overall rate being the result of several mechanisms acting in parallel. The most likely mechanisms are those of volume and grain boundary diffusion.

7. SUGGESTIONS FOR FUTURE WORK.

1. The techniques for the preparation of iron powder from oxalates used in this work started with a commercial grade of oxalate. Purer forms of oxalate could be made chemically by precipitation from solutions in oxalic acid. Thus, the effect of precipitation from either weak or concentrated solutions on the morphology of the powders produced would provide an interesting line of study.

2. An attempt should be made to lower the temperature of the reduction stage from oxide to metal, in order to minimise sintering of the powder mass at this stage, thus yielding finer powders. A better method might be to combine the reduction and sintering stage, so that oxide compacts are reduced and sintered at the same time, thereby making better use of the inherent "activity" of fine powders, and minimising risks of pyrophoncity.

3. Direct measurement, by means of quantitative microscopy, on the change in shape, size, and distribution of pores during sintering, would provide a better method of assessing possible mechanisms, than the measurement of secondary properties such as density, resistance, tensile strength etc.

4. Adsorption isotherms of the type used to assess surface area in this work, could be used to provide more information on the morphology of the powders. This arises from the fact that the behaviour of the adsorption and desorption branches of the isotherm at relative pressures approaching unity (well above the accepted B.E.T. range) can be used to identify the nature of pores, cracks etc. present on the surface of the particles themselves.

5. Incorporation of very fine oxide powders into the fine iron powders to produce a dispersed phase of low inter-particle spacing may lead to improvements in dispersion hardening systems.

TABLE 1.

Values of constants in model sintering equations

Mechanism	'n' in Eqt $^{n}_{4}$	M in Equation 4	p=(n-m) in Equation(6)	Reference
Viscous or Plastic Flow	2	1	1	9
Evaporation and Condensation	3	1	2	11
	7	3	4	14
Lattice Diffusion	5	2	3	11
	4	1	3	14
Surface Diffusion	7	3	4	11,26
	5	2	3	15
	3	1	2	16

TABLE 2.

Bulk Diffusion Data for α and γ Iron

	DIFFUSION COEFFICIENT Do - mm^2/sec		ACTIVATION ENERGY Q - kJ/mole		REFERENCE
	α Fe	γ Fe	α Fe	γ Fe	
VOLUME DIFFUSION	230,000	5,800	306	310	54
	580	58	249	284	55
	5,300		280		56
	1.9	130	198	284	57
	320		232		58
	11,800		281		59
	1,800		268		60
	190	18	239	270	61
	200		251		
		76		284	62
		44		280	63
		1.85		251	64
			278		65
				284	67
GRAIN BOUNDARY DIFFUSION		100		167	64
			188	171	65
	650		167		66
				128	67
			188	188	68,69
SURFACE DIFFUSION	$4x10^8$		266		24
	$5x10^7$		249		
	$3x10^9$		267		
	10^7	$4x10^5$	233	205	103
	$5.4x10^7$		241		104

TABLE 3.

Activation Energy Data for the Sintering of Iron Powders

Temperature Range C	Sintering Rate Exponent 'n'	Activation Energy Q, kJ/mole	Remarks	Reference
710 - 880	0.2 - 0.33	151	Hydrogen Atmosphere Powder Size 20 μm.	44
710 - 880	- 0.50	151		
920 - 1000	+ 0.40	288		
710 - 750	+ 0.20	760	Vacuum	
750 - 880	- 0.50	184		
< 740	+ 0.2	326	Mean Powder Size 20 μm.	45
	+ 0.33	222		
750 - 790	+ 0.2	150		
	- 0.5	146		
710 - 800	+ 0.2	760	Mean Powder Size 20 μm.	46
800 - 880	+ 0.2	192		
	- 0.05	176		
910 - 1000	+ 0.40	288		
< 910	-	167	Carbonyl Iron used	47
910 - 1250	-	292		
up to 900	-	≏ 62.7	Submicron powders used 8 - 11 m^2/gm surface area	48
-	-	300	-	49
750 - 1100	-	288	-	50
600 - 800	-	167	-	51
> 910	-	188	-	
800 and 900	1.0 → 1.25	100	Electrolytic Iron used 75 μm Particle Size	52
730 - 890	0.65	125	Carbonyl Iron used Particle Size 3-20 μm	53
1380 - 1460				
760 - 890	-	230	Electrolytic Iron used 50-103 μm Particle Size	24
450 - 900	-	172	Carbonyl Iron used of 6.3 μm mean size	114

TABLE 4.

Values of Activation Energies calculated from Sintering Data.

Material	Activation Energies	
	at 15 t.s.i.	at 50 t.s.i.
Carbonyl Iron Grade MCHP	92.1 kJ/mole	92.1 kJ/mole
Iron ex Johnson Mathey Oxide	120 kJ/mole	147.2 kJ/mole
Iron ex Ferrous Oxalate	145 kJ/mole	177 kJ/mole

NOTE: 1 k cal/mole = 4.186 kJ/mole.

TABLE 5.

Analyses of Materials Used in this Work

ANALYSES OF MATERIALS	
FERROUS OXALATE * Suppliers Analysis (Laboratory Grade)	Fe^{2+} 29 - 31% Chloride (Max Limits) 0.005% Nitrate " " 0.01 % Sulphate " " 0.05 % Ammonia " " 0.5 % Fe^{3+} " " 0.5 %
FERRIC OXIDE (High Purity)	Fe_2O_3 99.99%
IRON POWDER ex FERROUS OXALATE (Analysed on sintered compact)	C 0.105% Ca trace (<0.02) Cr <0.04 Mn 0.4 Ni <0.05 Cu <0.04 Zn present (<0.5%) but difficult to estimate Sn <0.02 Mo <0.05
CARBONYL IRON POWDER. GRADE MCHP (Manufacturers Information)	C <0.02 O_2 <0.2 N_2 <0.02 7.0 µm Average Particle Size 3.2 gm/cc Bulk Density

* This is obviously not a rigorous analysis since a spot check carried out on this powder, with Sodium Bismuthate, gave an intense permanganate colour confirming the presence of Mn, probably as an oxalate.

TABLE 6.

Surface Area calculated from B.E.T. Measurements

MATERIAL	Point 'B' Surface Area m^2/g	B.E.T. Surface Area m^2/g	B.E.T. Constant, 'C'
Carbonyl Iron	0.209	0.147	28.6
Iron Powder (ex Oxalate)	3.31	2.83	13.5
Iron Powder (ex Johnson Mathey Oxide)	3.56	2.52	Negative Intercept
Johnson Mathey Oxide	2.94	2. 2	125
Iron Oxide from decomposition of Ferrous Oxalate	—	78	143

TABLE 7.

Data from Gas Sorption Analysis at Liquid Nitrogen Temperatures for Iron Powder ex Ferrous Oxalate

Volume Sorbed ΔV ccs	Relative Pressure x_J	B.E.T. Parameter $= \frac{x_J}{\Delta v(1-x_J)}$
0.0199	0.1214	6.95
0.02703	0.2017	9.35
0.02877	0.2357	10.72
0.0385	0.4480	Outside B.E.T. range

TABLE 8.

Data from Gas Sorption Analysis at Liquid Nitrogen Temperatures for High Purity Iron Oxide

Volume Sorbed ΔV cos	Relative Pressure x_J	B.E.T. Parameter $= \frac{x_J}{\Delta v(1-x_J)}$
0.04090	0.0835	2.2278
0.04542	0.1411	3.617
0.04725	0.1617	4.0823
0.05359	0.3075	8.286
0.05737	0.4224	Outside B.E.T. range
0.0615	0.5666	Outside B.E.T. range

TABLE 9.

Data from Gas Sorption Analysis at Liquid Nitrogen Temperatures for Iron Powder ex High Purity Oxide.

Volume Sorbed ΔV cos	Relative Pressure x_J	B.E.T. Parameter $= \frac{x_J}{\Delta v(1-x_J)}$
0.1209	0.1462	1.417
0.1313	0.2332	2.316
0.1350	0.2637	2.653
0.1457	0.5002	Outside B.E.T. range

TABLE 10.

Data from Gas Sorption Analysis at Liquid Nitrogen Temperatures for Carbonyl Iron Powder

Volume Sorbed ΔV ccs	Relative Pressure x_J	B.E.T. Parameter $= \frac{x_J}{\Delta v(1-x_J)}$
0.0129	0.1247	11.08
0.0138	0.1470	12.52
0.0183	0.2958	22.95
0.0209	0.4283	Outside B.E.T. range
0.0239	0.6128	Outside B.E.T. range

TABLE 11.

Data from Gas Sorption Analysis at Liquid Nitrogen Temperatures, for Iron Oxide powder ex Ferrous Oxalate

Volume Sorbed ΔV ccs	Relative Pressure x_J	B.E.T. Parameter $= \frac{x_J}{\Delta v(1-x_J)}$
0.1349	0.04657	0.3621
0.1431	0.0559	0.4138
0.1452	0.05782	0.4227
0.1512	0.06902	0.4902
0.1547	0.08442	0.5962

AVERAGE GREEN DENSITY AT 15 t.s.i. gm/cc	SINTERED DENSITY AT 15 t.s.i. gm/cc	AVERAGE GREEN DENSITY AT 50 t.s.i. gm/cc	SINTERED DENSITY AT 50 t.s.i. gm/cc	TEMPERATURE (°C)	TIME (HOURS)	POROSITY = $\frac{Pt - Ps}{Ps}$ at 15 t.s.i.	POROSITY AT 50 t.s.i.
4.81	5.29	6.46	6.71		½	0.489	0.173
4.84	5.58	6.53	6.95		2	0.411	0.132
4.89	5.70	6.58	7.09	600	4	0.381	0.110
4.87	5.83	6.55	7.10		8	0.350	0.108
4.86	5.93	6.58	7.19		16½	0.328	0.095
4.84	5.66	6.58	7.06		½	0.391	0.115
4.81	5.93	6.52	7.20		2	0.328	0.093
4.90	6.10	6.56	7.23	700	4	0.290	0.089
4.85	6.19	6.54	7.28		8	0.272	0.081
4.88	6.36	6.53	7.40		16½	0.238	0.064
4.86	5.95	6.54	7.29		½	0.323	0.080
4.86	6.21	6.52	7.31		2	0.257	0.077
4.87	6.35	6.59	7.41	800	4	0.240	0.062
4.86	6.50	6.53	7.43		8	0.211	0.059
4.82	6.69	6.55	7.56		16½	0.177	0.041
4.84	5.95	6.55	7.14		½	0.323	0.102
4.88	5.92	6.58	7.14		2	0.330	0.102
4.88	6.17	6.59	7.20	900	4	0.276	0.093
4.88	5.95	6.42	7.12		8	0.323	0.105
4.89	6.31	6.56	7.21		16½	0.248	0.092

TABLE 12. Results of Sintering Experiments Iron Powder reduced at 300°C from High Purity Iron Oxide.

AVERAGE GREEN DENSITY AT 15 t.s.i. gm/cc	SINTERED DENSITY AT 15 t.s.i. gm/cc	AVERAGE GREEN DENSITY AT 50 t.s.i. gm/cc	SINTERED DENSITY AT 50 t.s.i. gm/cc	TEMPERATURE (°C)	TIME (HOURS)	POROSITY = $\frac{Pt - Ps}{Ps}$ AT 15 t.s.i.	POROSITY AT 50 t.s.i.
3.70	5.84	5.05	6.80	600	½	0.348	0.158
3.68	6.00	5.04	6.95		2	0.312	0.132
3.66	6.02	5.03	7.01		4	0.308	0.123
3.67	6.26	5.07	7.09		8	0.258	0.110
3.69	6.28	5.06	7.20		16½	0.254	0.093
3.62	6.53	4.96	7.13	700	½	0.205	0.104
3.70	6.42	5.08	7.17		2	0.226	0.098
3.64	6.73	4.94	7.26		4	0.170	0.084
3.62	6.66	5.02	7.29		8	0.182	0.080
3.62	6.70	4.91	7.28		16½	0.175	0.081
3.80	7.22	5.09	7.39	800	½	0.090	0.065
3.71	7.12	5.06	7.32		2	0.105	0.075
3.78	7.31	5.07	7.38		4	0.077	0.067
3.77	7.26	5.07	7.34		8	0.084	0.072
3.75	7.30	5.09	7.39		16½	0.078	0.065
3.69	7.22	5.08	7.33	900	½	0.090	0.074
3.65	7.15	4.99	7.35		2	0.101	0.071
3.64	7.19	4.99	7.32		4	0.095	0.075
3.67	7.22	5.00	7.35		8	0.090	0.071
3.62	7.07	4.98	7.29		16½	0.113	0.080

TABLE 13. Results of Sintering Experiments on Iron Powder, reduced at 300°C from Iron Oxide obtained from the decomposition of Ferrous Oxalate.

AVERAGE GREEN DENSITY AT 15 t.s.i. gm/cc	SINTERED DENSITY AT 15 t.s.i. gm/cc	AVERAGE GREEN DENSITY AT 50 t.s.i. gm/cc	SINTERED DENSITY AT 50 t.s.i. gm/cc	TEMPERATURE (°C)	TIME (HOURS)	POROSITY = Pt - Ps / Ps AT 15 t.s.i.	POROSITY AT 50 t.s.i.
5.50	5.63	7.06	7.10	600	½	0.398	0.108
5.59	5.86	7.01	7.10		2	0.343	0.108
5.49	6.01	7.02	7.21		4	0.309	0.092
5.52	6.00	7.04	7.28		8	0.312	0.081
5.43	6.11	6.94	7.21		16½	0.288	0.092
5.49	5.79	6.98	7.10	700	½	0.360	0.108
5.48	6.10	6.94	7.23		2	0.290	0.089
5.46	6.27	6.87	7.24		4	0.256	0.087
5.49	6.51	6.97	7.40		8	0.209	0.064
5.53	6.71	6.98	7.47		16½	0.173	0.054
5.48	6.08	6.97	7.21	800	½	0.294	0.092
5.49	6.48	6.96	7.37		2	0.215	0.068
5.45	6.72	6.97	7.40		4	0.171	0.064
5.42	6.86	6.97	7.44		8	0.146	0.058
5.45	6.99	6.97	7.52		16½	0.126	0.047
5.44	5.78	6.99	7.18	900	½	0.362	0.096
5.45	6.01	6.96	7.17		2	0.310	0.098
5.48	5.97	6.94	7.13		4	0.318	0.104
5.49	6.12	6.95	7.12		8	0.246	0.105
5.41	6.07	6.97	7.24		16½	0.298	0.087

TABLE 14. Results of Sintering Experiments on Iron Powder obtained by decomposition of Iron Carbonyl.

TABLE 15.

Temperatures of α / γ Transformation in the Powders as determined by Dilatometry

POWDER	ARRESTS ON HEATING	ARRESTS ON COOLING
CARBONYL IRON	Start 890°C Finish 900°C	883°C 870°C
IRON POWDER ex JOHNSON MATHEY OXIDE	Start 905°C Finish 910°C	888°C 880°C
IRON POWDER ex FERROUS OXALATE	Start Uncertain * Finish 908°C	870°C Uncertain *

* $<$900°C

TABLE 16.

Grain Size Measurements on Iron Powder, ex High Purity Iron Oxide.

AVERAGE LINEAL INTERCEPT mms.	TIME (HOURS)	TEMP. °C
0.0073	2	600
0.01	4	
0.011	8	
0.0095	$16\frac{1}{2}$	
0.012	$\frac{1}{2}$	700
0.012	2	
0.016	4	
0.016	8	
0.019	$16\frac{1}{2}$	
0.014	$\frac{1}{2}$	800
0.016	2	
0.020	4	
0.019	8	
0.022	$16\frac{1}{2}$	
0.037	$\frac{1}{2}$	900
0.035	2	
0.033	4	
0.033	8	
0.048	$16\frac{1}{2}$	

TABLE 17.

Grain Size Measurements on Iron Powder, ex Ferrous Oxalate

AVERAGE LINEAL INTERCEPT mms.	TIME (HOURS)	TEMP. °C.
0.0022	½	800
0.0030	4	
0.0036	8	
0.0038	16½	
0.0062	2	900
0.026	4	
0.021	8	
0.052	16½	

TABLE 18.

Grain Size Measurements on Carbonyl Iron Powder

AVERAGE LINEAL INTERCEPT mms.	TIME (HOURS)	TEMP °C
0.01	½	600
0.0099	2	
0.013	4	
0.011	8	
0.017	16½	
0.013	2	700
0.014	4	
0.014	8	
0.017	16½	
0.011	½	800
0.013	2	
0.014	4	
0.017	8	
0.02	16½	
0.032	2	900
0.036	4	
0.037	8	
0.033	16½	

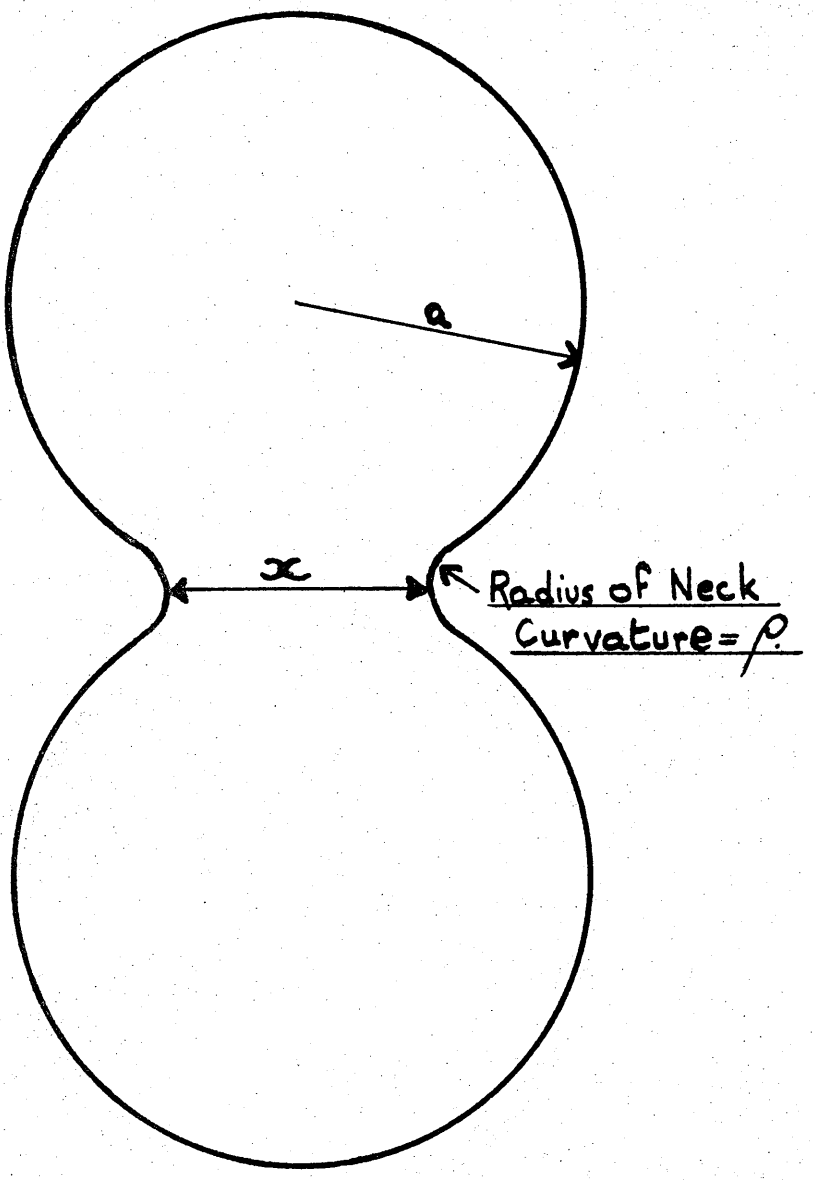

Figure 1. Neck Growth between particles

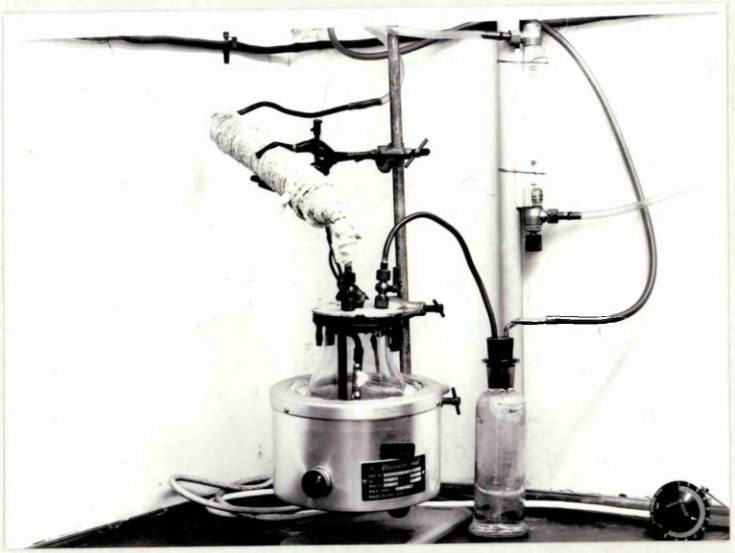

Figure 2. Preheating furnace and Reduction chamber used for preparation of Iron powder from oxides.

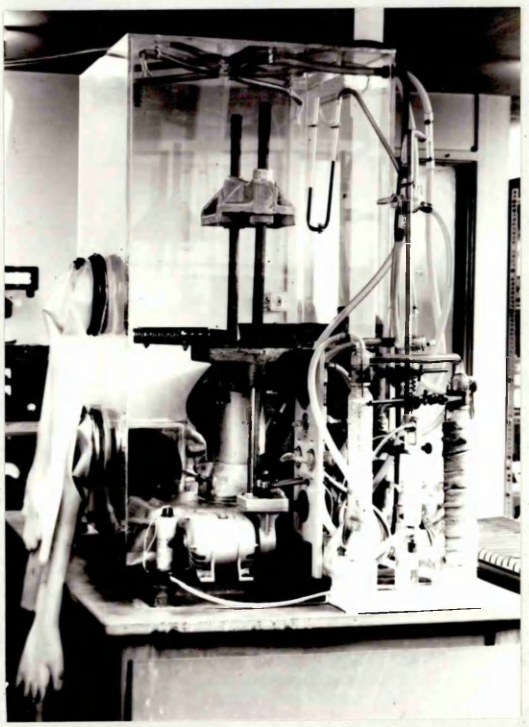

Figure 3. Glove Box used for pressing "green" compacts.

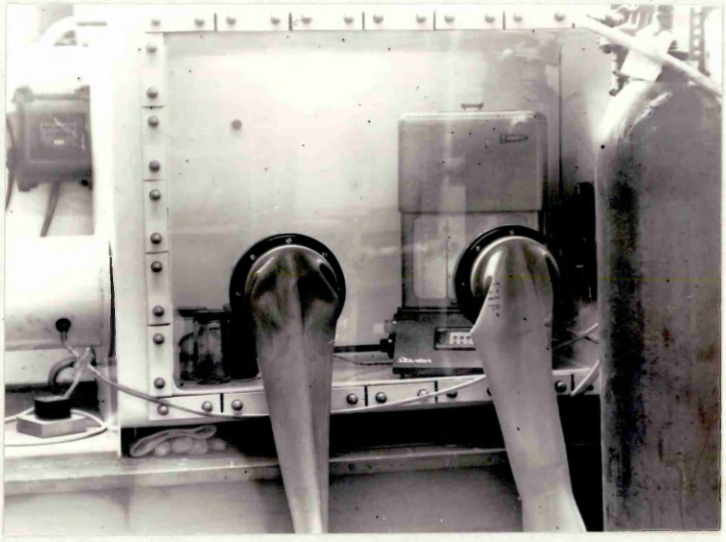

Figure 4. Glove Box used for storing and weighing powders.

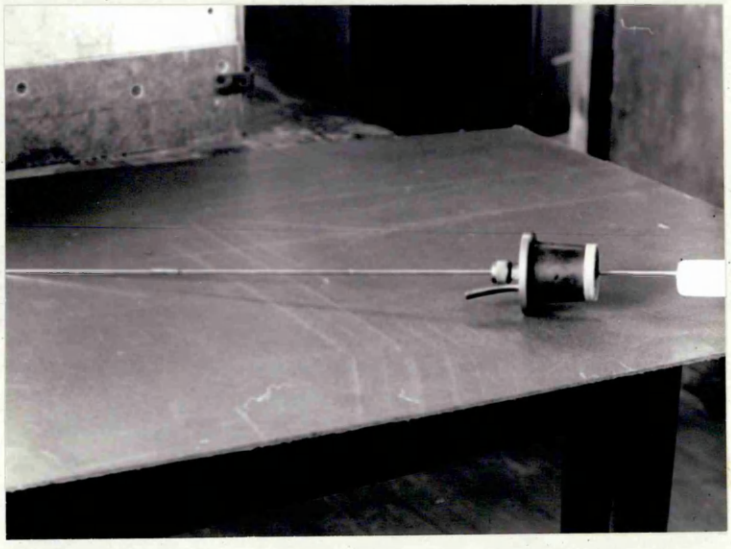

Figure 5. Transfer System used for placing compacts in Furnace under an inert atmosphere.

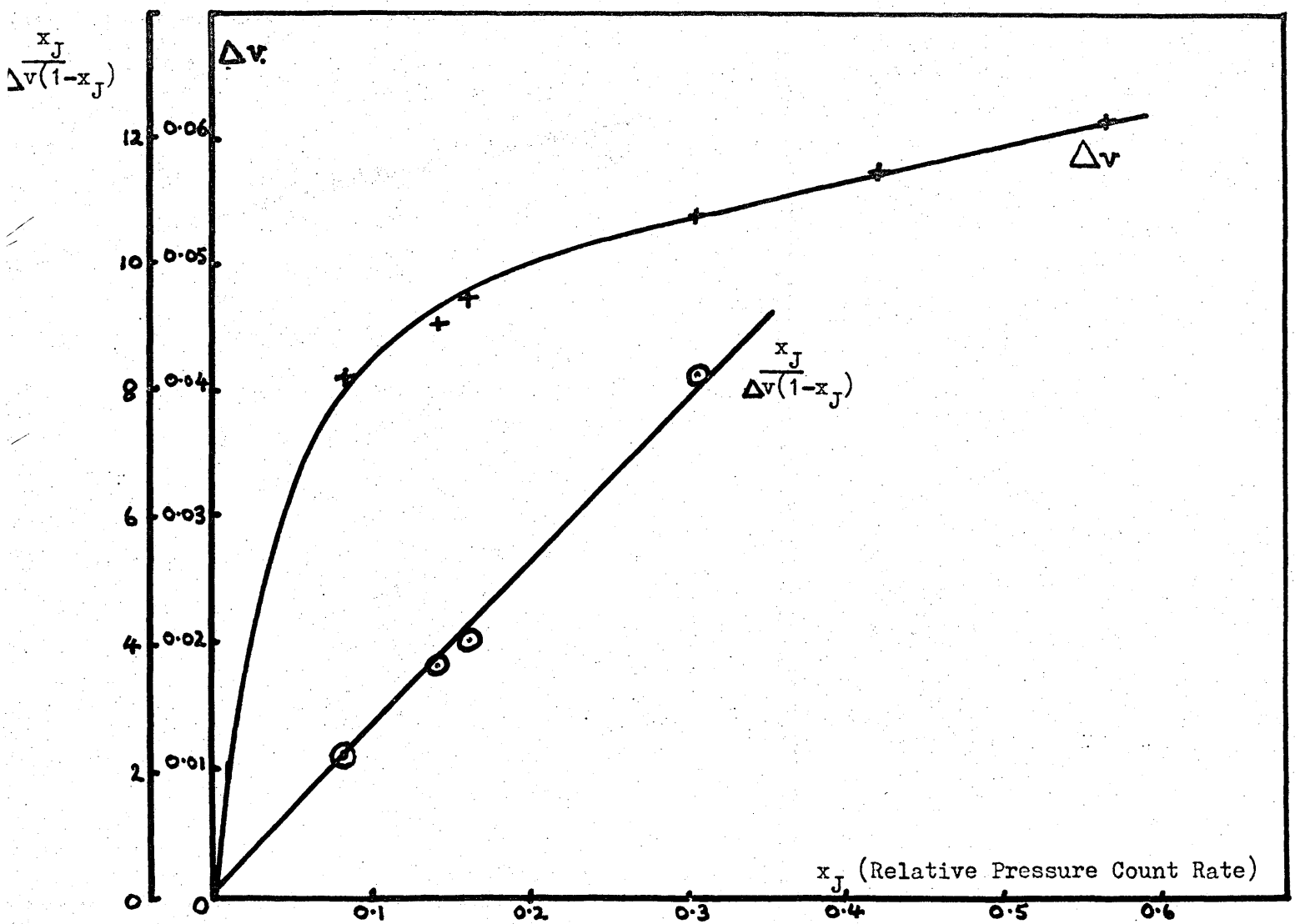

Figure 6. Krypton Sorption Isotherm and B.E.T. Plot for High Purity Iron Oxide

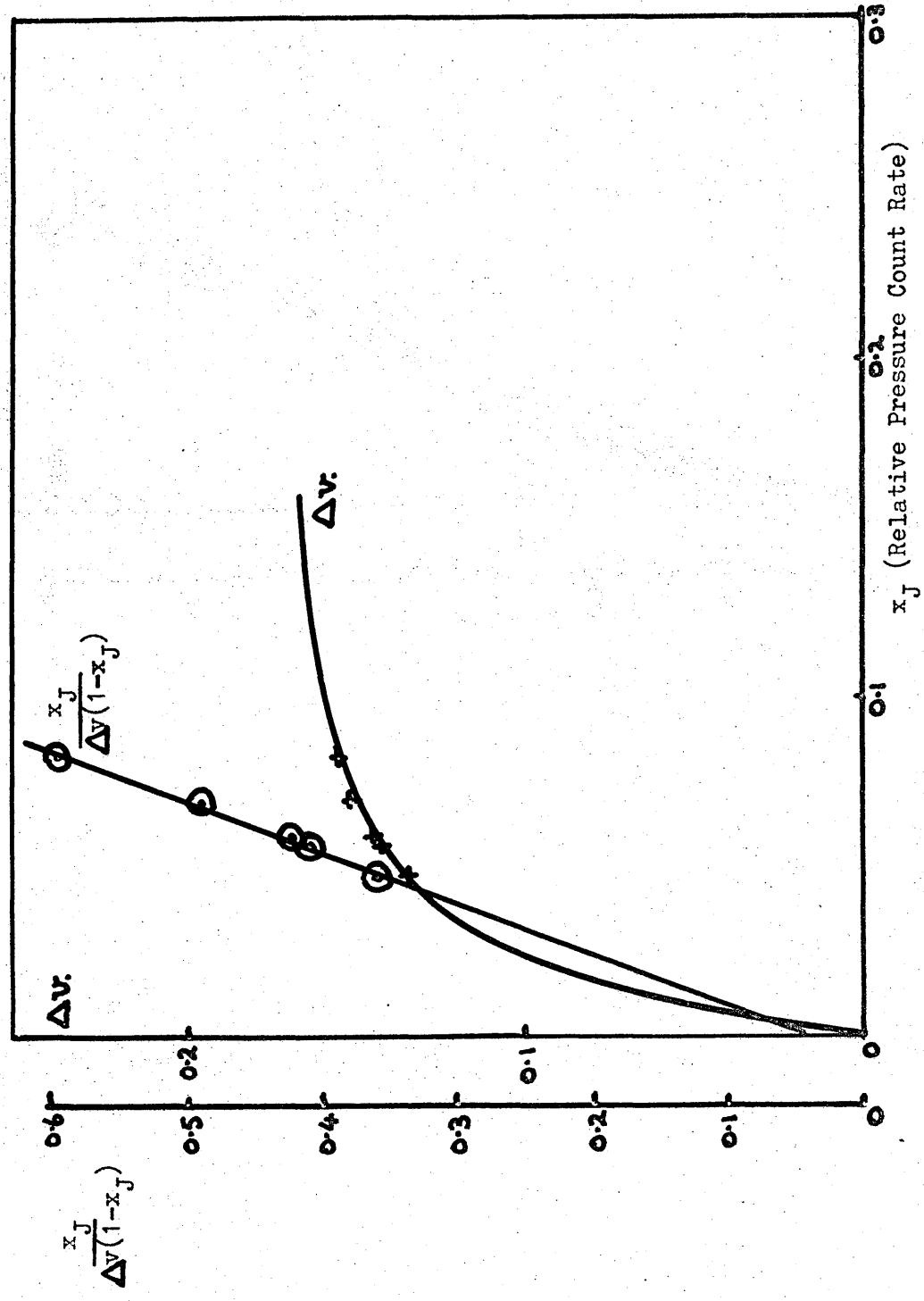

Figure 7. Krypton Sorption Isotherm and B.E.T. Plot For Iron Oxide ex Ferrous Oxalate

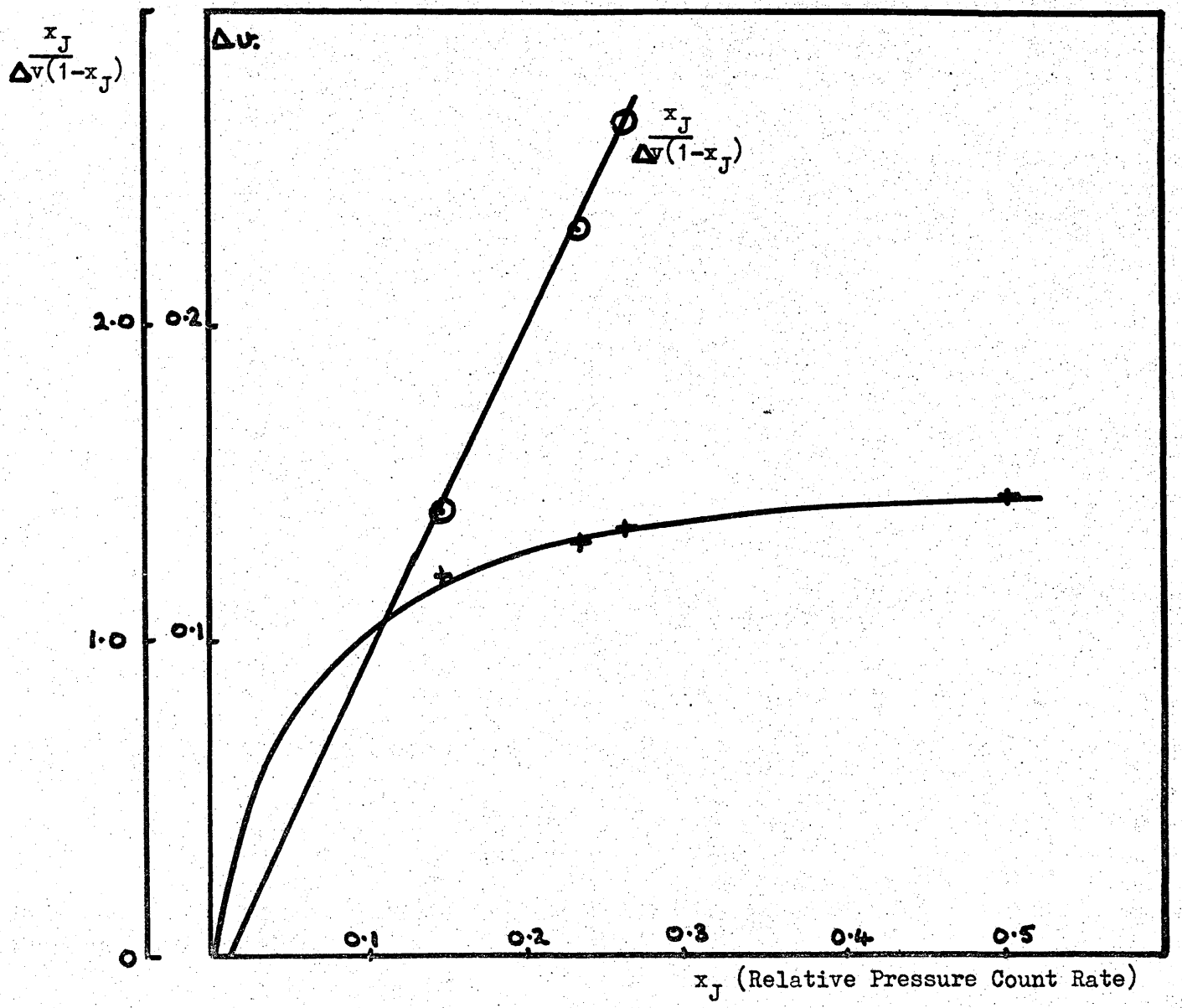

Figure 8. Krypton Sorption Isotherm and B.E.T. Plot For Iron Powder ex High Purity Oxide

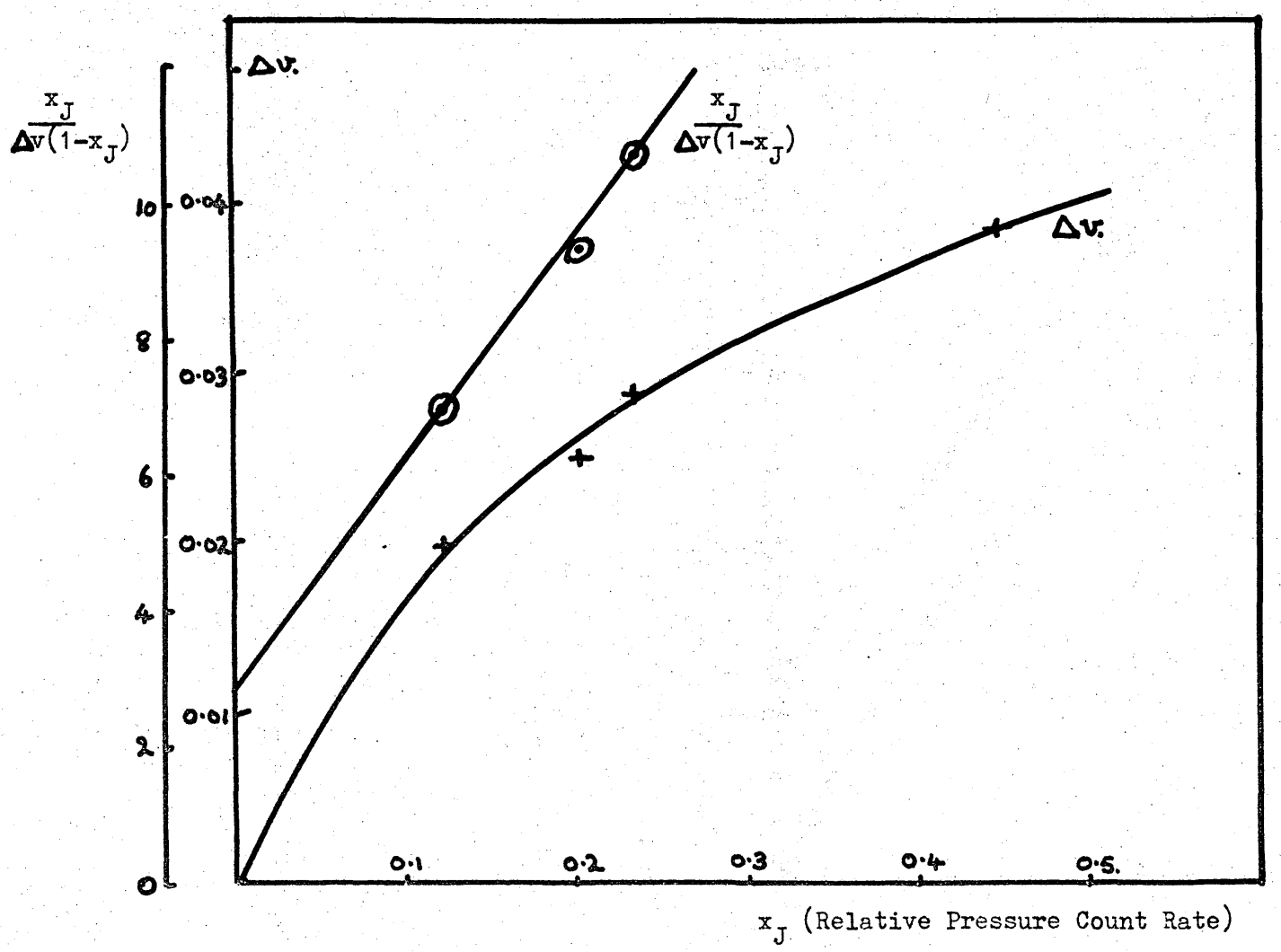

Figure 9. Krypton Sorption Isotherm and B.E.T. Plot for Iron Powder ex Ferrous Oxalate

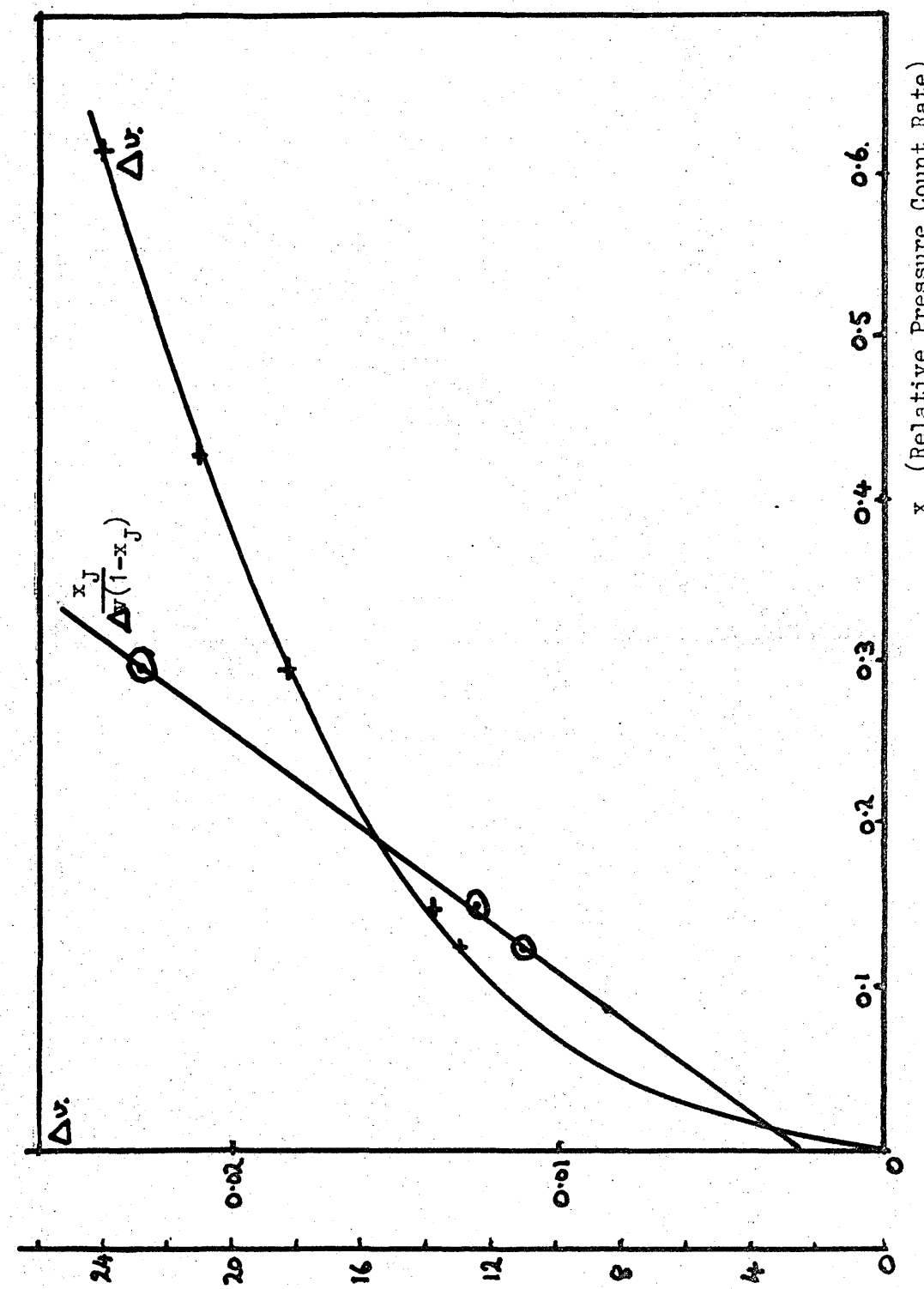

Figure 10. Krypton Sorption Isotherm and B.E.T. Plot for Carbonyl Iron Powder

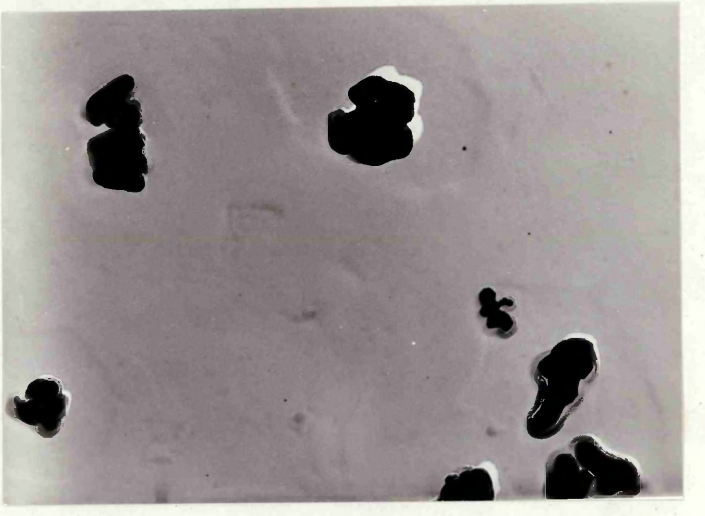

Figure 11. Electron Micrograph of High Purity Iron Oxide (x20,000)

Figure 12. Electron Micrograph of High Purity Iron Oxide (x60,000)

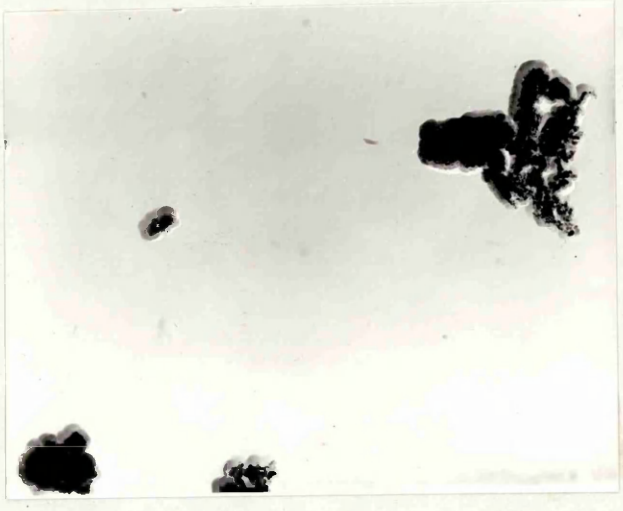

Figure 13. Electron Micrograph of Iron Oxide, ex Ferrous Oxalate (x20,000)

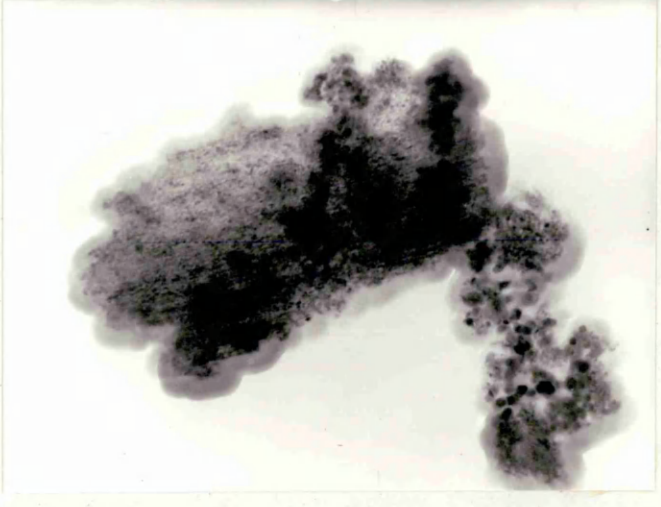

Figure 14. Electron Micrograph of Iron Oxide, ex Ferrous Oxalate (x40,000)

Figure 15. Electron Micrograph of Iron powder, ex Ferrous Oxalate (x30,000)

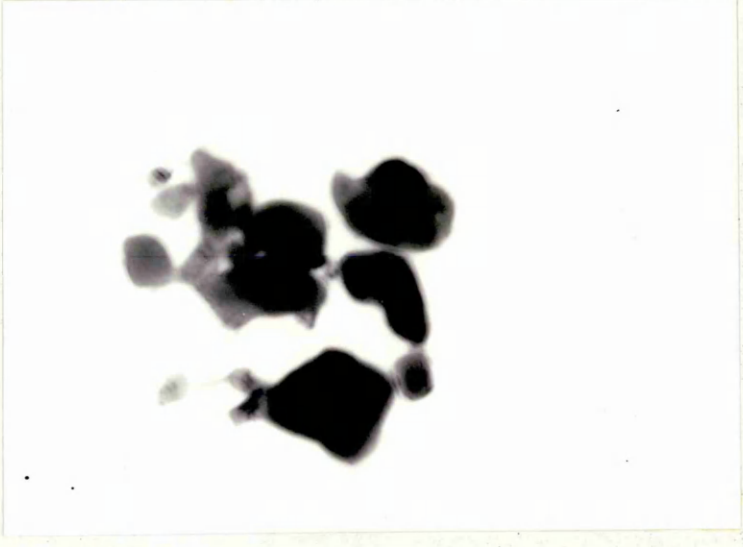

Figure 16. Electron Micrograph of Iron powder, ex Ferrous Oxalate (x60,000)

Figure 17. Electron Micrograph of Iron powder, ex High Purity Oxide (x12,000)

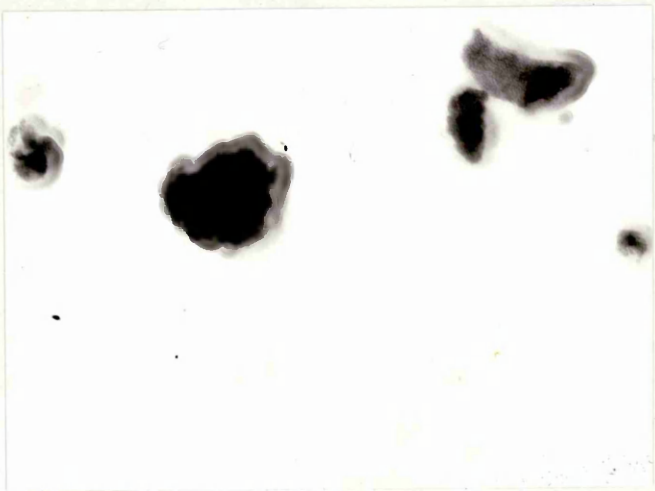

Figure 18. Electron Micrograph of Iron powder, ex High Purity Oxide (x60,000)

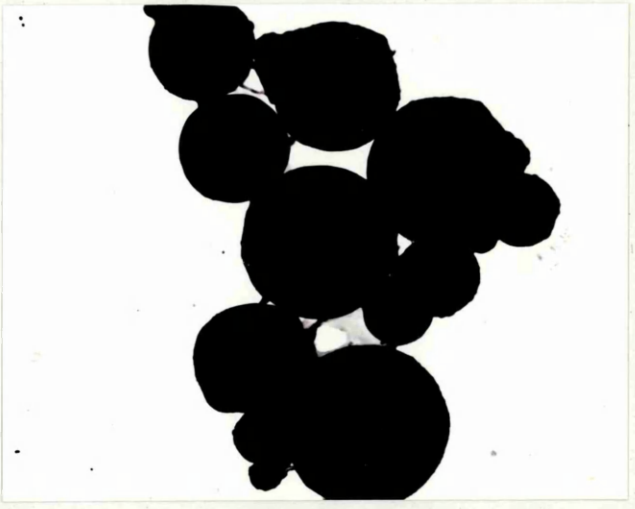

Figure 19. Electron Micrograph of Carbonyl Iron powder

(x4,000)

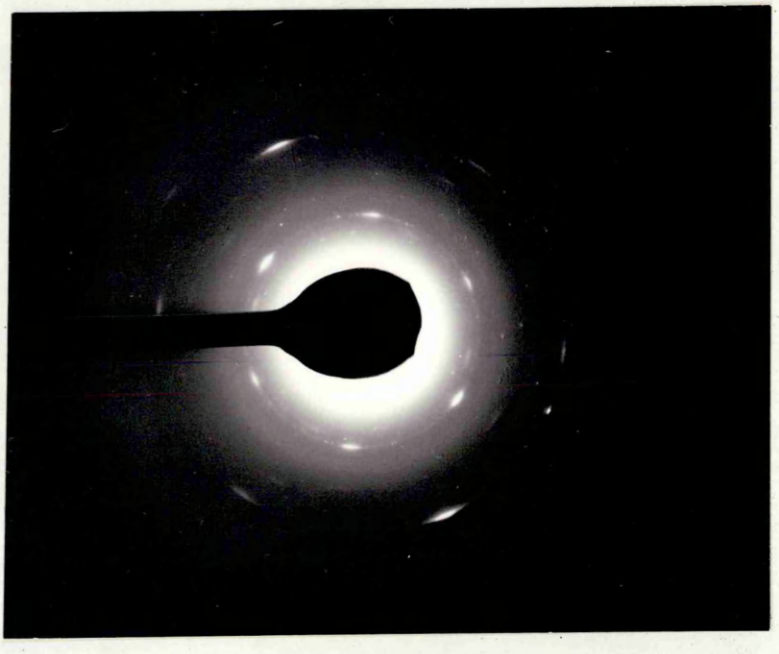

Figure 20. Diffraction Pattern of oxide obtained from decomposition of Ferrous Oxalate.

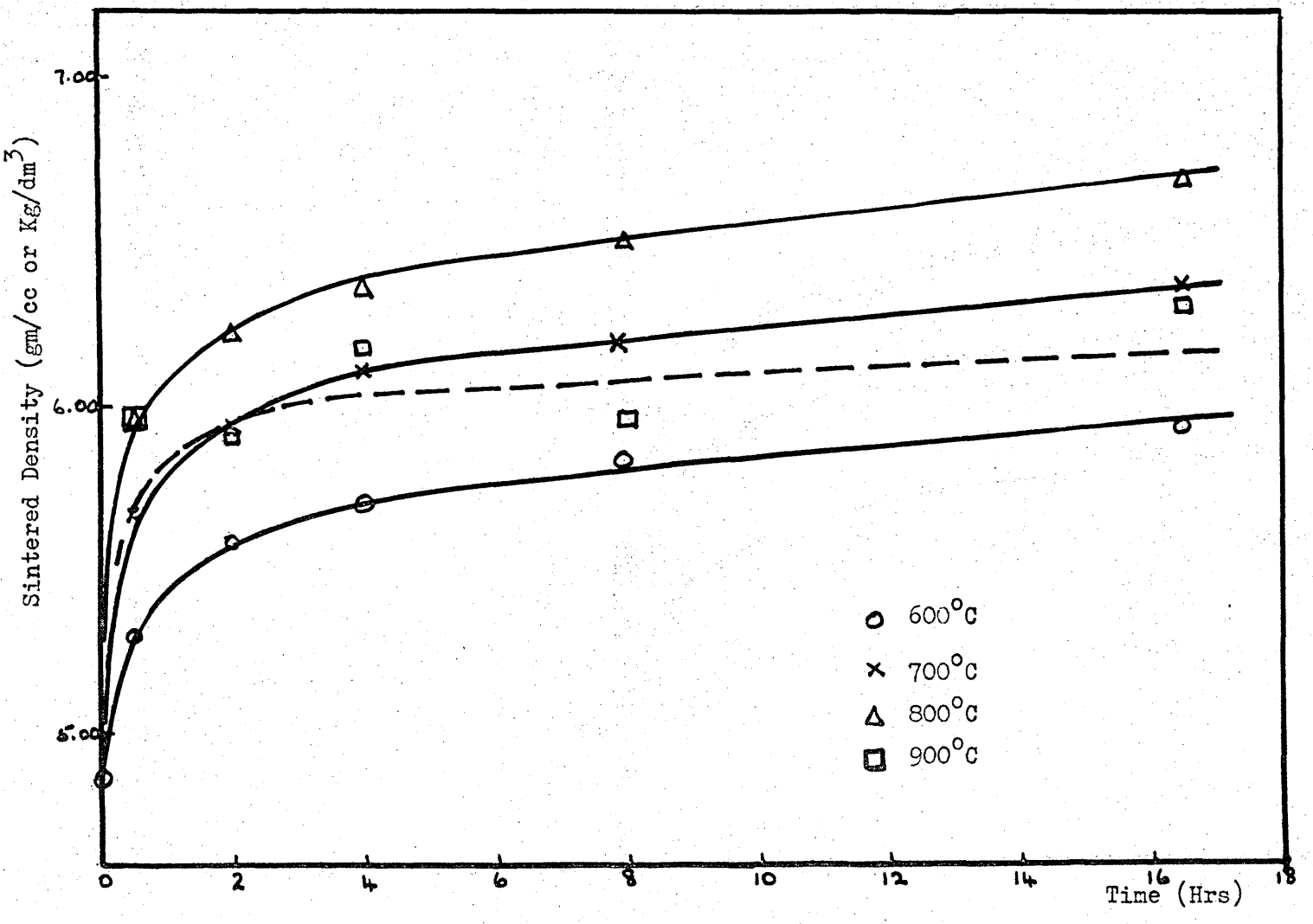

Figure 21. Isothermal Sintering Curves for Iron Powder produced from High Purity Iron Oxide at 300°C and pressed at 15 tsi (231MN/m^2)

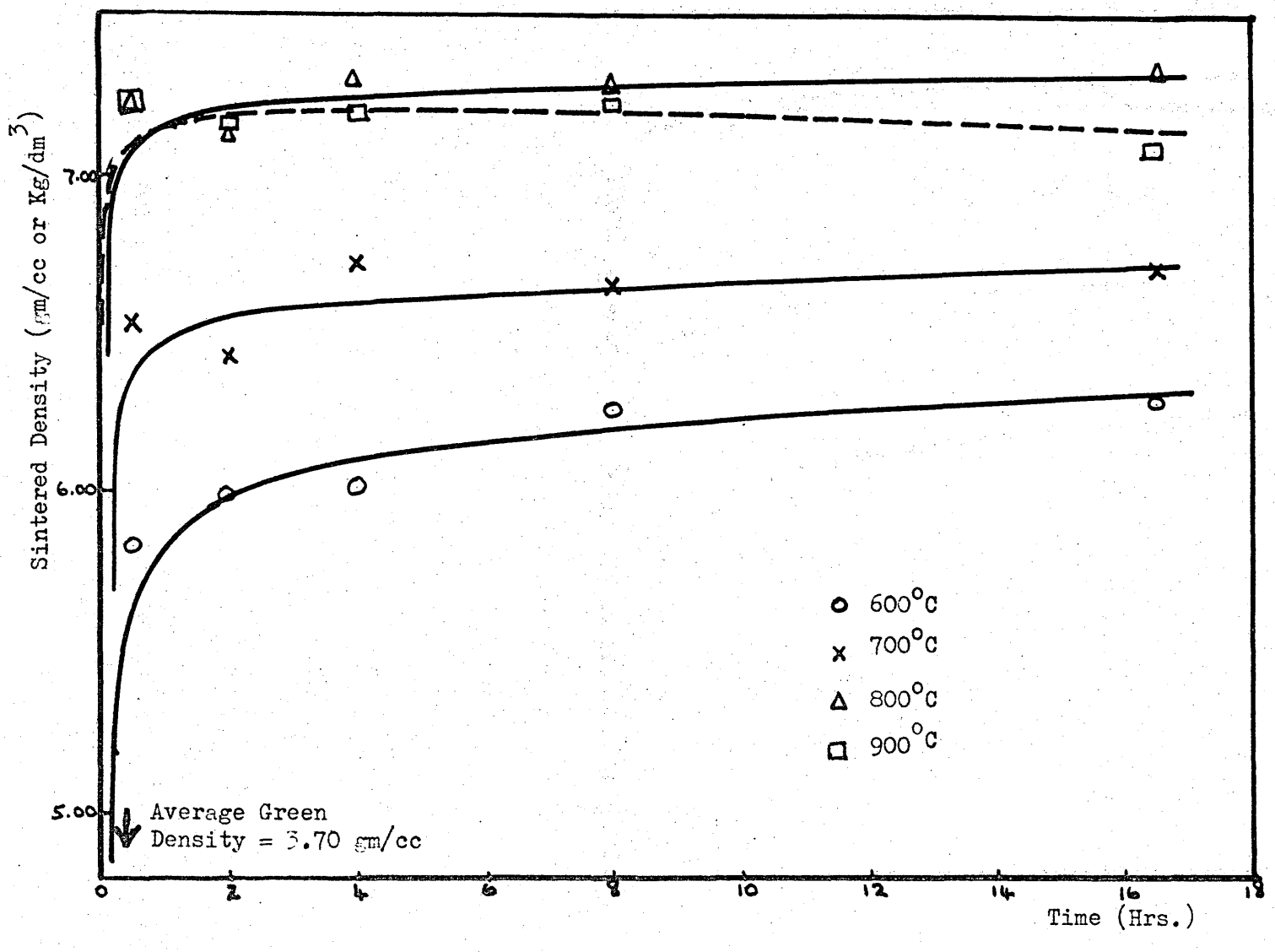

Figure 22. Isothermal Sintering Curves for Iron Powder produced from Ferrous Oxalate at 300°C and pressed at 15tsi (231 MN/m^2)

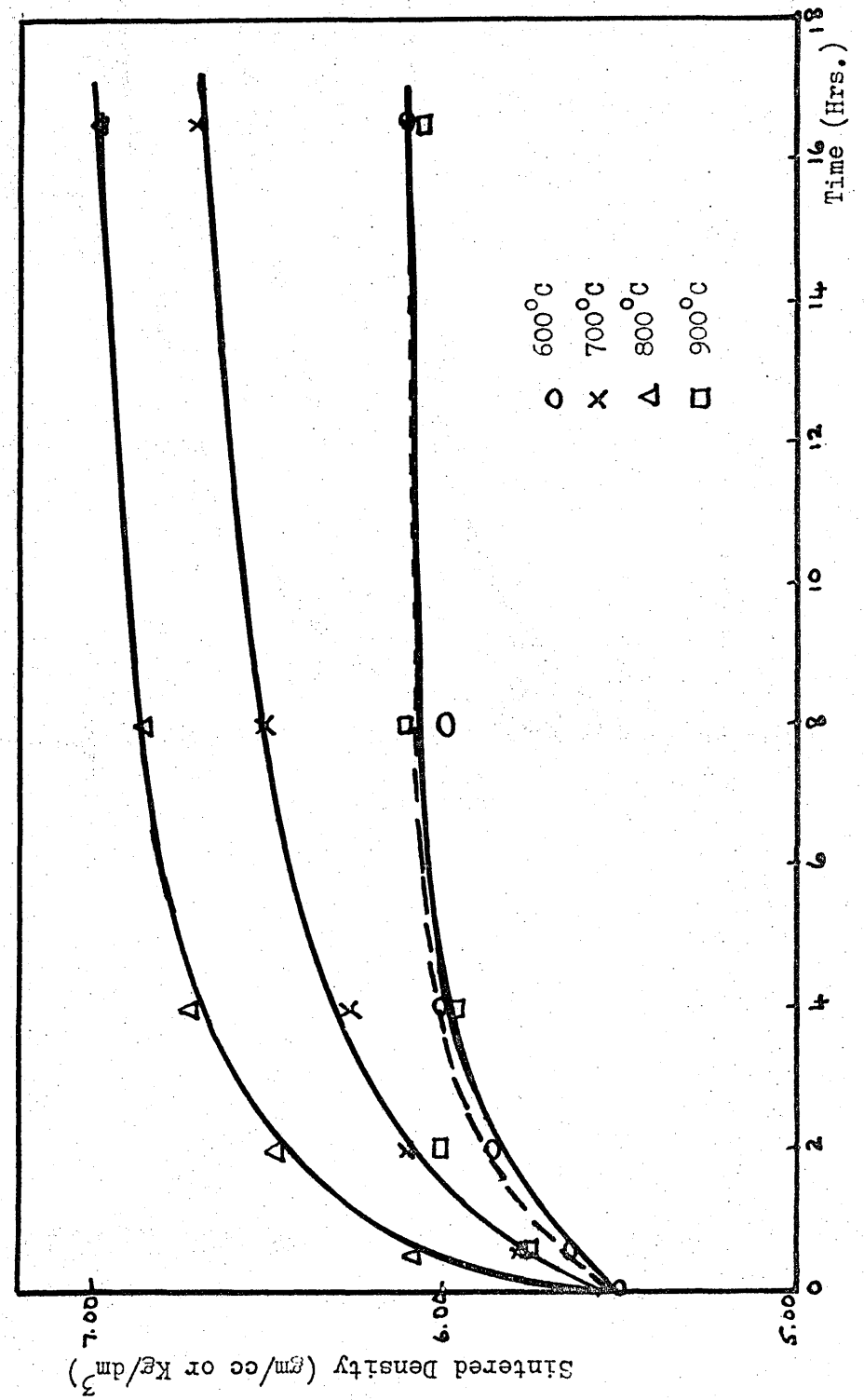

Figure 23. Isothermal Sintering Curves for Iron Powder (ex Iron Carbonyl) pressed at 15tsi (231MN/m^2)

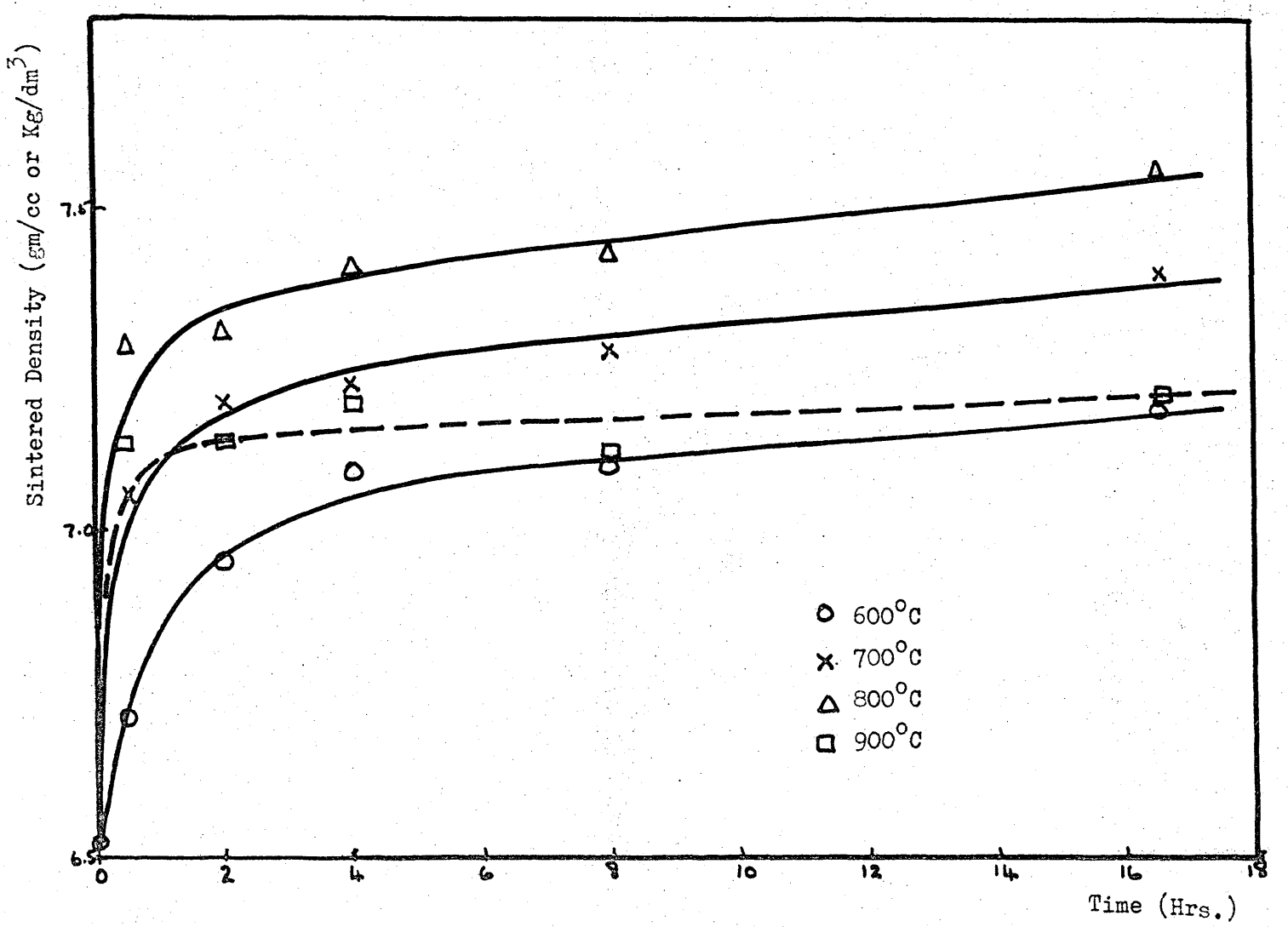

Figure 24. Isothermal Sintering Curves for Iron Powder produced from High Purity Iron Oxide at 300°C and pressed at 50tsi (770MN/m^2)

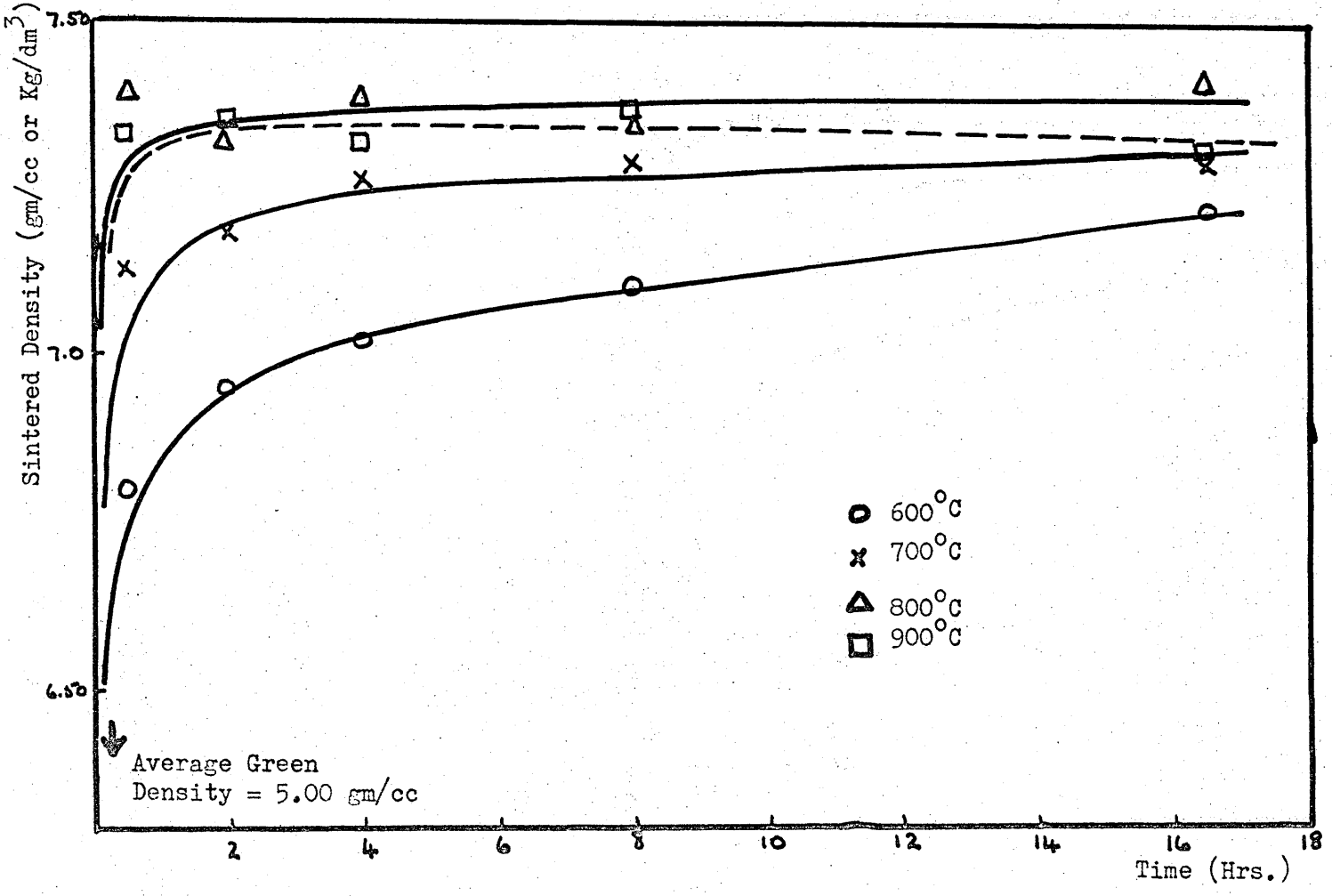

Figure 25. Isothermal Sintering Curves for Iron Powder produced from Iron Oxalate at 300°C and pressed at 50tsi (770 MN/m^2)

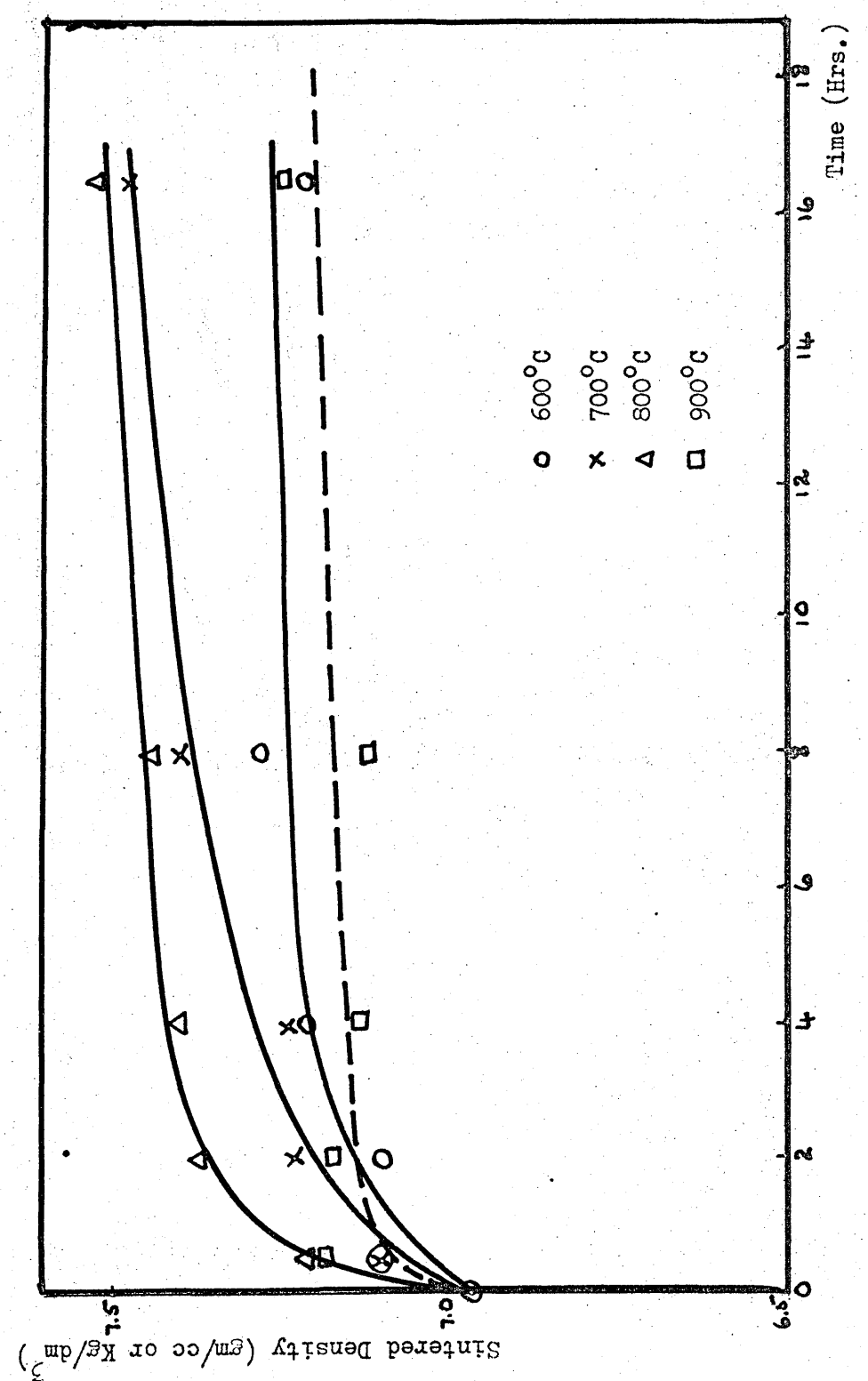

Figure 26. Isothermal Sintering Curves for Iron Powder (ex Iron Carbonyl) pressed at 50 tsi (770 MN/m^2)

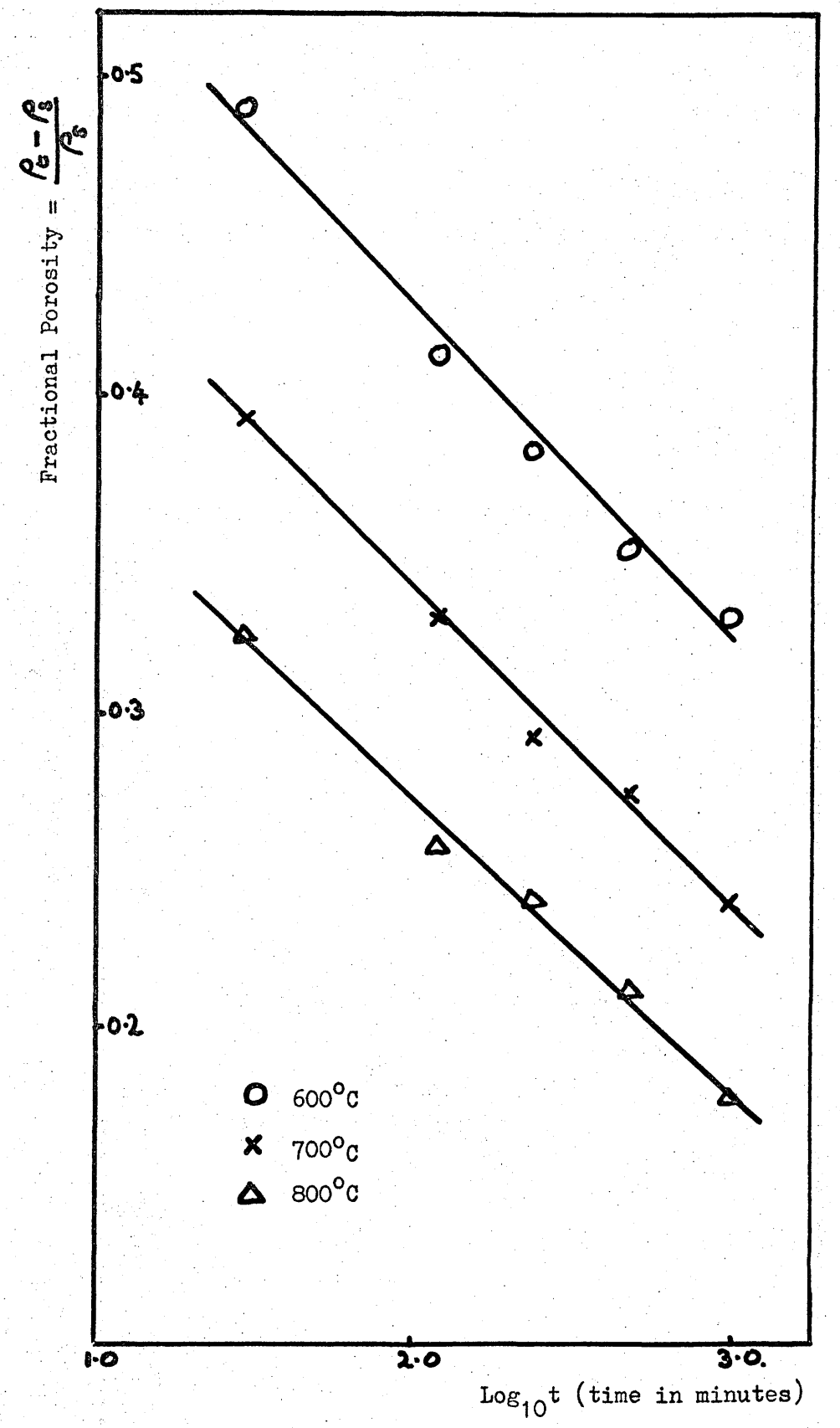

Figure 27. Semi Logarithmic Plot of the Sintering Data for Iron Powder ex High Purity Oxide pressed at 15tsi (231 MN/m^2)

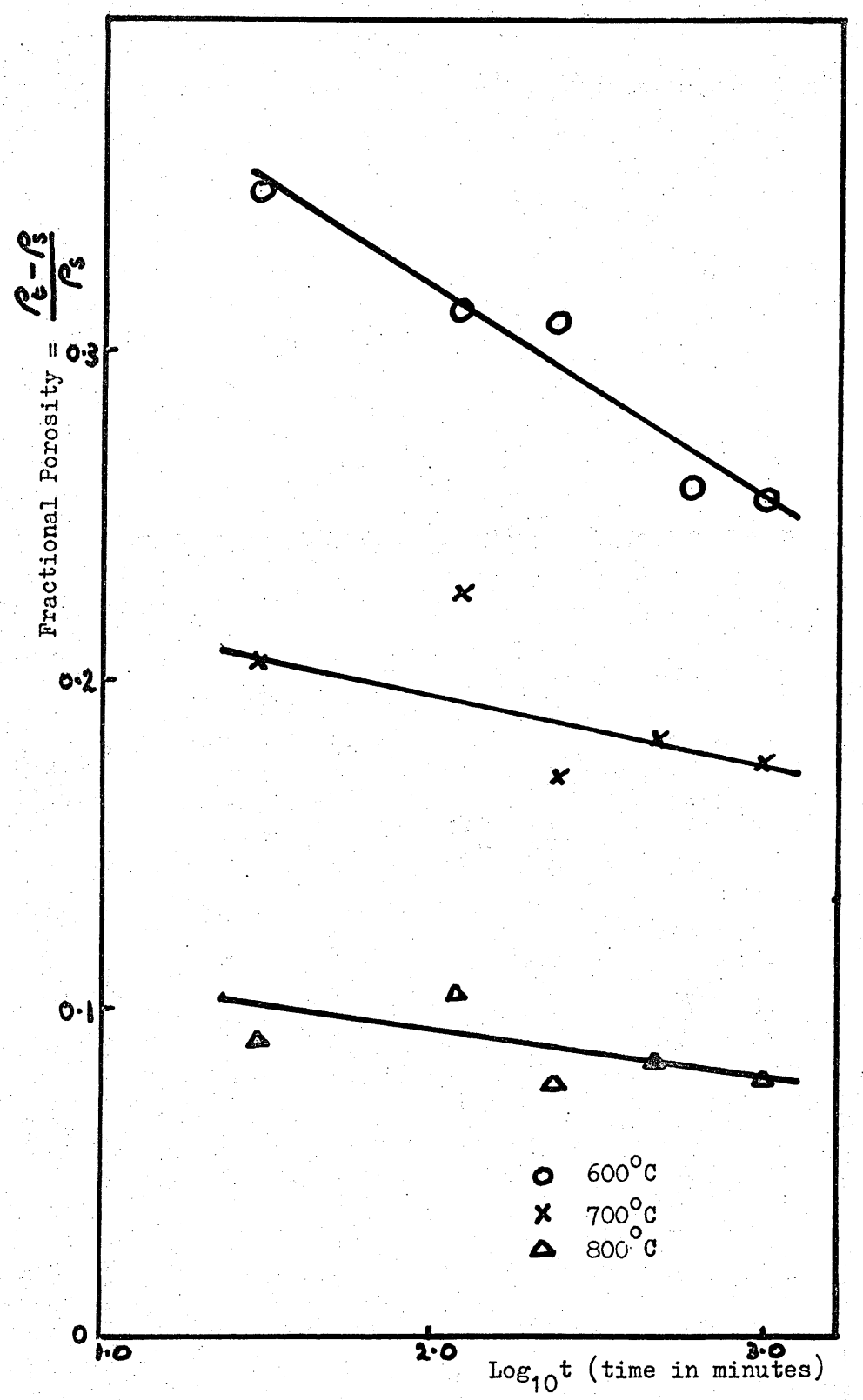

Figure 28. Semi Logarithmic Plot of the Sintering Data for Iron Powder ex Ferrous Oxalate pressed at 15tsi (231 MN/m^2)

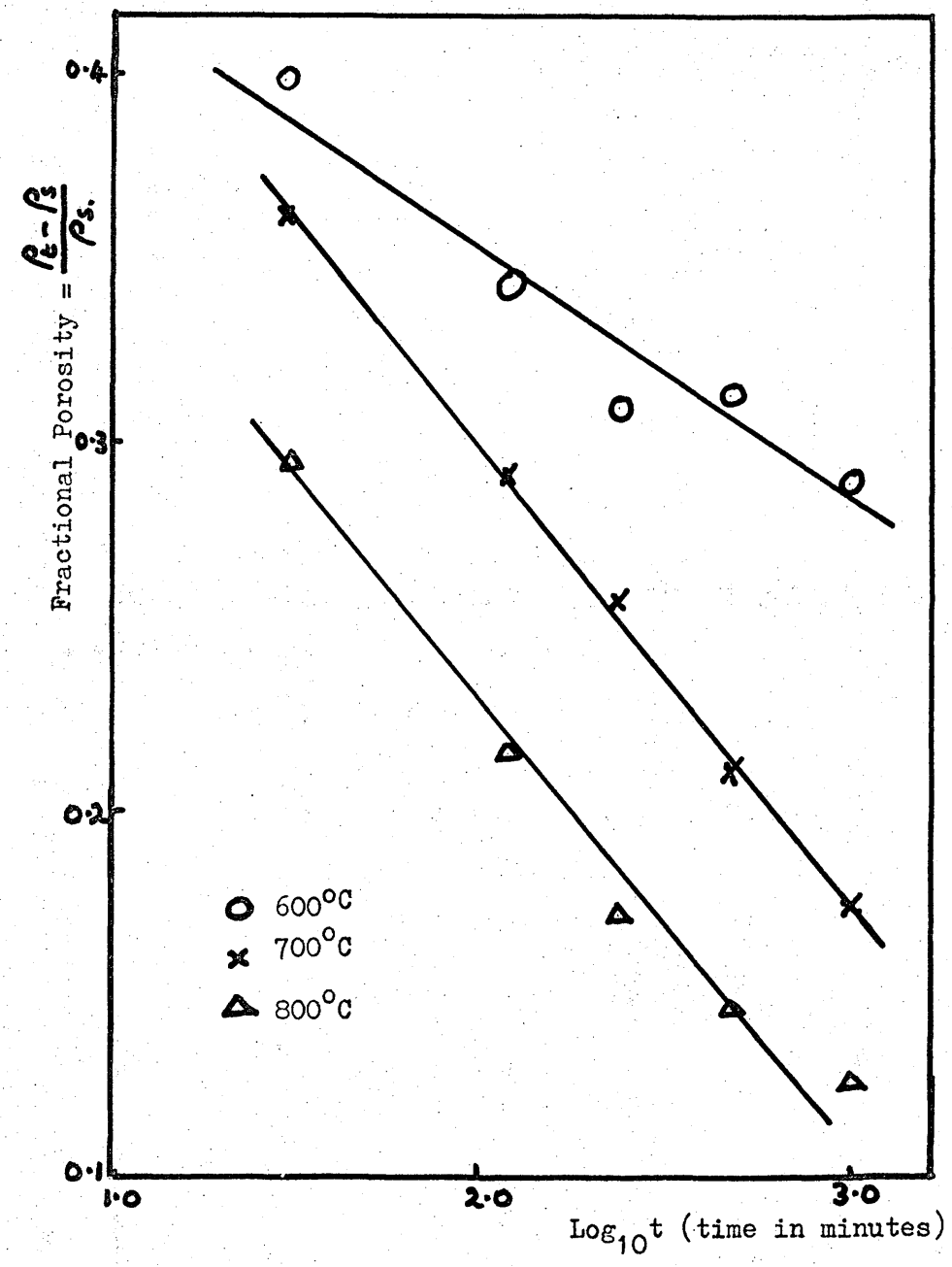

Figure 29. Semi Logarithmic Plot of the Sintering Data for Carbonyl Iron Powder pressed at 15tsi (231 MN/m^2)

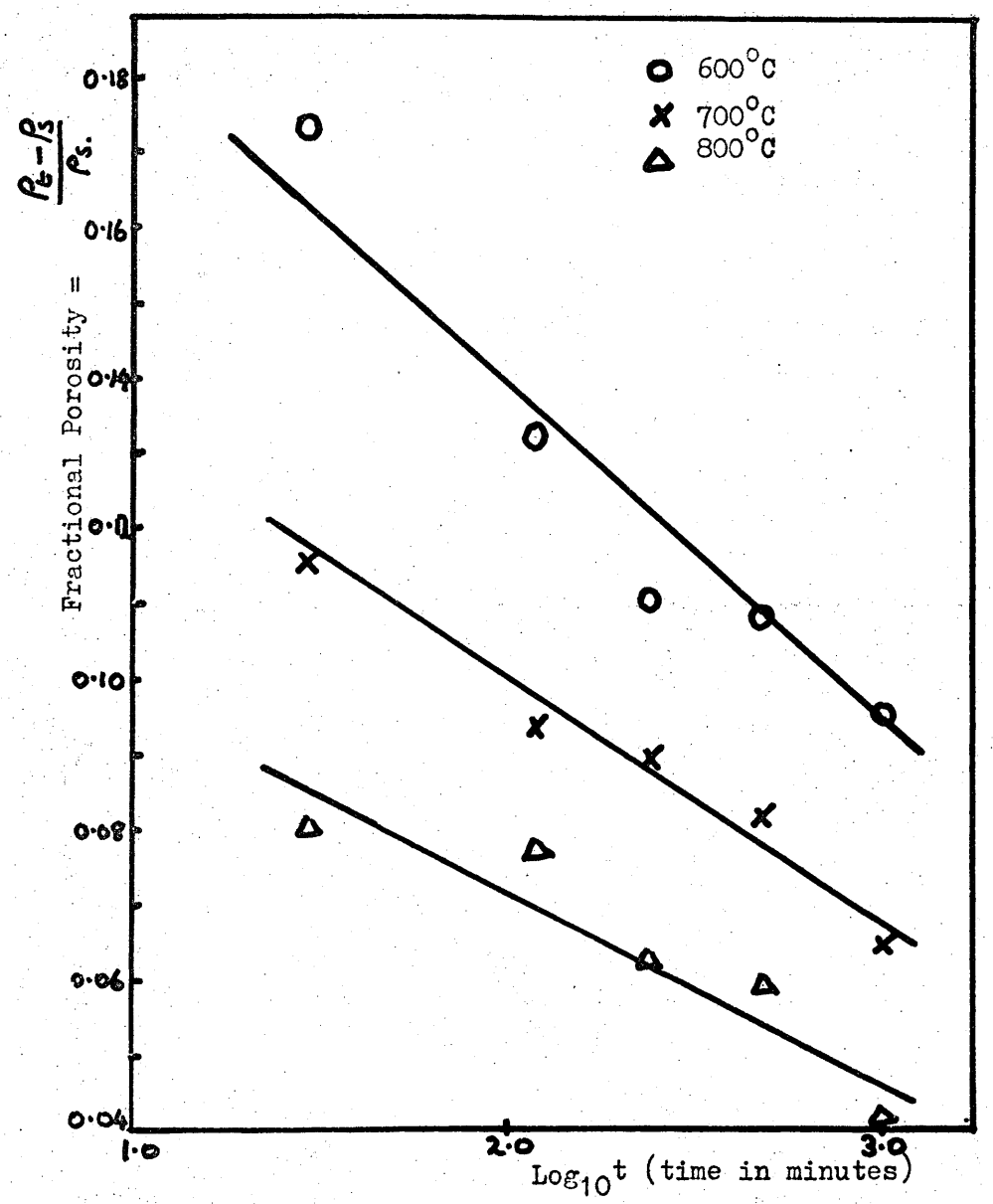

Figure 30. Semi Logarithmic Plot of the Sintering Data for Iron Powder ex High Purity Iron Oxide pressed at 50tsi (770 MN/m^2)

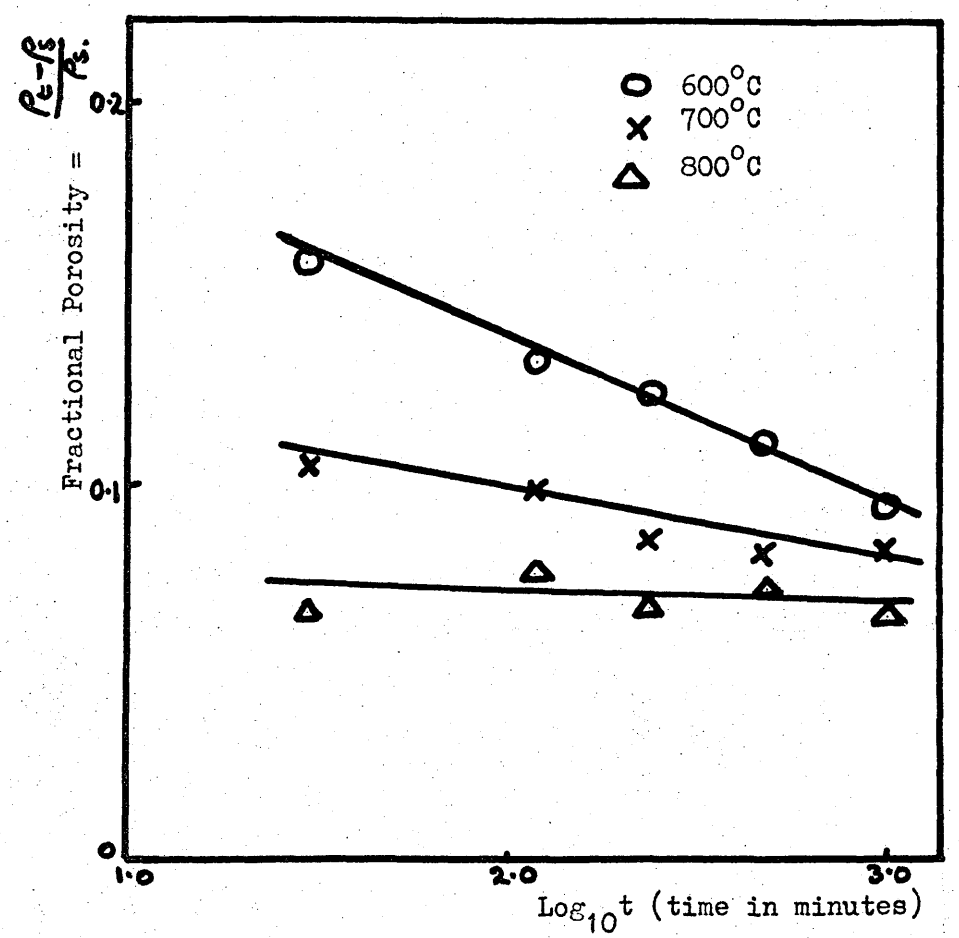

Figure 31. Semi Logarithmic Plot of the Sintering Data for Iron Powder ex Ferrous Oxalate pressed at 50tsi (770 MN/m^2)

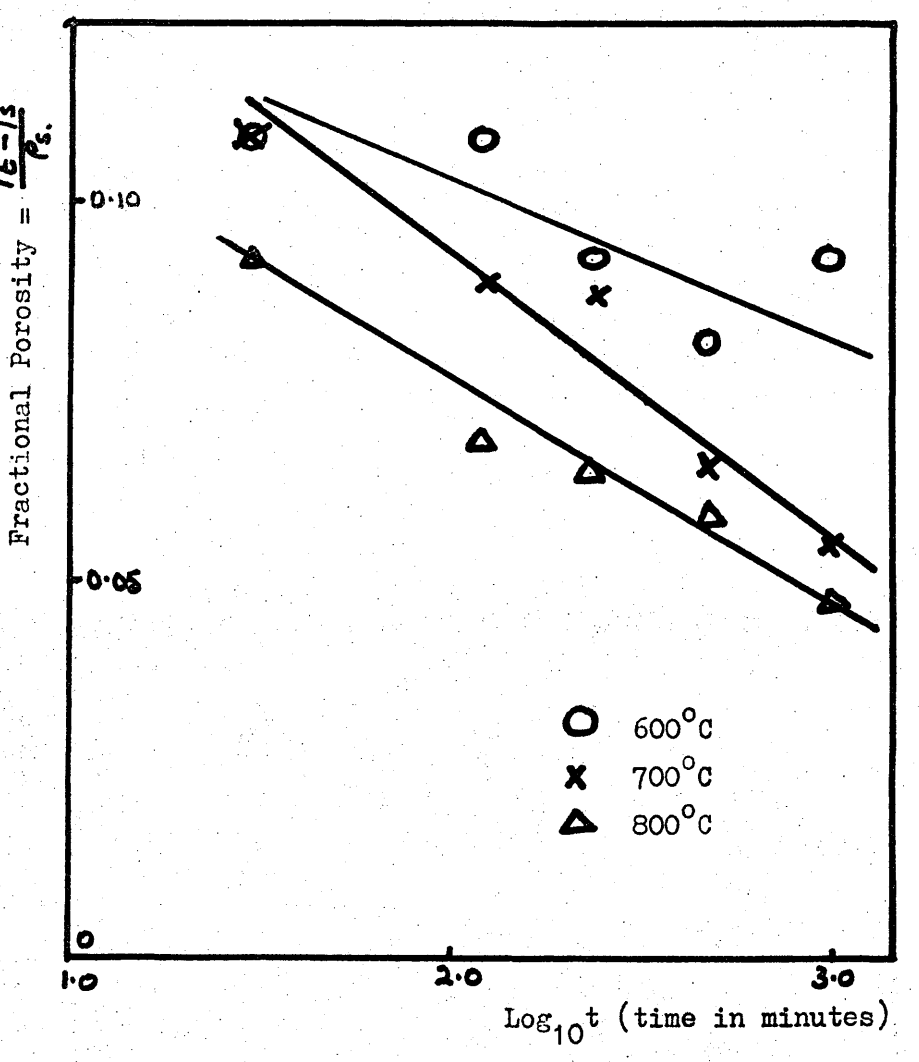

Figure 32. Semi Logarithmic Plot of the Sintering Data for Carbonyl Iron Powder pressed at 50tsi (770MN/m^2)

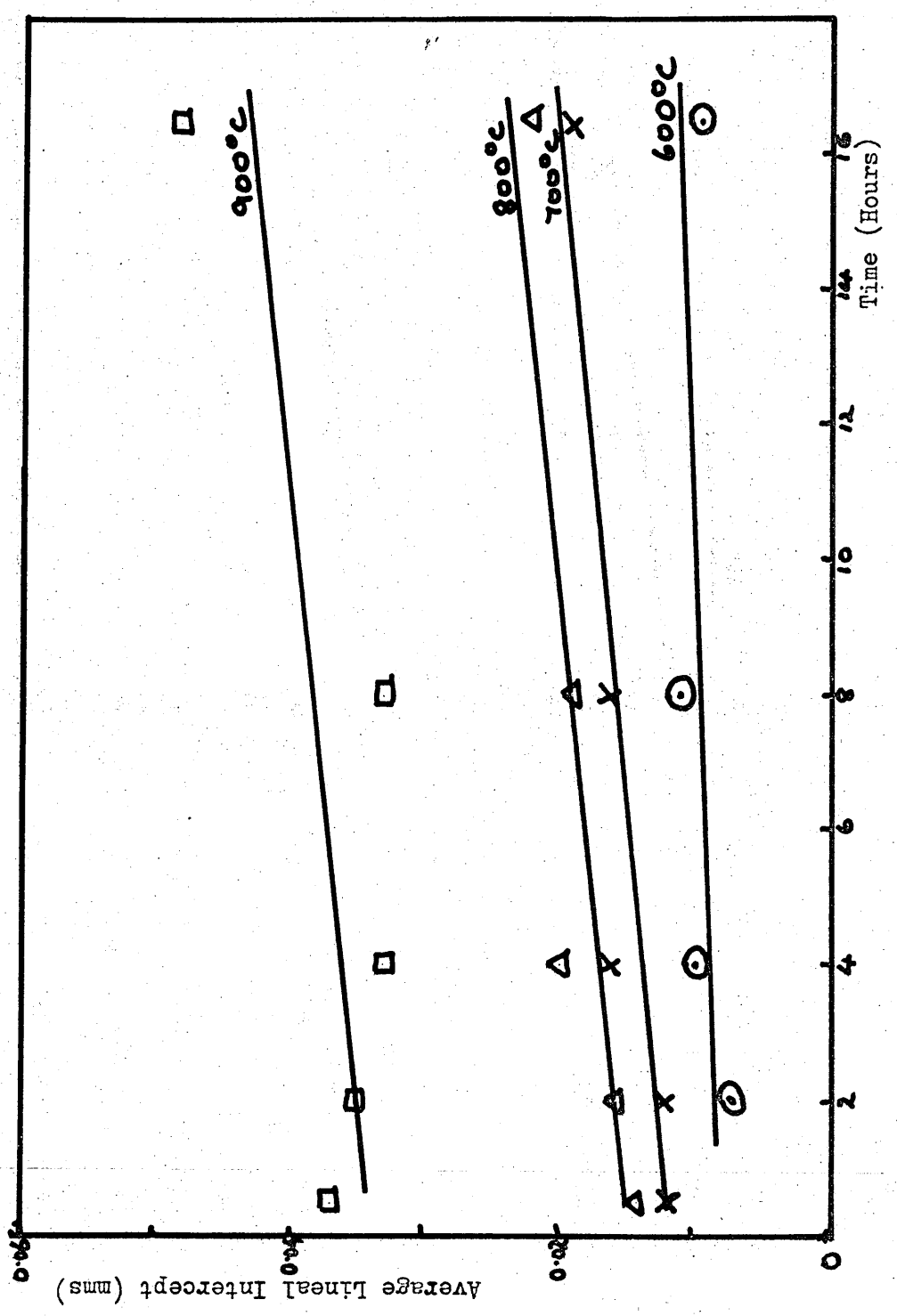

Figure 33. Grain Size Measurements on Iron Powder, ex High Purity Oxide, pressed at 15tsi (231 MN/m^2)

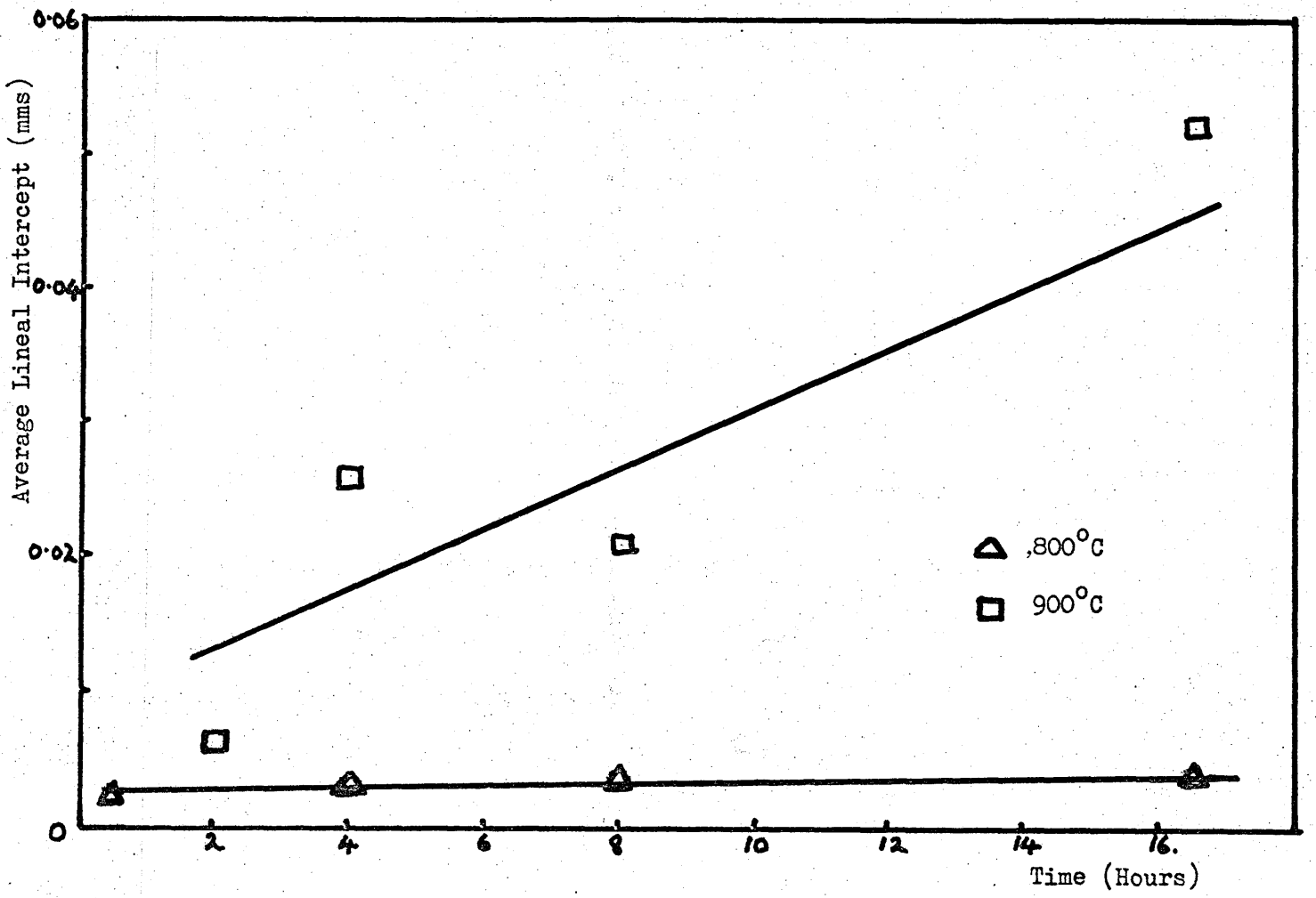

Figure 34. Grain Size Measurements on Iron Powder, ex Ferrous Oxalate, pressed at 15tsi (231 MN/m^2)

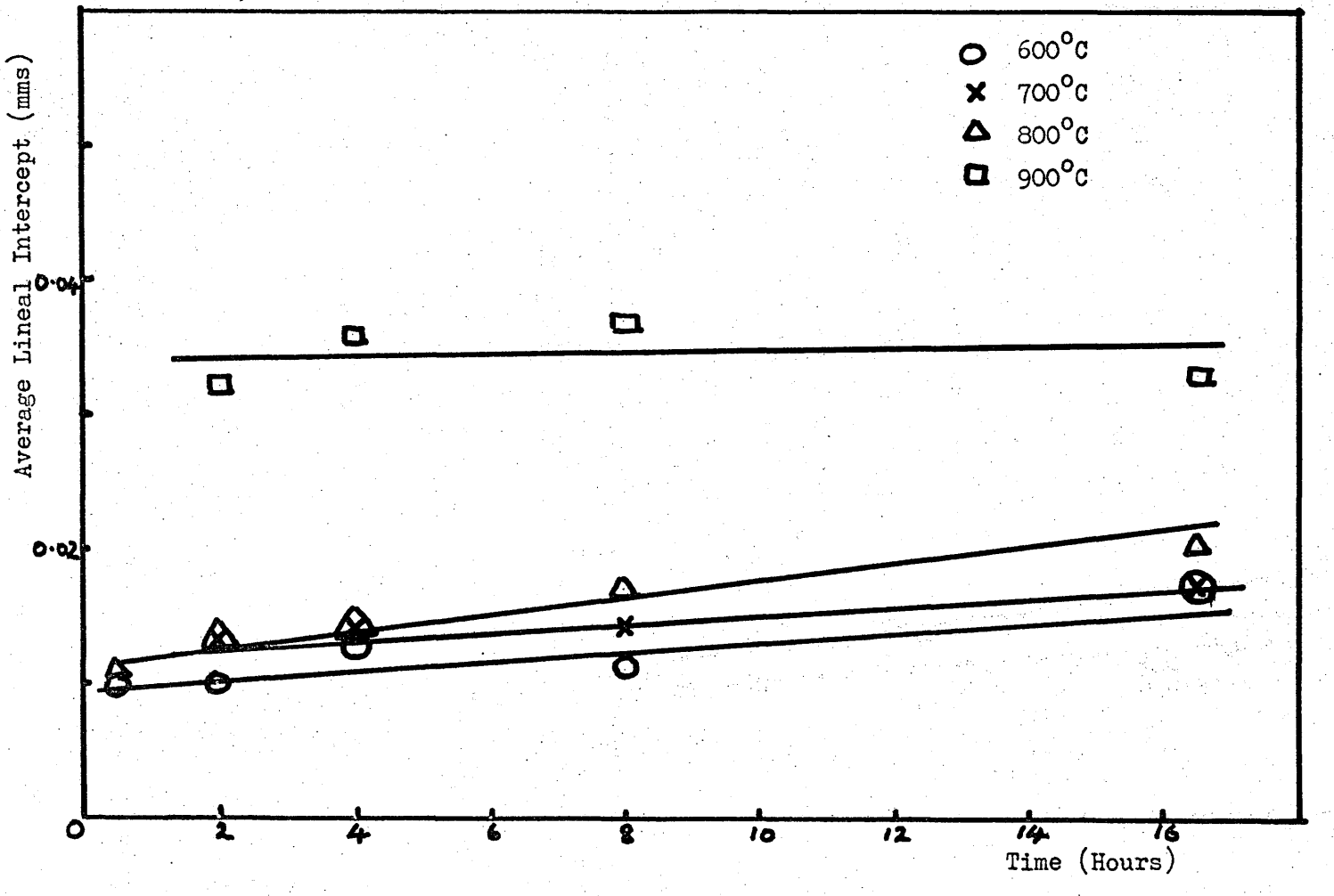

Figure 35. Grain Size Measurements on Iron Powder for Carbonyl Iron Powder, pressed at 15tsi (231 MN/m^2)

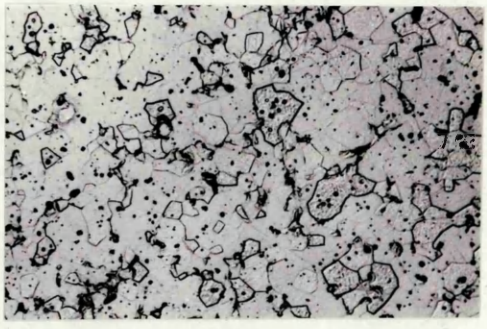

Etch 2% Nital.

Figure 36. Iron Powder, ex High Purity Oxide

Sintered 16½ hours at 800°C. (Pressed 15 t.s.i.) (x250 approx)

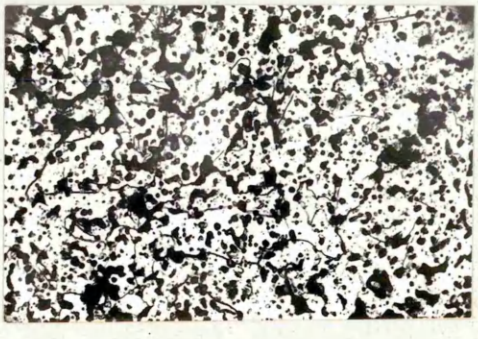

Etch 2% Nital.

Figure 37. Iron Powder, ex High Purity Oxide (x250 approx)

Sintered Two Hours at 900°C. (Pressed 15 t.s.i.)

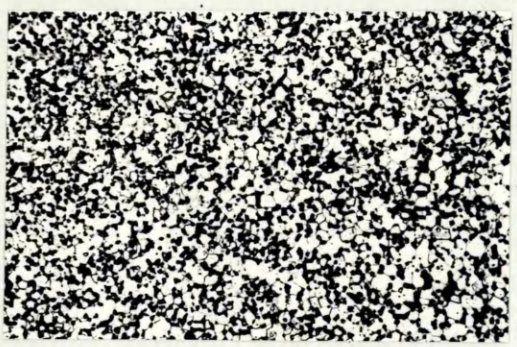

Etch 2% Nital.

Figure 38. Iron Powder, ex Ferrous Oxalate, (x200 approx)
Sintered 8 hours at 800°C. (Pressed 15 t.s.i.)

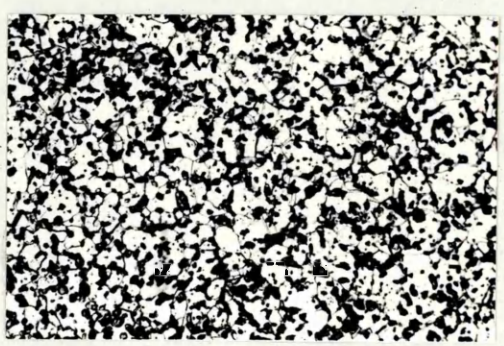

Etch 2% Nital.

Figure 39. Iron Powder, ex Ferrous Oxalate, (x200 approx)
Sintered 8 hours at 900°C. (Pressed 15 t.s.i.)

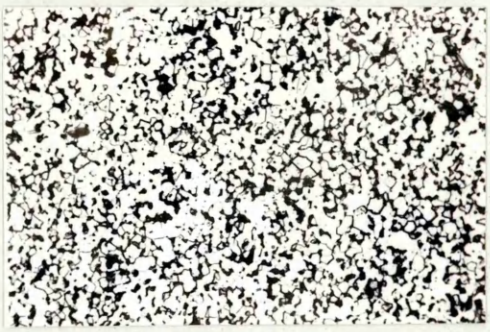

Etch 2% Nital.

Figure 40. Carbonyl Iron Powder, sintered 16½ hours (x200 approx) at 600°C. (Pressed 15 t.s.i.)

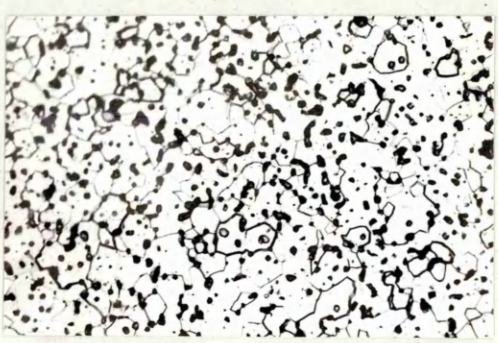

Etch 2% Nital

Figure 41. Carbonyl Iron Powder, sintered 16½ hours (x200 approx) at 800°C (Pressed 15 t.s.i.).

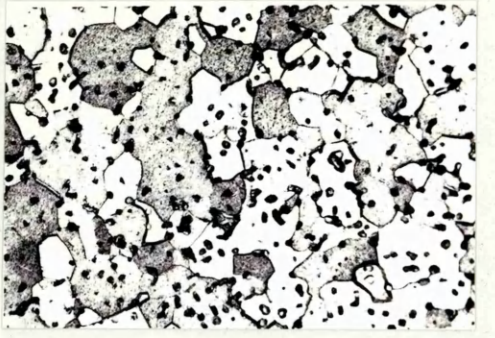

Etch 2% Nital.

Figure 42. Carbonyl Iron Powder, sintered 16½ hours (x200 approx) at 900°C. (Pressed 15 t.s.i.)

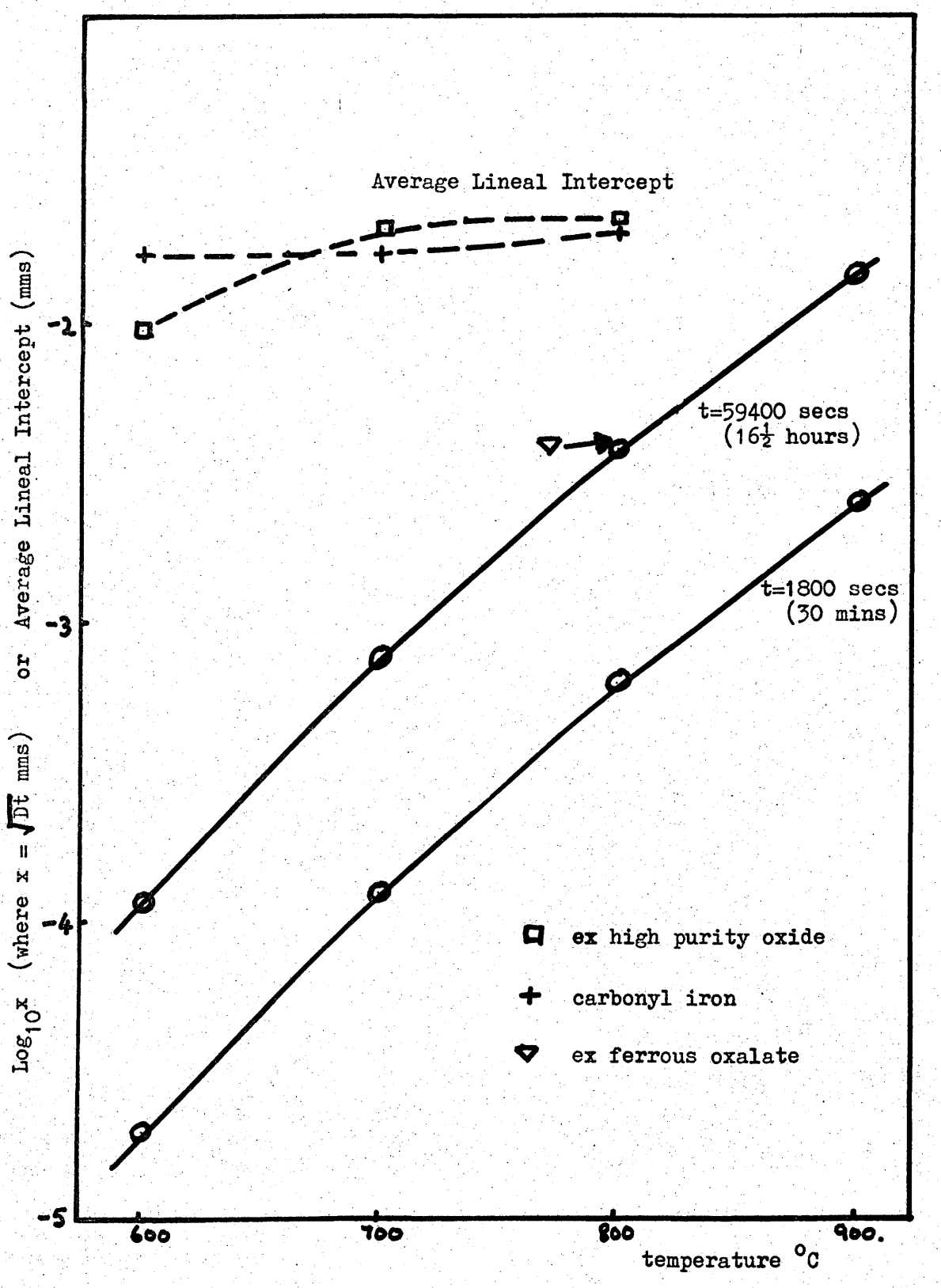

Figure 43. Comparison of Diffusion Distances attained by Volume Diffusion, with the maximum grain size in the powders after sintering at different temperatures

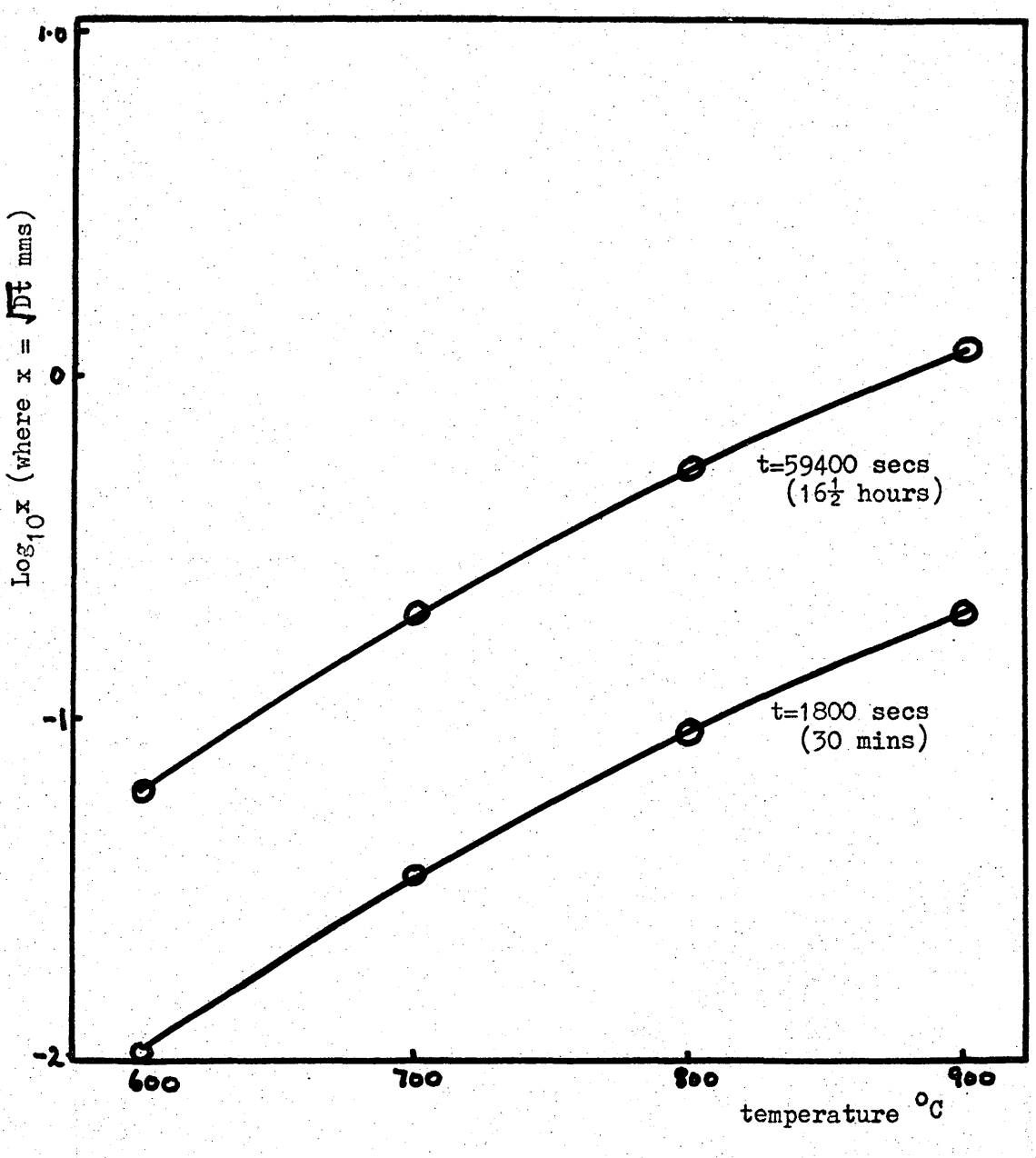

Figure 44. Diffusion distances attained under Grain Boundary Diffusion conditions, at different temperatures

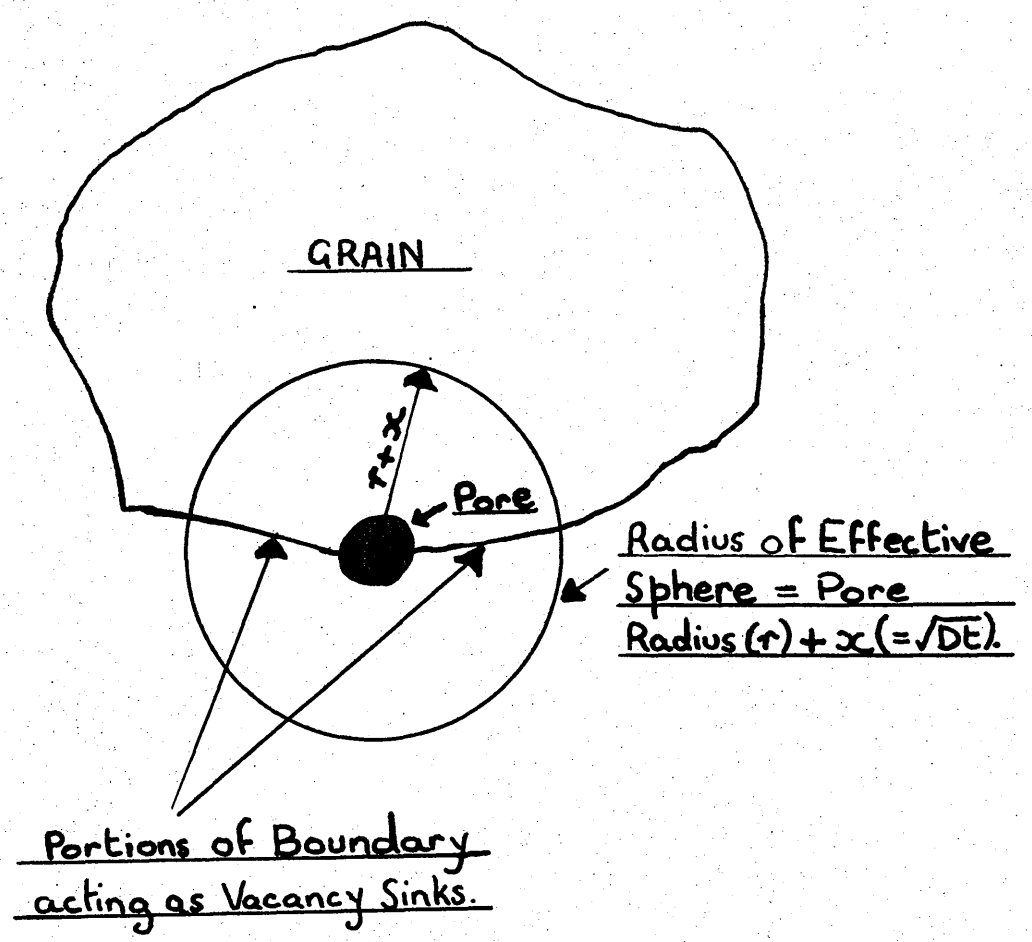

Figure 45. Diagram showing effective area of boundary operating as a Vacancy Sink under Volume Diffusion conditions

REFERENCES

1. F. Thummler and W. Thomma, "The Sintering Process". Metallurgical Review No. 115, 1967.

2. R.C. Smith, J. Chem. Soc. 123, 1923, 2088.

3. W. Eitel, "The Physical Chemistry of the Silicates". University of Chicago Press, 1954.

4. W.D. Jones, "Principles of Powder Metallurgy". Edward Arnold, 1937.

5. C.G. Goetzel, "Treatise on Powder Metallurgy", vols, I - III. Interscience Publishers, 1949 - 1952.

6. J. Frenkel, J. Physics, U.S.S.R. 9, 1945, 385.

7. G. Kuczynski, Trans. Amer. Inst. Min. Met. Eng. 185, 1949, 169. J. Appl. Physics 21, 1950, 632.

8. H.H. Hausner, "The Role of Surface Diffusion in Powder Metallurgy Sintering". Second International Powder Metallurgy Conference Report, Czechoslovakia 1966.

9. R.L. Coble and J.E. Burke, "Progress in Ceramics Science". (Ed. J.E. Burke) Vol. III p.197, 1963. Pergammon Press.

10. F.N. Rhines, Proc. Metal Powders Association, 1958. P.91.

11. G. Kuczynski, "Powder Metallurgy", (Ed. W. Leszynski). Interscience Publishers, 1961.

12. C. Herring, J. Appl. Physics, 21, 1950, 301.

13. R.G. Bernard, Powder Metallurgy 3, 1959, 86.

14. B. Ya Pines, Uspekhi Fiz. Nauk. 52, 1954, 501.

15. N. Cabrera, Trans. Amer. Inst. Min. Met. Eng. 188, 1950, 667.

16. P. Schwed, ibid, 191, 1951, 245.

17. R.T. de Hoff, D.R. Baldwin and F.N. Rhines, Planseeber Pulvermet 10, 1962, 24.

18. G.D. Rieck and J.G.R. Rockland, ibid, 13, 1965, 3.

19. B. Clapson and D.A. Robins, Powder Metallurgy 3, 1959, 72.

20. R.S. Barnes, Phil. Mag. 43, 1952, 1221.

21. L. Seigle, "Kinetics of High Temperature Processes", (Ed. W. Kingery) p.172, 1959. John Wiley.

22. A.L. Pranatis and L. Seigle, "Powder Metallurgy" (Ed. W. Leszynski) p.53, 1961. Interscience Publishers.

23. H. Fischmeister & R. Zahn. "Berichte uber die II Internat Pulvermet Tagung (Eisenach 1961) p.77 1962. Berlin (Akademie Verlag).

24. H. Fischmeister & R. Zahn "Modern Developments in Powder Metallurgy" Ed. H.H. Hausner. Vol II Applications 1966 New York (Plenum Press) p.12.

25. T.L. Wilson & P.G. Shewmon, Trans. Met. Soc. A.M.I.E. 236 1966, 49.

26. J.G.R. Rockland, Acta Metallurgica 14, 1966, 1273.

27. F.A. Nichols, Acta Metallurgica 15, 1967. Summary Issue No. 267.

28. L.F. Norris & G. Parravano, J.Amer. Ceram. Soc. 46, 1963, 449.

29. J. Brett & L. Seigle, Acta Metallurgica 14, 1966, 575.

30. J.K. Mackenzie & R. Shuttleworth, Proc. Phys. Soc. (London) 62, 1949, 833.

31. P.W. Clark, J.H. Cannon & J. White. Trans. Brit. Ceram. Soc. 52, 1953, 1.

32. B. Ya Pines, Physics of Metals, Metallography, 16, 1963, 55.

33. F.V. Lenel & G.S. Ansell. "Modern Developments in Powder Metallurgy" Ed. H.H. Hausner. Vol.1 "Fundamentals and Methods", 1966, New York. Plenum Press p.281.

34. F.R.N. Nabarro "Conference on the Strength of Solids". Physical Society London 1948.

35. C. Herring, J. Appl. Physics 21, 1950, 437.

36. B.H. Alexander & R.W. Baluffi Acta Met. 5, 1957, 666.

37. Kuczynski, G. "Theory of Residual Porosity in Powder Compacts" Powder Metallurgy, 1963 No. 12, p.1.

38. Kuczynski, G. & Ichinose, H. Unpublished work referred to in Ref. 39.

39. C.S. Smith, Trans. Amer. Inst. Min. Met. Eng. 175, 1948, 15.

40. N.A.L. Mansour & J. White. Powder Met. 12, 1963, 108.

41. W.D. Kingery & B. Francois J. Amer. Ceram. Soc. 48, 1965, 546.

42. H. Ichinose & G.C. Kuczynski. Acta Met. 10, 1962, 209.

43. C.B. Jordan & P. Duwez Trans. A.I.M.E. 188, 1950, 943.

44. M. Oxley and G. Cizeron, International J. Powder Met. 1, 1965, 15.

45. G. Cizeron and P. Lacombe, Compte Rend. 240, 1955, 427.

46. G. Cizeron, ibid 244, 1957, 2047.

47. C. Leymonie, Mlle. Lebrun and G. Cizeron, Memoires Scientifiques Rev. Metallurgy LXIII No.3, 1966.

48. G. Cizeron, J. Hui and C. Breugnot, ibid, LX No.11, 1963.

49. G. Bockstiegel, G. Masing and G. Zapf, J. Appl. Sci. Res. 4, 1954, 284.

50. N.C. Kothari, Ph.D. Thesis, referred to in Riso report No. 89, July 1964, of the Danish Atomic Energy Commission.

51. H.D. Dietze, Tech. Mitt. Krupp. 17, (3), 1959, 103.

52. S.L. Forss Ref. 24 Vol II p.3.

53. M.H. Tikkanen & S.A. Makipirtti. Internat J. Powder Met. 1, 1965, 15.

54. C.E. Birchenall & R.F. Mehl, Trans. A.I.M.E. 188 (1950), 144 and 1374.

55. F.S. Buffington, J.D. Bakalar & M. Cohen, The Physics of Powder Metallurgy, McGraw Hill (New York 1951), 92 - 107.

56. V.M. Golikov & V.T. Borisov. Promlemii Metallovedeniia i Fiziki Metallov, 1955, 528.

57. A.A. Joukhovitsky & V.A. Geodakyan, S. do Metallourgisdat, 1955, 267.

58. I.B. Borovsky, I.H. Miller and A.P. Tcherbakov, S. Isledovantai p o Jaroprotchnin Splabam (1957), Iz, Akad, Navk S.S.S.R., 2 (I.R.S.I.D. translation T 1070).

59. R.J. Borg & C.E. Birchenall, Trans. A.I.M.E. 218, 1960, 980.

60. C. Leymonie & P. Lacombe, Rev. Met. 55, 1958, 524.

61. F.S. Buffington, K. Hirano & M. Cohen, Acta Met., 9, 1961, 434.

62. P.L. Gruzin, Problemii Metallovedeniia i Fiziki Metallov 1952, Iz. Akad. Nauk. S.S.S.R. 1953, 383.

63. H.W. Mead & C.E. Birchenall, Trans. A.I.M.E., 206, 1956, 1336.

64. P. Lacombe, P. Guiraldenq & C. Leymonie, 2nd UNESCO Radioisotope Conference (Copenhagen, 1960).

65. C. Leymonie and P. Lacombe, Rev. Met. 56, 1959, 74.

66. C. Leymonie, Y. Adda, A. Kirianenko & P. Lacombe, Compt. Rend. Acad. Sci. 248, 1959, 1512.

67. S.Z. Bokstein, S.T. Kishkin and L.M. Moroz, Conf. Int. Radioisotopes, UNESCO (Paris 1957). Memoire RIC/193.

68. C. Leymonie, P. Lacombe and Libanti, C.C.R. Acad. Sci., Paris 246, 1958, 2614.

69. D.W. James & G.M. Leak. To be Published. Quoted in Grain Boundaries and Surface Properties of Metals by G.M. Leak. Prog in Applied Materials Research. 4, 29.

70. K. Torkar, H.J. Oel & A. Illigen. Ber Dent Keram Ges 43, 1966. 162.

71. R.L. Coble. Journal of Applied Physics, 32 No.5, 1961. 787 - 799.

72. H. Fischmeister, International Symposium on "Metallurgie des Poudres", (Paris 1964), St. Germain en Laye, (Editions Metaux), 1966.

73. F. Thummler & W. Thomma. Ref. 26, 1, 361.

74. P.E.D. Morgan & A.J.E. Welch. Ref. 20 p.105.

75. R.A. Brown. Amer. Ceram. Soc. Bull. 44, 1965, 483.

76. R.A. Brown ibid p.693.

77. J. Amer. Ceram. Soc. 48, 1965, 627.

78. E.C. Duderstadt & J.F. White. Amer. Ceram. Soc. Bull. 441, 1965, 907.

79. P. Ram, H.S. Gadiyar & P.K. Jena, J. Less Common Metals 10, 1966, 185.

80. J.T. Smith, J. Appl. Physics, 36, 1965, 395.

81. T. Vasilos & J.T. Smith, ibid 35, 1964, 215.

82. G. Bockstiegel, Int. Journal of Powder Met. 2, (4) 1966.

83. M.M. Tikkanen & S. Ylasaari. Ref. 26 Vol. I Fundamentals.

84. M.G. Nicholas, Trans. Met. Soc. A.I.M.E. 227, 1963, 250.

85. B. Ya Pines, A.F. Sirenko, N.I. Sukhinin Zhur Tekhn Fiziki 27, 1957, 1893.

86. A.R. Poster & H.H. Hausner, Industrial Heating May 1966. 841 - 850.

87. P. Ramakrishnan & G.S. Tendolkar. Powder Met. 7, (13). 1964, 34.

88. L.E. Russell, Powder Metallurgy 10, No.20. 1967, 239 - 263.

89. Rhines, Birchenall & Hughes, Trans. A.I.M.E. 188, 1950, 378.

90. C.A. Calow & C.R. Tottle, Powder Met. 8, 1965, 1 - 19.

91. E.H. Carman, Metallurgia October 1955, 165 - 168.

92. A.J. Shaler, J. Metals 15 (5) 1963, 355 - 357.

93. C.G. Goetzel & M.A. Steinberg. "A New Technology based on Submicron Powders". Vol.1 Ref. 26. p.194.

94. W.S. Cremens. "Use of Submicron metal & Non metal powders for Dispersion Strengthened Alloys". Ultra Fine Particles Symposium. Edited W.E. Kuhn. Published Wiley, p.457.

95. P.J. Clough. "Ultra fine Powders - Their Production and Characteristics", A.I.M.E. Symposium No. 23, "New Types of Metal Powders", H.H. Hausner, published Gordon & Breach, New York 1964.

96. H. Lamprey & R.L. Ripley, "Ultra fine Tungsten & Molybdenum Powders", J. Electrochem. Soc. 109 (8), 1962, 713 - 716.

97. M. Quatinetz, R.J. Schafer & C.R. Smeal, "The Production of Sub-micron Powders by Ball Milling with Grinding Aids". Ref. 96, p.271.

98. L.L. Szego & D.H. Houseman. Powder Metallurgy 8, 1965, 162.

99. A.D. Franklin & R.B. Campbell. J. Phys. Chem. 59, 1, 1955 65 - 67.

100. D.W. Aylmore & W.B. Jepson. J. Sci. Instruments 38, 1961, 156.

101. S. Brunauer, P.H. Emmett & E. Teller. J. Amer. Chem. Soc. 60, 1938, 309.

102. K.S.W. Sing & D. Swallow. Proc. Brit. Ceram. Soc. 5, 1965, 39.

103. J.M. Blakely & H. Mykura. "Metal Surfaces", American Society for Metals p.132.

104. J.M. Blakely & H. Mykura. Acta. Met. 10, 1962, 565.

105. C. Leymonie. "Radioactive Tracers in Physical Metallurgy", Chapman & Hall, 1963.

106. R.J. Borg & C.E. Birchenall, Trans A.I.M.E. 218, 1960, 980.

107. F.S. Buffington, K. Hirano & M. Cohen, Acta. Met. 9, 1961, 434.

108. M. Aucouturier, M.O. Pinheiro, R. de Castro & P. Lacombe, Acta. Met. 13, 1965, 125.

109. P. Guiraldenq, Compte Rendue, 254, 99, 1962, 1994.

110. M.J. Donachie & M.F. Burr. Journal of Metals, November, 1963, 849.

111. B.N. Singh. Powder Metallurgy 14, No.28, 1971, 277.

112. J.S. Hirschhorn & M.W. Garey. International Journal of Powder Metallurgy 5, 1969, 35.

113. R.W.K. Honeycombe. "The Plastic Deformation of Metals", Arnold 1968.

114. J.J. Bacmann & G. Cizeron. International Journal of Powder Metallurgy 5, (2) 1969, 39.

115. G. Matsumura. Acta. Metallurgica 19, August 1971, 851.

116. J.E. Hilliard. Metal Progress 85, 1964, 99.

117. M. Robbins, J.H. Swisher, H.M. Gladstone & R.C. Sherwood, J. Electrochem Soc. 117, (1), Jan. 1970, 137 - 139.

118. D.A. Everest, I.G. Sayce, & B. Selton. J. Materials Science 6 (3), March, 1971, 218 - 224.

119. M.A. Gussein, Yu. G. Kiryanov, N.S. Rabotnikov, A.S. Sakhiev and V.G. Syrkin, Sov. Powder Met. Metal Ceram. 12, (96) Dec. 1970, 962 - 965.

120. D. Dollimore and D. Nicholson. J. Chem. Soc. 1962, 960 - 965.

121. D. Dollimore, D.L. Griffiths & D. Nicholson. J. Chem. Soc. 1963, 2617 - 2623.

122. J. Amiel & Colette Malard, International Symposium on the Reactivity of Solids. Munich 1964. Published 1965, 614 - 622.

123. H. Frydrych. Polska Akad Nauk, Prace Kom Metal-Odlew 12, 1969 (Metalurgia) 7 - 42.

124. L. Forss. Iron Powder Metallurgy. Perspectives in Powder Metallurgy 3, 1968, 211 - 220.

125. D.L. Johnson. Journal of Applied Physics 40 (1) 1969, 192.

126. H.G. Van Bueren & J. Hornstra. "Reactivity in Solids". Elsevier Amsterdam 1960. p.112.

127. R.C. Gifkins. J. Australian Inst. of Metals. 14 (2) 1969, 92 - 97.

128. N.A. Gjostein. "Metal Surfaces", American Society for Metals 1962, p.99.

129. B.N. Singh & D.H. Houseman. Powder Metallurgy International 3 (1) 1971, 1 - 4.

130. A.D. Franklin, R. Campbell & J. Weinman. J. Applied Physics 24 (8) 1953. 1040 - 1045

131. S.J. Gregg & K.J. Hill. J. Chem Society 14 1953, 3945 - 3951.

132. M.J. Pryor & U.R. Evans. J. Chem Society 4 1949, 3330 - 3336.

133. F. Lihl Monatsh Chem 81 1950, 632.

134. R.P. Zerwekh & C.M. Wayman. Acta. Metallurgica 13. February 1965, 99 - 107.